Doctoral Thesis Reviewed by Ritsumeikan University

Advanced Positioning Algorithms for Automotive Single Frequency Receivers Based on PPP/VPPP GR Models

(PPP/VPPP GRモデルによる 車両用1周波受信機の測位アルゴリズムの高度化)

September 2017

2017年9月

Doctoral Program in Advanced Electrical, Electronic and Computer Systems
Graduate School of Science and Engineering

Ritsumeikan University

立命館大学大学院理工学研究科

電子システム専攻博士課程後期課程

MOURI Atsushi

毛利 篤史

Supervisors : Professor KUBO Yukihiro

研究指導教員：久保 幸弘 教授

Acknowledgements

The author would like to express his sincere gratitude to Professor Yukihiro Kubo of Ritsumeikan University for his supervisions, suggestion and continuous warm encouragement in the preparation of this thesis.

The author would also like to express his sincere gratitude to Professor Sueo Sugimoto of Ritsumeikan University for his supervisions, suggestion and continuous warm encouragement in the preparation of this thesis.

The author would also like to acknowledge their suggestion, guidance and continuous warm encouragement of Professor Kiyotsugu Takaba and Professor Yoshitaka Kawabata of Ritsumeikan University.

The author is also grateful to Dr. Masaharu Ohashi, Mr. Masahiro Ozaki, Mr. Yoshifumi Karatsu, and Mr. Goshi Okuda, for their helpful discussions and suggestions. Thanks are due to the author's colleagues in Information Communication System (Kubo) Laboratory who contributed to realize this thesis.

The author would like to thank Car Multimedia System Engineering Department of Sanda works, Mitsubishi Electric Corporation for allowing the author to enroll in a Ph.D program as an adult student for three years. The author's final thanks go to the author's father and mother for leading the author to path for learning, and the author's wife and daughter for always watching over the author with warm hearts.

Abstract

This thesis addresses more reliable and precise novel positioning algorithms for automotive applications using low-end single-frequency Global Navigation Satellite System (GNSS) receivers. In addition, it refers to the detection and correction of Doppler-observable outliers and precise point positioning (PPP)/very precise point positioning (VPPP) algorithms using single or double-difference (SD/DD) observables based on the GNSS regression (GR) models.

First, mathematical models of pseudoranges, Doppler shifts, and carrier-phase measurements are derived as basic equations for the positioning. The GR models for DD-based observables are shown, which are similar to the GR models for relative positioning algorithms; however, all antenna positions are unknown. The Kalman filtering algorithms for recursive estimation of all antenna positions and DD-based integer ambiguity of all carrier-phases are derived.

Second, methods of detecting Doppler outliers that cause positioning errors at Doppler-aided GNSS positioning for automotive applications and methods of correcting these errors are referred. The detection method based on the innovation process in Kalman filtering and that based on the measurements made on the basis of the difference between C/A code pseudoranges and Doppler shift range-rates are referred. Then, two correction methods, namely the Doppler outlier exclusion and Doppler outlier estimation, are proposed.

VPPP update algorithms based on geometric distance constraints estimate the parameters more precisely, including antenna positioning and integer ambiguities. Observables by four antennas on a squared board in a static situation are used for the positioning. Compared with the conventional PPP/VPPP algorithms, DD-based PPP/VPPP algorithms are shown to generate more precise positioning results, i.e. approximately 50-cm root-mean-square errors.

Finally, the estimation algorithms of Euler angles based on baseline vectors for attitude estimation are referred. When we obtain very precise positions of antennas disposed in a plane, we estimate the Euler angles from the baseline vectors of multiple antennas using the least-squares method. The so-called GNSS gyro can be realized as an application of the above-proposed positioning methods.

Contents

Chapter 1

Introduction

A key issue in Global Navigation Satellite Systems (GNSS) for advanced driving assistant systems (ADAS) or active safety systems (ASS) is to stably obtain the sub-meter-level vehicle positions by autonomous driving. Multi-GNSS positioning by single-frequency receivers contributes lower dilution of precision (DOP) values even in satellite-signal blockage areas; however, the bias error sources of the positioning, e.g. ionospheric delay, are remained, and the positioning performances are approximately limited to more than one meter. In order to achieve sub-meter-level accuracy, carrier-phase observables are additionally utilized, and estimation methods of the bias errors are applied for more precise autonomous positioning.

1.1 Overview of the Global Navigation Satellite Systems

Global Positioning System (GPS), initiated by the U.S. Department of Defense, first became operational (initial operational capability) with 24 satellites in 1993. By receiving the navigation messages from four or more satellites, a GPS receiver can effectively fix any three-dimensional positions on the earth. The GPS was originally developed for military purpose, and is comprised of space segment of satellites, control segment of monitor stations and ground antennas, and user segment of receivers. After removing selective

availability in 2000, the GPS has achieved several meter-level positioning by standard point positioning (SPP), and rapidly been expanded to civil application markets [1]–[4].

In recent years, the GNSS or Regional Navigation Satellite Systems (RNSS), namely not only GPS by the US, but also GLONASS by Russia, BeiDou Satellite System (BDS) by China, Galileo by EU, and Quasi-Zenith Satellite System (QZSS) by Japan, have been initiated or planning [5]–[8]. Until 2020, worldwide navigation satellite counts will surpass 130 satellites. Especially in Asian area, a receiver will be able to track more than 30 satellites at a time under open sky environments. QZSS by Japan will become operational in April 2018, and can complement or augment the GPS for more accurate positioning. Furthermore GNSS/RNSS will support multi-frequency signals, not only L1 band, but also L2/L5 bands in the future. The multi-frequency observations can be utilized for real-time kinematic (RTK) or precise point positioning (PPP) in order to correct ionospheric propagation delays or to resolve carrier-phase ambiguities.

The GNSS has been applied in a wide range of fields, and played more and more significant roles, e.g. SPP for various types of mobile vehicles planes/ships/cars or moving human, or differential GPS (DGPS)/relative positioning based on monitor stations for topographic surveying. The GPS time can be utilized for time synchronization functions. The multi-GNSS positioning can provide more precise positions recently, and is expected to contribute to more precise applications, e.g. lane-keep assistance or autonomous-brake system in ADAS/ASS.

1.2 Positioning Methods for Automotive Applications

In recent years, the required specifications for automotive applications are dramatically changing from (A) car navigations to (C) ADAS/ASS/automatic driving. The higher

accuracy positioning are also required by the changes as shown in Figure 1.1. In the case of (A), SPP basically utilizes just C/A code pseudoranges of low-end single-frequency receivers without augmentation data from reference stations. The SPP positioning methods can provide los-cost solutions and higher availability, however, have lower reliability of observables and lower positioning accuracy. On the other hand, in the case of (B), relative positioning for topographic surveying additionally utilizes carrier-phase (CP) observables which provide approximately one hundred times more precise pseudoranges, and multi-frequency observables, namely L1 and also L2/L5/L6 bandwidth. The augmentation data are also transmitted from reference stations through communication means. Therefore the positioning has approximately centimeter-level accuracy. The positioning accuracy of (B) targets less than (a)1.0 m, (b)0.5 m, and (c)0.1 m in stages. (B) employs

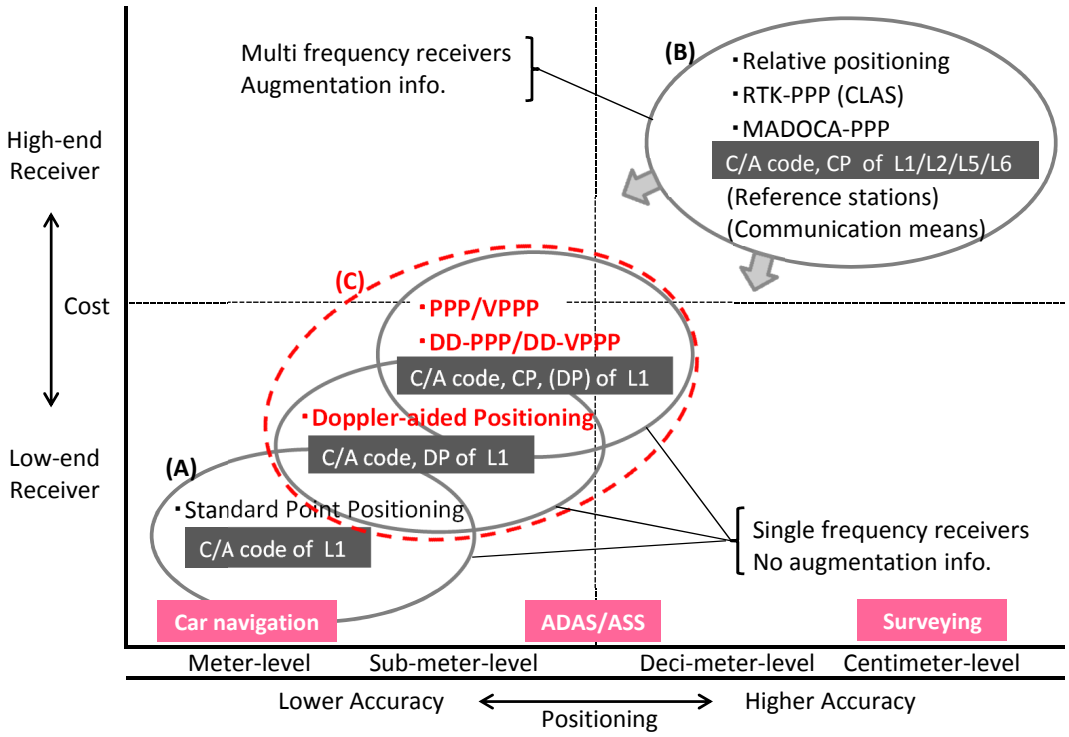

Figure 1.1: Target of this study (C)

RTK equivalent positioning methods with augmentation information, such as RTK-PPP (CLAS: centimeter-level augmentation system) or MADOCA-PPP (multi-GNSS advanced demonstration tool for orbit and clock analysis). The positioning techniques of these high-end receivers are gradually expanded to automotive commodity products. In the case of this study (C), the target positioning accuracy is sub-meter level required for ADAS/ASS applications. The positioning methods utilize not only code pseudoranges but also Doppler shift frequency and carrier-phase pseudoranges of single-frequency receivers without augmentation data. Advanced positioning algorithms can provide higher reliability of observables and higher positioning accuracy by Doppler-aided positioning or PPP-based positioning.

In general, there are three major error sources of GNSS positioning [1]. First one is GNSS satellite-related error source, e.g. clocks or orbits. Second one is GNSS signal travel path-related source, e.g. ionospheric or tropospheric signal delays. Third one is receiver-related source, e.g. observables or multi-path. GNSS observables for positioning are affected by these error sources, and caused bias or random errors. The satellite-related errors are globally caused, and the path-related errors are locally caused. According to standard error model for code pseudoranges, the bias noises are dominant except for multi-path, and the total amount of the errors is approximately five meters.

PPP-based positioning which utilizes carrier-phase observables needs to resolve integer ambiguities. They are comparatively easy to be resolved by fixed-point positioning under open sky environments, however, they have degraded positioning accuracy under signal blockage areas or multi-path environments. Under these difficult environments, Doppler shift observables (DP) are effectively utilized to improve positioning accuracy or availability.

In order to improve the reliability of these observables, the outlier detection and correction methods based on the GNSS observables. Although there are a lot of literature about detection of the outlier or the robust Kalmanfilter [9], [10] to overcome these problems, we propose the following two methods: 1) statistical tests on the innovation processes of the Kalman filter, 2) statistical test on the difference between C/A code delta-ranges and Doppler-shift range-rates. Method-1 is derived by modifying the cycle slip detection algorithm in [11], [12]. Method-2 can be also applied to carrier-phase delta-ranges.

Augmentation data utilized by the high-end receivers depends on positioning infrastructures, e.g. reference stations. In order to remove these error sources and realize the accuracy equivalent to relative positioning, the high-end receivers utilize the various methods with augmentation data, namely Satellite Based Augmentation System (SBAS), L1 band experimental signals (LEX) and so on. SBAS broadcasts wide-area differential augmentation data from geostationary satellites, and can correct the satellite orbits and clocks and the ionospheric signal delays, and achieve one meter or less positioning accuracy [13]. RTK-PPP based on LEX signals broadcasts State Space Representation (SSR) data from QZSS, and correct satellite orbits or clocks, and ionospheric or tropospheric signal delays and achieve centimeter-level positioning accuracy [14]. However, the GNSS observables of reference stations at the same timing are needed to generate augmentation data. MSAS (SBAS by Japan) needs the observables obtained at 12 monitor stations, and LEX needs the observables obtained at approximately 200 reference stations of GEONET in Japan. As the numbers of reference stations are not sufficient in the developing areas, the precise positioning based on augmentation data likewise RTK-PPP becomes impossible.

In order to resolve the issues of infrastructure dependency, the autonomy-oriented PPP are effective to improve positioning accuracy for automotive applications. PPP uti-

lizes carrier-phase observables from multiple rover antennas (receivers) by low-end single-frequency receivers without any augmentation information [15]–[20]. We have enhanced our previous PPP algorithms, and applied double-difference (DD) observables among multiple antennas to the algorithms and derived the DD-based GR models (DD-PPP). The DD-based technique needs additional rover antennas (receivers), however, it utilizes the cancellation of several bias error sources by DD-based observables at added antennas without any externally transmitted data. Additionally we have been developing Very Precise Point Positioning (VPPP) algorithms [21]–[25], the geometrical distances among the antennas are utilized as the constraints to improve PPP positioning estimates. VPPP is also applied to DD-PPP by the geometrical distance constraints.

1.3 Summary of Contents

This thesis mainly addresses following three topics:

i) Detection and correction of observable outliers for automotive

ii) PPP/VPPP algorithms by or not by DD-based observables among multiple antennas

iii) Euler-angle estimation by baseline vectors among multiple antennas

In Chapter 2, the mathematical models and the characteristic features of three independent GNSS observables, namely L1-C/A code psudoranges, L1 frequency carrier-phase pseudoranges, and Doppler frequency shifts, are referred. Then, the GR models for PPP/SD-PPP/DD-PPP algorithms among multiple antennas are derived, and the development to Kalman filtering positioning are shown.

In Chapter 3, the methods of detecting Doppler outliers which cause positioning errors at Doppler-aided GNSS positioning for automotive, and correcting the errors are referred. The detection methods are based on the innovation process in Kalman filtering, and based

on the measurements, namely the differences among C/A code delta-ranges, carrier-phase delta-ranges and Doppler range-rates. The correction methods are the Doppler outlier exclusion, and the estimation.

In Chapter 4, VPPP algorithms are applied to PPP/SD-PPP/DD-PPP with multiple antennas by using constraints of geometrical distances among antennas' positions and common receivers' clock errors based on the minimum mean square (MMS) methods. Then, the experimental results of the following four positioning methods among multiple antennas in a static environment are shown.

(a) PPP (Precise Point Positioning)

(b) VPPP (Very Precise Point Positioning)

(c) DD-PPP (Double-Difference Precise Point Positioning)

(d) DD-VPPP (Double-Difference Very Precise Point Positioning)

In Chapter 5, the GR model of baseline-vector estimation based on the DD-PPP GR model is derived, and the updating equations based on baseline-vector length constraints are also derived. The estimation algorithms of Euler angles based on baseline vectors for attitude estimation are referred. The experimental results of the Euler-angle values by least-squares method using six baseline vectors of four antennas are shown for the so-called GNSS gyro.

Chapter 2

GNSS Regression (GR) Models

2.1 Introduction

GNSS receivers basically generate three types of raw measurements, namely C/A code pseudoranges, carrier-phases pseudoranges, and Doppler shift frequencies. The raw data means the source data for calculating the fixed antenna positions connected to the receivers, and are generated at baseband processes after down-converter processes of GNSS RF signals. In general, L1-C/A code pseudoranges and Doppler-shift frequencies are measured at the acquisition stage of satellite signals in GNSS receivers. Receivers conduct a search process over the space of code-phase shifts and Doppler-frequency shifts, and routinely measure them in the carrier tracking loop of an acquisition stage. Doppler observables are obtained by frequency-locked loop (FLL) and less affected by noises or multipath compared with C/A code pseudorange observables obtained by delay-locked loop (DLL), and more robust than carrier-phase observables obtained by phase-locked loop (PLL) [3]. GNSS receivers have the same hardware components of the DLL, the FLL, and the PLL, however, their loop bandwidth affect the noise characteristic and the signal dynamics of the raw data [26]. Therefore high-end GNSS receivers for millimeter-level topographic surveying can provide less positioning fluctuations of SPP which mainly utilizes C/A code

pseudoranges compared with single-frequency GNSS receivers for meter-level mobile applications. Our proposed PPP/VPPP positioning algorithms are applied to economical single-frequency GNSS receivers.

In this chapter, first, the mathematical models and the characteristic features of measurements are referred. The GNSS measurement equations are referred in a lot of literature [1]–[3]. Regardless of the kinds of receivers, the same mathematical equation models can be applied to the measurements. The models are composed of the geometrical distance based on the measurement principle and the error terms composed of satellite-related, signal travelling-related, receiver-related sources, and observation noises.

Second, the GR models of conventional PPP algorithms for a single antenna are shown. PPP techniques are basically one approach to achieve sub-meter level positioning accuracy using carrier-phase observables without baseline vector analysis from reference stations. Then, the expansion equations by individually applying the PPP algorithms to multiple rover antennas (receivers) are shown.

Lastly the GR models of novel PPP algorithms based on the single difference (SD) or the double difference (DD) GNSS observables among multiple antennas (receivers) are referred. The models are derived from the GR models of relative positioning algorithms, however, all antennas' positions are unknown parameters.

2.2 Mathematical Models and Features of GNSS Measurements

The C/A code pseudoranges $\rho_u^p(t)$ at GPS time (GPST) t is derived from the signal travelling time as follows [26]:

$$\rho_u^p(t) = c\left[t_u(t) - t^p(t - \tau_u^p)\right] + e_u^p(t), \tag{2.1}$$

where c ($\approx 2.99792458 \times 10^8$[m/s]) denotes the speed of light, $t^p(t-\tau_u^p)$ is the emission time measured by the satellite clock, and $t_u(t)$ is the arrival time measured by the user's receiver clock. τ_u^p is the signal travelling time from the satellite to the receiver for the code pseudoranges, and e_u^p is the measurement error.

The relationship between the time of the satellite or the receiver clocks and the GPST are as follows:

$$t^p(t-\tau_u^p) = (t-\tau_u^p) + \delta t^p(t-\tau_u^p), \quad t_u(t) = t + \delta t_u(t), \tag{2.2}$$

where δt^p is the satellite clock bias, and δt_u is the receiver clock bias. Eqs. (2.2) are substituted in Eq. (2.1), and then we obtain the following equation:

$$\begin{aligned}\rho_u^p(t) &= c\left[t + \delta t_u(t) - ((t-\tau_u^p) + \delta t^p(t-\tau_u^p))\right] + e_u^p(t) \\ &= c\tau_u^p + c\left[\delta t_u(t) - \delta t^p(t-\tau_u^p)\right] + e_u^p(t).\end{aligned} \tag{2.3}$$

The travelling time τ_u^p multiplied by the speed of light can be modeled as follows:

$$c\tau_u^p = r_u^p(t, t-\tau_u^p) + \delta I_u^p(t) + \delta T_u^p(t), \tag{2.4}$$

where $r_u^p(t, t-\tau_u^p)$ is the geometric distance between the receiver position at time t and the satellite position at $(t-\tau_u^p)$. δI_u^p and δT_u^p reflect the delays of GNSS signals travelling through the ionosphere and the troposphere, respectively. Finally we obtain the mathematical model of C/A code pseudoranges as follows:

$$\rho_u^p(t) = r_u^p(t, t-\tau_u^p) + c\left[\delta t_u(t) - \delta t^p(t-\tau_u^p)\right] + \delta I_u^p(t) + \delta T_u^p(t) + e_u^p(t). \tag{2.5}$$

The carrier-phase observables $\phi_u^p(t)$ at GPST t is derived from the signal travelling time τ_u^p as follows:

$$\phi_u^p(t) = \phi_u(t) - \phi^p(t-\tau_u^p) + N_u^p + \epsilon_u^p(t), \tag{2.6}$$

where $\phi_u(t)$ is the phase of the signal generated by the receiver clock at the arrival time, and $\phi^p(t-\tau_u^p)$ is the phase of the signal generated by the satellite at the emission time. N_u^p is the integer ambiguity. $\epsilon_u^p(t)$ is the measurement error. We simplify Eq. (2.6) by the following equation:

$$\phi^p(t-\tau_u^p) = \phi^p(t) - f \times \tau, \tag{2.7}$$

then we obtain as follows:

$$\begin{aligned} \phi_u^p(t) &= f \times \tau + N_u^p + \epsilon_u^p(t) = \frac{r_u^p(t, t-\tau_u^p)}{\lambda} + N_u^p + \epsilon_u^p(t), \\ \lambda\phi_u^p(t) &= r_u^p(t, t-\tau_u^p) + \lambda N_u^p + \lambda\epsilon_u^p(t), \end{aligned} \tag{2.8}$$

where f and λ are the carrier frequency and wavelength, respectively. $r_u^p(t, t-\tau_u^p)$ is the geometric distance between the receiver position at time t and the satellite position at $(t-\tau_u^p)$:

$$\lambda\phi_u^p(t) = r_u^p(t, t-\tau_u^p) + c\left[\delta t_u(t) - \delta t^p(t-\tau_u^p)\right] + \delta I_u^p(t) + \delta T_u^p(t) + \lambda N_u^p + \lambda\epsilon_u^p(t). \tag{2.9}$$

Doppler shift frequencies are equivalent to the range rate, and can be regarded as a projection of the relative velocity on the satellite line-of-sight vector [26],[27]. The Doppler shift is actually measured as the pseudorange rate, and proportional to the line-of-sight velocity of the user relative to the satellite over the time interval. The mathematical model of Doppler shift can be obtained by differentiating Eq. (2.5) as follows:

$$\dot{\rho}_u^p(t) = \dot{r}_u^p(t, t-\tau_u^p) + c\left[\delta\dot{t}_u(t) - \delta\dot{t}^p(t-\tau_u^p)\right] + \delta\dot{I}_u^p(t) + \delta\dot{T}_u^p(t) + \dot{\epsilon}_u^p(t), \tag{2.10}$$

where $\delta\dot{t}_u(t)$ and $\delta\dot{t}^p(t-\tau_u^p)$ are the receiver and satellite clock drifts.

We analyze Doppler frequency shift accuracy compared with L1-C/A code pseudoranges. C/A code delta-ranges are the time-differenced pseudorange observables over two

consecutive times (epochs), namely $\rho^p_{CA,u}(t)$ - $\rho^p_{CA,u}(t-1)$. On the other hand, Doppler shift range-rates are receiver-satellite values based on Doppler frequency shift observables, namely $\lambda_1 D^p_{L1,u}(t)$. $\rho^p_{CA,u}(t)$ is a C/A code pseudorange, and $D^p_{L1,u}(t)$ is a Doppler frequency shift between satellite p and receiver u at epoch t. λ_1 is wave length of carrier wave and calculated by c/f_1. c denotes the speed of light, and f_1 is L1 central frequency, namely $f_1 = 2 \times 77 \times 10.23$ [MHz] $= 1575.42$ [MHz]. In theory delta-ranges are nearly equal to range-rates. C/A code pseudoranges and Doppler shifts observables are proved to be independent (p.186 in [2]).

Fig. 2.1 shows an example of the comparison between the delta-ranges (red line) obtained from code pseudoranges and the range-rates (blue line) obtained from Doppler shifts. The observables was collected from a u-blox NEO-7N receiver equipped in the test vehicle moved in Tokyo, Japan, on April 2, 2014. The satellite elevation is 55-56 degrees

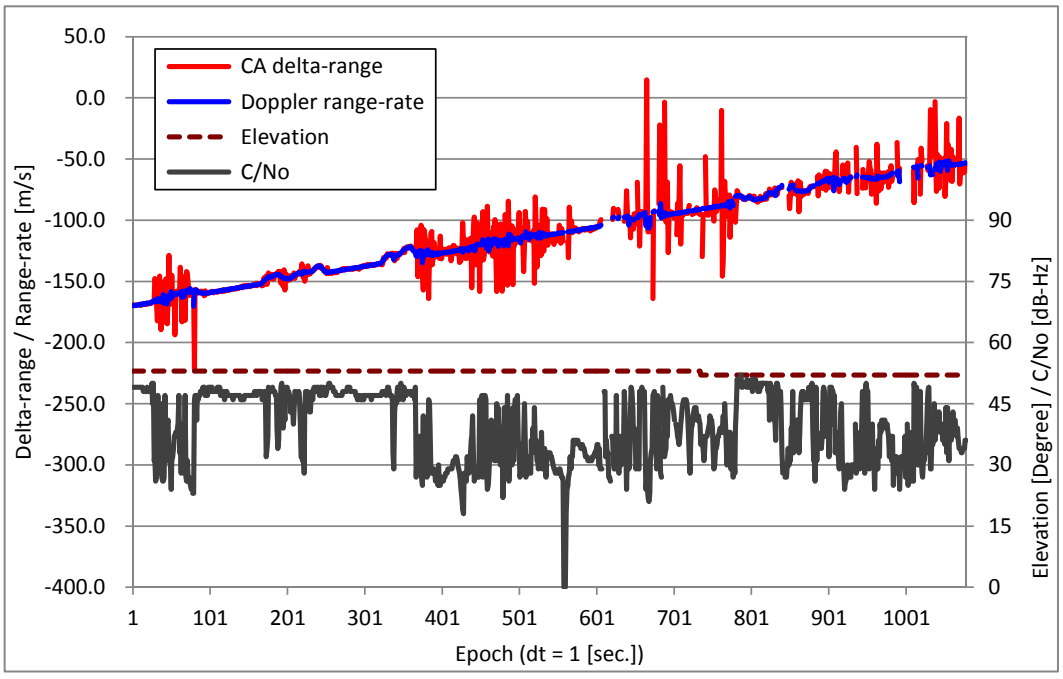

Figure 2.1: CA code delta-range / Doppler shift range-rate

(brown line), and the C/No (Carrier to Noise ratio) values [28] (black line) calculated by the baseband process of the receiver are degraded to approximately 30 dB-Hz from 45 dB-Hz because of multipath indirect waves. The delta-ranges have several tens of meter fluctuations when the C/No degradations. On the other hand the range-rates have small fluctuations. The Doppler shifts are less affected by the indirect waves, and can stay more accurate than code pseudoranges even under multipath environments. Doppler observables therefore have the potential to be utilized to smooth the code pseudorange noises in GNSS difficult environment.

2.3 GNSS Regression Models among Multiple Antennas

2.3.1 GR Equations for GNSS Measurements

First of all, similarly to [15]–[20], we formulate all observed positioning data consisting of the L1 carrier-phase, pseudoranges based on C/A code, and Doppler shift frequency by using the GNSS regression models. The natural extensions of GNSS regression models for multiple frequencies of GPS, Galileo, Compass/BeiDou, GLONASS, and US-GPS modernization are also similarly formulated. Namely, we consider the following fundamental measurements of L1 band carrier-phases $\varphi^p_{L1,u}(t)$ (equivalently, $\Phi^p_{L1,u}(t)$ as the unit of length), pseudoranges $\rho^p_{CA,u}(t)$ based on the C/A code, and Doppler shift frequency

$\dot{\rho}^p_{DL1,u}(t)$, respectively, as follows [2], [26], [29], [31]:

$$\begin{aligned}\rho^p_{CA,u}(t) &= r^p_u(t, t-\tau^p_u) + \delta I^p_u(t) + \delta T^p_u(t) + c\,[\delta t_u(t) - \delta t^p(t-\tau^p_u)] \\ &\quad +\delta b_{CA,u} - \delta b^p_{CA} + e^p_{CA,u}(t), \qquad (2.11)\\ \Phi^p_{L1,u}(t) &= \lambda_1 \varphi^p_{L1,u}(t) \\ &= r^p_u(t, t-\tau^p_u) - \delta I^p_u(t) + \delta T^p_u(t) + c\,[\delta t_u(t) - \delta t^p(t-\tau^p_u)] \\ &\quad +\delta b_{L1,u} - \delta b^p_{L1} + \lambda_1 N^p_u + \lambda_1 \varepsilon^p_{L1,u}(t), \qquad (2.12)\\ \dot{\rho}^p_{DL1,u}(t) &= \dot{r}^p_u(t, t-\tau^p_u) + \delta \dot{I}^p_u(t) + \delta \dot{T}^p_u(t) + c\left[\delta \dot{t}_u(t) - \delta \dot{t}^p(t-\tau^p_u)\right] \\ &\quad +\delta b_{DL1,u} - \delta b^p_{DL1}(t) + \varepsilon^p_{DL1,u}(t), \qquad (2.13)\end{aligned}$$

where c ($\cong 2.99792458 \times 10^8$[m/s]) denotes the speed of light, and f_1 and λ_1 are the central frequency and the wave length of the L1 carrier wave

$$f_1 = 2 \times 77 \times 10.23 \text{ [MHz]} = 1575.42 \text{ [MHz]}.$$

In Eqs. (2.11)-(2.13), the so-called receiver's biases, $\{\delta b_{CA,u},\ \delta b_{L1,u},\ \delta b_{DL1,u}\}$, and the satellite biases, $\{\delta b^p_{CA},\ \delta b^p_{L1},\ \delta b^p_{DL1}\}$, are contained in the usual observed positioning data consisting of the L1 carrier-phase, pseudorange based on the C/A codes [32], and Doppler shift frequency. Also $r^p_u(t, t-\tau^p_u)$ is the geometric distance between the receiver u at the time t and the satellite p at the time $t-\tau^p_u$ (τ^p_u denotes the travel time from the satellite p ($p = 1, \ldots, n_s$) to the receiver u ($u = 1, \ldots, n_r$)). Namely,

$$\begin{aligned}r^p_u(t) &\equiv r^p_u(t, t-\tau^p_u) \\ &= \left[\left(x_u(t) - x^p(t-\tau^p_u)\right)^2 + \left(y_u(t) - y^p(t-\tau^p_u)\right)^2 + \left(z_u(t) - z^p(t-\tau^p_u)\right)^2\right]^{1/2} \\ &= ||u(t) - s^p(t-\tau^p_u)||, \qquad (2.14)\end{aligned}$$

where $u \equiv \left[x_u, y_u, z_u\right]^{\mathrm{T}}$ and $s^p \equiv \left[x^p, y^p, z^p\right]^{\mathrm{T}}$ are a user (unknown) and satellite positions, respectively. Also n_s denotes the number of the observable satellites. n_r denotes the

number of the receivers one-on-one connected to multiple antennas. Further in Eqs. (2.11)-(2.12), $\delta I_u^p(t)$ and $\delta T_u^p(t)$ reflect the delay or the advance associated with the transmission of the L1 signal through the ionosphere and the troposphere, respectively. $\delta t_u(t)$ and $\delta t^p(t-\tau_u^p)$ are the clock errors of the receiver u at the time t and the satellite p at the time $t-\tau_u^p$. N_u^p denotes integer ambiguity between the satellite p and the receiver u, and $e_{CA,u}^p(t),\ \varepsilon_{L1,u}^p(t),\ \varepsilon_{DL1,u}^p(t)$ denote measurement errors.

Eq. (2.14) contains the satellite orbital errors. The estimated satellite orbits are obtained from the navigation messages which are decoded from the transmitted L1 signal. Let us denote $\hat{s}^p$ as the estimated position of the satellite s^p at the time $t-\tau_u^p$. Eq. (2.14) is expressed by nonlinear terms based on satellites s^p and receiver u. We use the following relations of the derivatives,

$$\frac{\partial r_u^p}{\partial x_u} = \frac{(x_u - x^p)}{r_u^p}, \quad \frac{\partial r_u^p}{\partial y_u} = \frac{(y_u - y^p)}{r_u^p}, \quad \frac{\partial r_u^p}{\partial z_u} = \frac{(z_u - z^p)}{r_u^p}, \quad (p = 1, 2, \ldots, n_s), \tag{2.15}$$

and

$$\frac{\partial r_u^p}{\partial x^p} = -\frac{(x_u - x^p)}{r_u^p}, \quad \frac{\partial r_u^p}{\partial y^p} = -\frac{(y_u - y^p)}{r_u^p}, \quad \frac{\partial r_u^p}{\partial z^p} = -\frac{(z_u - z^p)}{r_u^p}, \quad (p = 1, 2, \ldots, n_s). \tag{2.16}$$

Then we have the relation:

$$\frac{\partial r_u^p}{\partial u} = -\frac{\partial r_u^p}{\partial s^p}. \tag{2.17}$$

Thus the 1st order Taylor series approximation of Eq. (2.14) around the previous estimated

value $u = \hat{u}^{(\nu)}$ (ν : iteration counts of the estimation) and $s^p = \hat{s}^p$ is given by

$$\begin{aligned} r_u^p &\cong r_{\hat{u}^{(\nu)}}^{\hat{p}} + (g_{\hat{u}^{(\nu)}}^{\hat{p}})^{\mathrm{T}}[u - s^p - (\hat{u}^{(\nu)} - \hat{s}^p)] \\ &= ||\hat{u}^{(\nu)} - \hat{s}^p|| + \frac{(\hat{u}^{(\nu)} - \hat{s}^p)^{\mathrm{T}}}{||\hat{u}^{(\nu)} - \hat{s}^p||}[u - s^p - (\hat{u}^{(\nu)} - \hat{s}^p)] \\ &= \frac{(\hat{u}^{(\nu)} - \hat{s}^p)^{\mathrm{T}}}{||\hat{u}^{(\nu)} - \hat{s}^p||}(u - s^p) \end{aligned} \tag{2.18}$$

for $p = 1, 2, \ldots, n_s$, where

$$g_{\hat{u}^{(\nu)}}^{\hat{p}} \equiv \left[\frac{\partial r_u^p}{\partial u}\right]_{u=\hat{u}^{(\nu)}, s^p=\hat{s}^p} = \frac{(\hat{u}^{(\nu)} - \hat{s}^p)}{||\hat{u}^{(\nu)} - \hat{s}^p||}. \tag{2.19}$$

In order to employ the same estimation method as that of previous PPP methods, the linearized gradient vectors $g_{\hat{u}}^{\hat{p}}$ are utilized for Extended Kalman filter of the DD-based PPP method. From Eqs. (2.11)-(2.13), we therefore have the approximations:

$$\rho_{CA,u}^p \cong (g_{\hat{u}^{(\nu)}}^{\hat{p}})^{\mathrm{T}}(u - s^p) + \delta I_u^p + \delta T_u^p + c(\delta t_u - \delta t^p) + \delta b_{CA,u} - \delta b_{CA}^p + e_{CA,u}^p, \tag{2.20}$$

$$\begin{aligned} \Phi_{L1,u}^p &\cong (g_{\hat{u}^{(\nu)}}^{\hat{p}})^{\mathrm{T}}(u - s^p) - \delta I_u^p + \delta T_u^p + c(\delta t_u - \delta t^p) + \delta b_{L1,u} - \delta b_{L1}^p + \lambda_1 N_{L1,u}^p \\ &\quad + \lambda_1 \varepsilon_{L1,u}^p, \end{aligned} \tag{2.21}$$

$$\begin{aligned} \dot{\rho}_{DL1,u}^p &= \lambda_1 D_{L1,u}^p \\ &\cong (g_{\hat{u}^{(\nu)}}^{\hat{p}})^{\mathrm{T}}(\dot{u} - \dot{s}^p) + \delta \dot{I}_u^p + \delta \dot{T}_u^p + c(\delta \dot{t}_u - \delta \dot{t}^p) + \delta b_{DL1}^p + \varepsilon_{DL1,u}^p. \end{aligned} \tag{2.22}$$

Define the $n_s \times 3$ matrix:

$$G_{\hat{u}^{(\nu)}}^{\hat{p}} \equiv \begin{bmatrix} (g_{\hat{u}^{(\nu)}}^{\hat{1}})^{\mathrm{T}} \\ (g_{\hat{u}^{(\nu)}}^{\hat{2}})^{\mathrm{T}} \\ \vdots \\ (g_{\hat{u}^{(\nu)}}^{\hat{n}_s})^{\mathrm{T}} \end{bmatrix} = \begin{bmatrix} \frac{\partial r_{\hat{u}^{(\nu)}}^{\hat{1}}}{\partial \hat{x}_u^{(\nu)}} & \frac{\partial r_{\hat{u}^{(\nu)}}^{\hat{1}}}{\partial \hat{y}_u^{(\nu)}} & \frac{\partial r_{\hat{u}^{(\nu)}}^{\hat{1}}}{\partial \hat{z}_u^{(\nu)}} \\ \frac{\partial r_{\hat{u}^{(\nu)}}^{\hat{2}}}{\partial \hat{x}_u^{(\nu)}} & \frac{\partial r_{\hat{u}^{(\nu)}}^{\hat{2}}}{\partial \hat{y}_u^{(\nu)}} & \frac{\partial r_{\hat{u}^{(\nu)}}^{\hat{2}}}{\partial \hat{z}_u^{(\nu)}} \\ \vdots & \vdots & \vdots \\ \frac{\partial r_{\hat{u}^{(\nu)}}^{\hat{n}_s}}{\partial \hat{x}_u^{(\nu)}} & \frac{\partial r_{\hat{u}^{(\nu)}}^{\hat{n}_s}}{\partial \hat{y}_u^{(\nu)}} & \frac{\partial r_{\hat{u}^{(\nu)}}^{\hat{n}_s}}{\partial \hat{z}_u^{(\nu)}} \end{bmatrix}. \tag{2.23}$$

In order to simplify the expression, superscript (ν) for the iteration counts of the estimation is omitted hereafter.

2.3.2 GR Models for PPP

Eqs. (2.11)-(2.13) are denoted for the observables of L1-CA code pseudoranges, L1 carrier-phases and Doppler shifts. The equations can be applied for L2-CA, L1-PY, L2-PY and other kinds of observables for multi-frequencies and multi-GNSS navigation signals. It was pointed out in [32] that the magnitude of the satellite's hardware delay bias δb_*^p is usually in the range of (several nanosecond $\times c$), while the receiver's hardware biases $\delta b_{*,u}$ could exceed (10 nanoseconds $\times c$). we therefore assume that the satellite's hardware delay biases are negligible, and the receiver's hardware biases are not disregarded, and defined as the terms of the 3×1 vector: $\delta b_u \equiv [\delta b_{CA,u}, \delta b_{L1,u}, \delta b_{DL1,u}]^{\mathrm{T}}$. $\delta \dot{I}_u^p(t)$ and $\delta \dot{T}_u^p(t)$ which are the delay changes for a short time are very small and negligible.

Here, we define the vectors:

$$
\begin{aligned}
\rho_{CA,u}^p &\equiv \begin{bmatrix} \rho_{CA,u}^1 \\ \vdots \\ \rho_{CA,u}^{n_s} \end{bmatrix}, \quad \Phi_{L1,u}^p \equiv \begin{bmatrix} \Phi_{L1,u}^1 \\ \vdots \\ \Phi_{L1,u}^{n_s} \end{bmatrix}, \quad D_{L1,u}^p \equiv \begin{bmatrix} D_{L1,u}^1 \\ \vdots \\ D_{L1,u}^{n_s} \end{bmatrix}, \\
c\delta t^p &\equiv \begin{bmatrix} c\delta t^1 \\ \vdots \\ c\delta t^{n_s} \end{bmatrix}, \quad s \equiv \begin{bmatrix} s^1 \\ \vdots \\ s^{n_s} \end{bmatrix}, \quad \dot{s} \equiv \begin{bmatrix} \dot{s}^1 \\ \vdots \\ \dot{s}^{n_s} \end{bmatrix}, \\
\delta I_u &\equiv \begin{bmatrix} \delta I_u^1 \\ \vdots \\ \delta I_u^{n_s} \end{bmatrix}, \quad \delta T_u \equiv \begin{bmatrix} \delta T_u^1 \\ \vdots \\ \delta T_u^{n_s} \end{bmatrix}, \quad N_{L1,u}^p \equiv \begin{bmatrix} N_{L1,u}^1 \\ \vdots \\ N_{L1,u}^{n_s} \end{bmatrix}, \\
e_{CA,u} &\equiv \begin{bmatrix} e_{CA,u}^1 \\ \vdots \\ e_{CA,u}^{n_s} \end{bmatrix}, \quad \varepsilon_{L1,u} \equiv \begin{bmatrix} \varepsilon_{L1,u}^1 \\ \vdots \\ \varepsilon_{L1,u}^{n_s} \end{bmatrix}, \quad \varepsilon_{DL1,u} \equiv \begin{bmatrix} \varepsilon_{DL1,u}^1 \\ \vdots \\ \varepsilon_{DL1,u}^{n_s} \end{bmatrix}. \qquad (2.24)
\end{aligned}
$$

Furthermore, from Eq. (2.23), we define a block diagonal matrix with the size $(n_s \times 3n_s)$:

$$G^{\hat{p}}_{D,\hat{u}} \equiv \begin{bmatrix} (g^{\hat{1}}_{\hat{u}})^{\mathrm{T}} & O & O & \cdots & O \\ O & (g^{\hat{2}}_{\hat{u}})^{\mathrm{T}} & O & \cdots & O \\ \vdots & & \ddots & & \vdots \\ \vdots & & & \ddots & O \\ O & \cdots & \cdots & O & (g^{\hat{n}_s}_{\hat{u}})^{\mathrm{T}} \end{bmatrix}. \tag{2.25}$$

Then from Eqs. (2.20)-(2.22), we have the following vector regression equation:

$$y^p_u = H^{\hat{p}}_{\hat{u}}\theta_u + v_u, \tag{2.26}$$

where

$$y^p_u \equiv \begin{bmatrix} \rho^p_{CA,u} \\ \Phi^p_{L1,u} \\ \lambda_1 D^p_{L1,u} \end{bmatrix}, \quad H^{\hat{p}}_{\hat{u}} \equiv \begin{bmatrix} G^{\hat{p}}_{\hat{u}} & \mathbf{1} & \mathbf{1} & -I & -G_D & & I & I & \\ G^{\hat{p}}_{\hat{u}} & \mathbf{1} & \mathbf{1} & -I & -G_D & & I & I & I \\ G^{\hat{p}}_{\hat{u}} & \mathbf{1} & \mathbf{1} & & & -G_D & & & \end{bmatrix},$$

$$\begin{aligned} \theta_u &\equiv \left[u,\ \dot{u},\ c\delta t_u,\ c\dot{\delta} t_u,\ \delta b_u,\ c\delta t^p,\ s,\ \dot{s},\ \delta I_u,\ \delta T_u,\ \lambda_1 N_{L1,u}\right]^{\mathrm{T}}, \\ v_u &\equiv \left[e^{\mathrm{T}}_{CA,u},\ \lambda_1(\varepsilon^p_{L1,u})^{\mathrm{T}},\ \lambda_1(\varepsilon^p_{DL1,u})^{\mathrm{T}}\ \right]^{\mathrm{T}}, \end{aligned} \tag{2.27}$$

and I denote the $n_s \times n_s$ identity matrix and $\mathbf{1} \equiv [1, 1, \cdots, 1]^{\mathrm{T}}$: $n_s \times 1$ vector.

The navigation messages broadcasted from GNSS satellites include some knowledge of the satellite position s, the satellite velocity $\dot{s}$, the satellite clock error δt^p, as well as the delay or the advance due to the ionospheric and tropospheric effects, δI_u and δT_u are, for instance,

$$\begin{aligned} &\hat{s} = s + e_s, \quad \hat{\dot{s}} = \dot{s} + e_{\dot{s}}, \quad \hat{c\delta t^p} = c\delta t^p + e_{\delta t^p}, \\ &\hat{\delta I_u} = \delta I_u + e_{\delta I_u}, \quad \hat{\delta T_u} = \delta T_u + e_{\delta T_u}, \end{aligned} \tag{2.28}$$

where e_* show the estimation errors. Substituting the above relations Eqs. (2.28)-(2.28) into the GR equations Eqs. (2.20)-(2.21) to utilize Kalman filtering methods, and neglect $s, \dot{s}$, $c\delta t^p$, δI_u, δT_u, we have

$$\begin{bmatrix} y^{\hat{p}}_{CA,\hat{u}} \\ y^{\hat{p}}_{L1,\hat{u}} \\ y^{\hat{p}}_{DL1,\hat{u}} \end{bmatrix} = C^{\hat{p}}_{\hat{u}} \begin{bmatrix} u \\ \dot{u} \\ c\delta t_u \\ c\dot{\delta} t_u \\ \delta b_u \\ \lambda_1 N_{L1,u} \end{bmatrix} + v, \tag{2.29}$$

where

$$C^{\hat{p}}_{\hat{u}} = \begin{bmatrix} G^{\hat{p}}_{\hat{u}} & \mathbf{1} & \mathbf{1} & \\ G^{\hat{p}}_{\hat{u}} & \mathbf{1} & \mathbf{1} & I \\ G^{\hat{p}}_{\hat{u}} & \mathbf{1} & \mathbf{1} & \end{bmatrix}, \quad v = \begin{bmatrix} G^{\hat{p}}_{D,\hat{u}} e_s + e_{\delta t^p} - e_{\delta I_u} - e_{\delta T_u} + e_{CA,u} \\ G^{\hat{p}}_{D,\hat{u}} e_s + e_{\delta t^p} + e_{\delta I_u} - e_{\delta T_u} + \lambda_1 \varepsilon_{L1,u} \\ G^{\hat{p}}_{D,\hat{u}} e_{\dot{s}} + e_{\dot{\delta} t^p} + \lambda_1 \varepsilon_{DL1,u} \end{bmatrix}, \tag{2.30}$$

$$y^{\hat{p}}_{CA,\hat{u}} = \rho^s_{CA,u} + G^{\hat{p}}_{D,\hat{u}} \hat{s} + c\hat{\delta} t^p - \hat{\delta I}_u - \hat{\delta T}_u, \tag{2.31}$$

$$y^{\hat{p}}_{L1,\hat{u}} = \Phi^s_{L1,u} + G^{\hat{p}}_{D,\hat{u}} \hat{s} + c\hat{\delta} t^p + \hat{\delta I}_u - \hat{\delta T}_u, \tag{2.32}$$

$$y^{\hat{p}}_{DL1,\hat{u}} = \dot{\rho}^s_{DL1,u} + G^{\hat{p}}_{D,\hat{u}} \hat{\dot{s}}, \tag{2.33}$$

$$G^{\hat{p}}_{\hat{u}} \equiv \begin{bmatrix} s^{\hat{1}}_{\hat{u}} & s^{\hat{2}}_{\hat{u}} & \cdots & s^{\hat{n}_s}_{\hat{u}} \end{bmatrix}^{\mathrm{T}}, \tag{2.34}$$

$$G^{\hat{p}}_{D,\hat{u}} \equiv \mathrm{diag}\begin{pmatrix} (g^{\hat{1}}_{\hat{u}})^{\mathrm{T}} & (g^{\hat{2}}_{\hat{u}})^{\mathrm{T}} & \cdots & (g^{\hat{n}_s}_{\hat{u}})^{\mathrm{T}} \end{pmatrix}. \tag{2.35}$$

The above Eq. (2.29) is called GNSS regression model (GR model) [15]–[20]. In this thesis, the positioning results are obtained by the extended Kalman filtering methods based on the GR models.

Let us consider that multiple antennas $u_i = 1, \ldots, n_r$ are disposed with the given distance $d_{j,i}$ between any two antennas u_i and u_j. In this assumption, when we observe

C/A code pseudoranges and carrier-phases by multiple antennas, we have the following n_r single-frequency GR equations:

$$y_{\hat{u}_i} = C^{\hat{p}}_{\hat{u}_i}\theta_{u_i} + v_{u_i}, \tag{2.36}$$

for $i = 1, \ldots, n_r$, where

$$C^{\hat{p}}_{\hat{u}_i} = \begin{bmatrix} G^{\hat{p}}_{\hat{u}_i} & \mathbf{1} & \mathbf{1} & \\ G^{\hat{p}}_{\hat{u}_i} & \mathbf{1} & \mathbf{1} & I \\ G^{\hat{p}}_{\hat{u}_i} & \mathbf{1} & \mathbf{1} & \end{bmatrix}, \quad \theta_{u_i} = \begin{bmatrix} u_i \\ \dot{u}_i \\ c\delta t_{u_i} \\ c\dot{\delta} t_{u_i} \\ \delta b_{u_i} \\ \lambda_k N_{L1,u_i} \end{bmatrix}. \tag{2.37}$$

We show state equations and measurement equations for applying Kalman filtering. The receiver's clock errors $c\delta t_u$ are generally modeled as follows [1], [33], [34] (let us call the following model as the A-model of the receiver's clock error),

$$c\delta t_{u,t+1} = c\delta t_{u,t} + \Delta_t c\dot{\delta} t_{u,t} + w_{c\delta t_u,t}, \tag{2.38}$$

$$c\dot{\delta} t_{u,t+1} = c\dot{\delta} t_{u,t} + w_{c\dot{\delta} t_u,t}, \tag{2.39}$$

where Δ_t denotes the sampling interval of the receiver's clock error, and the noise $w_{c\delta t_u,t}$ and $w_{c\dot{\delta} t_u,t}$ are assumed as white Gaussian processes with zero means and covariances $q_{c\delta t}$ and $q_{c\dot{\delta} t}$, respectively. Then we can write

$$\begin{aligned} \begin{bmatrix} c\delta t_{u,t+1} \\ c\dot{\delta} t_{u,t+1} \end{bmatrix} &= \begin{bmatrix} 1 & \Delta_t \\ 0 & 1 \end{bmatrix} \begin{bmatrix} c\delta t_{u,t} \\ c\dot{\delta} t_{u,t} \end{bmatrix} + \begin{bmatrix} w_{c\delta t_u,t} \\ w_{c\dot{\delta} t_u,t} \end{bmatrix} \\ &\equiv F_{A,c\delta t} \begin{bmatrix} c\delta t_{u,t} \\ c\dot{\delta} t_{u,t} \end{bmatrix} + \begin{bmatrix} w_{c\delta t_u,t} \\ w_{c\dot{\delta} t_u,t} \end{bmatrix}. \end{aligned} \tag{2.40}$$

Then assuming that the time differential of receiver's clock error $c\delta t_u$ obeys first-order Malkov models on the time series analysis, we can derive the following equation:

$$\begin{aligned}\begin{bmatrix} c\delta t_{u,t+1} \\ c\dot{\delta} t_{u,t+1} \end{bmatrix} &= \begin{bmatrix} 1 & \Delta_t \\ 0 & \kappa \end{bmatrix} \begin{bmatrix} c\delta t_{u,t} \\ c\dot{\delta} t_{u,t} \end{bmatrix} + \begin{bmatrix} 0 \\ w_{c\dot{\delta} t_u,t} \end{bmatrix} \\ &\equiv F_{B,c\delta t} \begin{bmatrix} c\delta t_{u,t} \\ c\dot{\delta} t_{u,t} \end{bmatrix} + \begin{bmatrix} 0 \\ w_{c\dot{\delta} t_u,t} \end{bmatrix}. \end{aligned} \tag{2.41}$$

Now we present an approximated but simpler estimation algorithm of η_t. Namely define

$$\eta_t \equiv \left[\eta_{1,t},\ \eta_{2,t},\ \cdots,\ \eta_{n_r,t}\right]^{\mathrm{T}}, \tag{2.42}$$

where

$$\eta_{i,t} = \left[u_i,\ \dot{u}_i,\ c\delta t_{u_i},\ c\dot{\delta t}_{u_i},\ \delta b_{u_i},\ N_{L1,u_i}\right]^{\mathrm{T}}, \quad (i = 1, \cdots, n_r). \tag{2.43}$$

Then the state equation and measurement equation are given by

$$\eta_{i,t+1} = A_{i,t}\ \eta_{i,t} + w_{i,t}, \tag{2.44}$$

$$y_{\hat{u}_{i,t}} = C_{i,t}\ \eta_{i,t} + v_{i,t}, \tag{2.45}$$

where

$$A_{i,t} \equiv \begin{bmatrix} I_{3\times 3} & & & \\ & I_{3\times 3} & & \\ & & F_{*,c\delta t} & \\ & & & I \end{bmatrix}, \quad C_{i,t} \equiv \begin{bmatrix} G_{\hat{u}_i} & & 1 & 0 & 1 & \\ G_{\hat{u}_i} & & 1 & 0 & 1 & \lambda_1 I \\ & G_{\hat{u}_i} & 0 & 1 & 1 & \end{bmatrix}, \tag{2.46}$$

$$w_{i,t} \equiv \left[\mathbf{0}_3,\ \mathbf{0}_3,\ *,\ w_{c\dot{\delta t}_{ui}},\ \mathbf{0}_{2+n_{si}}\right]^{\mathrm{T}}. \tag{2.47}$$

Thus, for each state $\eta_{i,t}$, we can obtain the filtering estimate $\hat{\eta}_{i,t|t}$ and its error covariance matrix $\Sigma_{\eta_i,t|t}$ by applying the Kalman filter. The approximated estimate $\hat{\eta}_{t|t}$ and its error

covariance are obtained by

$$\hat{\eta}_{t|t} = \begin{bmatrix} \hat{\eta}_{1,t|t} \\ \vdots \\ \hat{\eta}_{n_r,t|t} \end{bmatrix}, \quad R_{\eta,t|t} = \begin{bmatrix} \Sigma_{\eta_1,t|t} & & O \\ & \ddots & \\ O & & \Sigma_{\eta_2,t|t} \end{bmatrix}. \tag{2.48}$$

2.3.3 GR Models for SD/DD-PPP

Let us consider GR equations of pseudoranges based on C/A code for satellites p and q, and the receivers (antennas) u_i and,u_j as follows:

$$\begin{aligned} \rho^p_{CA,u_i} &\cong (g^{\hat{p}}_{\hat{u}_i})^{\mathrm{T}}(u_i - s^p) + \delta I^p_{u_i} + \delta T^p_{u_i} + c(\delta t_{u_i} - \delta t^p) \\ &\quad + \delta b_{CA,u_i} - \delta b^p_{CA} + e^p_{CA,u_i}, \end{aligned} \tag{2.49}$$

$$\begin{aligned} \rho^p_{CA,u_j} &\cong (g^{\hat{p}}_{\hat{u}_j})^{\mathrm{T}}(u_j - s^p) + \delta I^p_{u_j} + \delta T^p_{u_j} + c(\delta t_{u_j} - \delta t^p) \\ &\quad + \delta b_{CA,u_j} - \delta b^p_{CA} + e^p_{CA,u_j}, \end{aligned} \tag{2.50}$$

$$\begin{aligned} \rho^q_{CA,u_i} &\cong (g^{\hat{q}}_{\hat{u}_i})^{\mathrm{T}}(u_i - s^q) + \delta I^q_{u_i} + \delta T^q_{u_i} + c(\delta t_{u_i} - \delta t^q) \\ &\quad + \delta b_{CA,u_i} - \delta b^q_{CA} + e^q_{CA,u_i}, \end{aligned} \tag{2.51}$$

$$\begin{aligned} \rho^q_{CA,u_j} &\cong (g^{\hat{q}}_{\hat{u}_j})^{\mathrm{T}}(u_j - s^q) + \delta I^q_{u_j} + \delta T^q_{u_j} + c(\delta t_{u_j} - \delta t^q) \\ &\quad + \delta b_{CA,u_j} - \delta b^q_{CA} + e^q_{CA,u_j}. \end{aligned} \tag{2.52}$$

Then we subtract Eq. (2.49) from Eq. (2.50), namely, taking the single difference between the measurements of the receivers u_i and u_j. The signal travelling paths to the adjacent GNSS antennas from the same satellite are very close, we therefore can assume

$$\delta I^p_{u_i} \cong \delta I^p_{u_j},\ \delta T^p_{u_i} \cong \delta T^p_{u_j},$$

then we have the relation for the single difference relation of satellite p:

$$\begin{aligned}\rho^{p}_{CA,u_ju_i} &\equiv \rho^{p}_{CA,u_j} - \rho^{p}_{CA,u_i} \\ &\cong (g^{\hat{p}}_{\hat{u}_j})^{\mathrm{T}}u_j - (g^{\hat{p}}_{\hat{u}_i})^{\mathrm{T}}u_i + (g^{\hat{p}}_{\hat{u}_j})^{\mathrm{T}}(-s^p) - (g^{\hat{p}}_{\hat{u}_i})^{\mathrm{T}}(-s^p) + c(\delta t_{u_j} - \delta t_{u_i}) \\ &\quad +\delta b_{CA,u_j} - \delta b_{CA,u_i} + e^{p}_{CA,u_j} - e^{p}_{CA,u_i}. \end{aligned} \tag{2.53}$$

Also we have the single-difference relation of satellite q:

$$\begin{aligned}\rho^{q}_{CA,u_ju_i} &\equiv \rho^{q}_{CA,u_j} - \rho^{q}_{CA,u_i} \\ &\cong (g^{\hat{q}}_{\hat{u}_j})^{\mathrm{T}}u_j - (g^{\hat{q}}_{\hat{u}_i})^{\mathrm{T}}u_i + (g^{\hat{q}}_{\hat{u}_j})^{\mathrm{T}}(-s^q) - (g^{\hat{q}}_{\hat{u}_i})^{\mathrm{T}}(-s^q) + c(\delta t_{u_j} - \delta t_{u_i}) \\ &\quad +\delta b_{CA,u_j} - \delta b_{CA,u_i} + e^{q}_{CA,u_j} - e^{q}_{CA,u_i}. \end{aligned} \tag{2.54}$$

Then, finally we have the following double-difference measurements equations for pseudoranges based on C/A code by subtracting Eq. (2.53) from Eq. (2.54). The u_i is the reference antenna position, and the p is the reference satellite:

$$\begin{aligned}\rho^{qp}_{CA,u_ju_i} &\equiv \rho^{q}_{CA,u_ju_i} - \rho^{p}_{CA,u_ju_i} \\ &\cong (g^{\hat{q}}_{\hat{u}_j})^{\mathrm{T}}u_j - (g^{\hat{q}}_{\hat{u}_i})^{\mathrm{T}}u_i - \left((g^{\hat{p}}_{\hat{u}_j})^{\mathrm{T}}u_j - (g^{\hat{p}}_{\hat{u}_i})^{\mathrm{T}}u_i\right) \\ &\quad +(g^{\hat{q}}_{\hat{u}_j})^{\mathrm{T}}(-s^q) - (g^{\hat{q}}_{\hat{u}_i})^{\mathrm{T}}(-s^q) - \left((g^{\hat{p}}_{\hat{u}_j})^{\mathrm{T}}(-s^p) - (g^{\hat{p}}_{\hat{u}_i})^{\mathrm{T}}(-s^p)\right) \\ &\quad +e^{q}_{CA,u_j} - e^{q}_{CA,u_i} - \left(e^{p}_{CA,u_j} - e^{p}_{CA,u_i}\right) \\ &= (g^{\hat{q}\hat{p}}_{\hat{u}_j})^{\mathrm{T}}u_j - (g^{\hat{q}\hat{p}}_{\hat{u}_i})^{\mathrm{T}}u_i - (g^{\hat{q}}_{\hat{u}_j\hat{u}_i})^{\mathrm{T}}s^q + (g^{\hat{p}}_{\hat{u}_j\hat{u}_i})^{\mathrm{T}}s^p + e^{qp}_{CA,u_ju_i}, \end{aligned} \tag{2.55}$$

where

$$\begin{aligned} g^{\hat{q}\hat{p}}_{\hat{u}_j} &\equiv g^{\hat{q}}_{\hat{u}_j} - g^{\hat{p}}_{\hat{u}_j} \quad g^{\hat{q}\hat{p}}_{\hat{u}_i} \equiv g^{\hat{q}}_{\hat{u}_i} - g^{\hat{p}}_{\hat{u}_i} \\ g^{\hat{q}}_{\hat{u}_j\hat{u}_i} &\equiv g^{\hat{q}}_{\hat{u}_j} - g^{\hat{q}}_{\hat{u}_i} \quad g^{\hat{p}}_{\hat{u}_j\hat{u}_i} \equiv g^{\hat{p}}_{\hat{u}_j} - g^{\hat{p}}_{\hat{u}_i} \\ e^{qp}_{CA,u_i} &\equiv e^{q}_{CA,u_i} - e^{p}_{CA,u_i} \quad e^{qp}_{CA,u_j} \equiv e^{q}_{CA,u_j} - e^{p}_{CA,u_j} \\ e^{qp}_{CA,u_ju_i} &\equiv e^{qp}_{CA,u_j} - e^{qp}_{CA,u_i}. \end{aligned}$$

Again let us consider GR equations of the L1 carrier-phase positioning data for satellites p, and the receivers (antennas) u_i and,u_j as follows:

$$\Phi^p_{L1,u_i} \cong (g^{\hat{p}}_{\hat{u}_i})^{\mathrm{T}}(u_i - s^p) - \delta I u^p_i + \delta T u^p_i + c(\delta t_{u_i} - \delta t^p) + \delta_{b_{L1},u_i} - \delta b^p_{L1} + \lambda_1 N^p_{L_1,u_i} + \lambda_1 \varepsilon^p_{L1,u_i}, \tag{2.56}$$

$$\Phi^p_{L1,u_j} \cong (g^{\hat{p}}_{\hat{u}_j})^{\mathrm{T}}(u_j - s^p) - \delta I u^p_j + \delta T u^p_j + c(\delta t_{u_j} - \delta t^p) + \delta_{b_{L1},u_j} - \delta b^p_{L1} + \lambda_1 N^p_{L_1,u_j} + \lambda_1 \varepsilon^p_{L1,u_j}, \tag{2.57}$$

$$\Phi^q_{L1,u_i} \cong (g^{\hat{q}}_{\hat{u}_i})^{\mathrm{T}}(u_i - s^q) - \delta I u^q_i + \delta T u^q_i + c(\delta t_{u_i} - \delta t^q) + \delta_{b_{L1},u_i} - \delta b^q_{L1} + \lambda_1 N^q_{L1,u_i} + \lambda_1 \varepsilon^q_{L1,u_i}, \tag{2.58}$$

$$\Phi^q_{L1,u_j} \cong (g^{\hat{q}}_{\hat{u}_j})^{\mathrm{T}}(u_j - s^q) - \delta I u^q_j + \delta T u^q_j + c(\delta t_{u_j} - \delta t^q) + \delta_{b_{L1},u_j} - \delta b^q_{L1} + \lambda_1 N^q_{L1,u_j} + \lambda_1 \varepsilon^q_{L1,u_j}. \tag{2.59}$$

Then we repeat the similar manner to take the differences for the L1 carrier-phase positioning data. By subtracting Eq. (2.56) from Eq. (2.57), we have the relation for the single difference relation of satellite p:

$$\begin{aligned}\Phi^p_{L1,u_ju_i} &\equiv \Phi^p_{CA,u_j} - \Phi^p_{CA,u_i} \\ &\cong (g^{\hat{p}}_{\hat{u}_j})^{\mathrm{T}}u_j - (g^{\hat{p}}_{\hat{u}_i})^{\mathrm{T}}u_i + (g^{\hat{p}}_{\hat{u}_j})^{\mathrm{T}}(-s^p) - (g^{\hat{p}}_{\hat{u}_i})^{\mathrm{T}}(-s^p) + c(\delta t_{u_j} - \delta t_{u_i}) \\ &\quad + \delta b_{L1,u_j} - \delta b_{L1,u_i} + \lambda_1(N^p_{L_1,u_j} - N^p_{L_1,u_i}) + \lambda_1(\varepsilon^p_{L_1,u_j} - \varepsilon^p_{L_1,u_i}),\end{aligned} \tag{2.60}$$

Also by subtracting Eq. (2.58) from Eq. (2.59), we have the relation for the single-difference relation of satellite q:

$$\begin{aligned}\Phi^q_{L1,u_ju_i} &\equiv \Phi^q_{CA,u_j} - \Phi^q_{CA,u_i} \\ &\cong (g^{\hat{q}}_{\hat{u}_j})^{\mathrm{T}}u_j - (g^{\hat{q}}_{\hat{u}_i})^{\mathrm{T}}u_i + (g^{\hat{q}}_{\hat{u}_j})^{\mathrm{T}}(-s^q) - (g^{\hat{q}}_{\hat{u}_i})^{\mathrm{T}}(-s^q) + c(\delta t_{u_j} - \delta t_{u_i}) \\ &\quad + \delta b_{L1,u_j} - \delta b_{L1,u_i} + \lambda_1(N^q_{L_1,u_j} - N^q_{L_1,u_i}) + \lambda_1(\varepsilon^q_{L_1,u_j} - \varepsilon^q_{L_1,u_i}),\end{aligned} \tag{2.61}$$

Finally we have the following double-difference equations: by subtracting Eq. (2.60) from Eq. (2.61):

$$\begin{aligned}\Phi^{qp}_{L_1,u_ju_i} &\equiv \Phi^{q}_{L1,u_ju_i} - \Phi^{p}_{L1,u_ju_i} \\ &\cong (g^{\hat{q}\hat{p}}_{\hat{u}_j})^{\mathrm{T}}u_j - (g^{\hat{q}\hat{p}}_{\hat{u}_i})^{\mathrm{T}}u_i - (g^{\hat{q}}_{\hat{u}_j\hat{u}_i})^{\mathrm{T}}s^q + (g^{\hat{p}}_{\hat{u}_j\hat{u}_i})^{\mathrm{T}}s^p + \lambda_1(N^q_{L_1,u_j} - N^q_{L_1,u_i} \\ &\quad -N^p_{L_1,u_j} + N^p_{L_1,u_i}) + \lambda_1(\varepsilon^q_{L_1,u_j} - \varepsilon^q_{L_1,u_i} - \varepsilon^p_{L_1,u_j} - \varepsilon^p_{L_1,u_i}) \\ &= (g^{\hat{q}\hat{p}}_{\hat{u}_j})^{\mathrm{T}}u_j - (g^{\hat{q}\hat{p}}_{\hat{u}_i})^{\mathrm{T}}u_i - (g^{\hat{q}}_{\hat{u}_j\hat{u}_i})^{\mathrm{T}}s^q + (g^{\hat{p}}_{\hat{u}_j\hat{u}_i})^{\mathrm{T}}s^p + \lambda_1 N^{qp}_{L_1,u_ju_i} + \lambda_1\varepsilon^{qp}_{L_1,u_ju_i}, \quad (2.62)\end{aligned}$$

where

$$\lambda_1\varepsilon^{qp}_{L1,u_i} \equiv \lambda_1\varepsilon^{q}_{L1,u_i} - \lambda_1\varepsilon^{p}_{DL1,u_i} \quad \lambda_1\varepsilon^{qp}_{L1,u_j} \equiv \lambda_1\varepsilon^{q}_{L1,u_j} - \lambda_1\varepsilon^{p}_{DL1,u_j}$$

$$\lambda_1\varepsilon^{qp}_{L1,u_ju_i} \equiv \lambda_1\varepsilon^{qp}_{L1,u_j} - \lambda_1\varepsilon^{qp}_{DL1,u_i}.$$

Let us consider GR equations of Doppler shift frequency data for satellites p and q, and the receivers (antennas) u_i and,u_j as follows:

$$\dot{\rho}^p_{DL1,u_i} \cong (g^{\hat{p}}_{\hat{u}_i})^{\mathrm{T}}(\dot{u}_i - \dot{s}^p) + \delta\dot{I}^p_{u_i} + \delta\dot{T}^p_{u_i} + c(\delta\dot{t}_{u_i} - \delta\dot{t}^p) + \delta\dot{b}^p_{DL1} + \lambda_1\dot{\varepsilon}^p_{DL1,u_i}, \quad (2.63)$$

$$\dot{\rho}^p_{DL1,u_j} \cong (g^{\hat{p}}_{\hat{u}_j})^{\mathrm{T}}(\dot{u}_j - \dot{s}^p) + \delta\dot{I}^p_{u_j} + \delta\dot{T}^p_{u_j} + c(\delta\dot{t}_{u_j} - \delta\dot{t}^p) + \delta\dot{b}^p_{DL1} + \lambda_1\dot{\varepsilon}^p_{DL1,u_j}, \quad (2.64)$$

$$\dot{\rho}^q_{DL1,u_i} \cong (g^{\hat{q}}_{\hat{u}_i})^{\mathrm{T}}(\dot{u}_i - \dot{s}^q) + \delta\dot{I}^q_{u_i} + \delta\dot{T}^q_{u_i} + c(\delta\dot{t}_{u_i} - \delta\dot{t}^q) + \delta\dot{b}^q_{DL1} + \lambda_1\dot{\varepsilon}^q_{DL1,u_i}, \quad (2.65)$$

$$\dot{\rho}^q_{DL1,u_j} \cong (g^{\hat{q}}_{\hat{u}_j})^{\mathrm{T}}(\dot{u}_j - \dot{s}^q) + \delta\dot{I}^q_{u_j} + \delta\dot{T}^q_{u_j} + c(\delta\dot{t}_{u_j} - \delta\dot{t}^q) + \delta\dot{b}^q_{DL1} + \lambda_1\dot{\varepsilon}^q_{DL1,u_j}. \quad (2.66)$$

Then we subtract Eq. (2.63) from Eq. (2.64), namely, taking the single difference between the measurements of the receivers u_i and u_j. Also if we can assume

$$\delta\dot{I}^p_{u_i} \cong \delta\dot{I}^p_{u_j}, \ \delta\dot{T}^p_{u_i} \cong \delta\dot{T}^p_{u_j},$$

then we have the relation for the single-difference relation of satellite p:

$$\begin{aligned}\dot{\rho}^{p}_{DL1,u_ju_i} &\equiv \dot{\rho}^{p}_{DL1,u_j} - \dot{\rho}^{p}_{DL1,u_i} \\ &\cong (g^{\hat{p}}_{\hat{u}_j})^{\mathrm{T}}\dot{u}_j - (g^{\hat{p}}_{\hat{u}_i})^{\mathrm{T}}\dot{u}_i + (g^{\hat{p}}_{\hat{u}_j})^{\mathrm{T}}(-\dot{s}^p) - (g^{\hat{p}}_{\hat{u}_i})^{\mathrm{T}}(-\dot{s}^p) + c(\delta t_{u_j} - \delta t_{u_i}) \\ &\quad +\delta b_{DL1,u_j} - \delta b_{DL1,u_i} + \lambda_1\varepsilon^{p}_{DL1,u_j} - \lambda_1\varepsilon^{p}_{DL1,u_i}. \end{aligned} \tag{2.67}$$

Also we have the single-difference relation of satellite q:

$$\begin{aligned}\dot{\rho}^{q}_{DL1,u_ju_i} &\equiv \dot{\rho}^{q}_{DL1,u_j} - \dot{\rho}^{q}_{DL1,u_i} \\ &\cong (g^{\hat{q}}_{\hat{u}_j})^{\mathrm{T}}\dot{u}_j - (g^{\hat{q}}_{\hat{u}_i})^{\mathrm{T}}\dot{u}_i + (g^{\hat{q}}_{\hat{u}_j})^{\mathrm{T}}(-\dot{s}^q) - (g^{\hat{q}}_{\hat{u}_i})^{\mathrm{T}}(-\dot{s}^q) + c(\delta t_{u_j} - \delta t_{u_i}) \\ &\quad +\delta b_{DL1,u_j} - \delta b_{DL1,u_i} + \lambda_1\varepsilon^{q}_{DL1,u_j} - \lambda_1\varepsilon^{q}_{DL1,u_i}. \end{aligned} \tag{2.68}$$

Then, finally we have the following double-difference measurements equations for pseudo-ranges based on C/A code by subtracting Eq. (2.67) from Eq. (2.68):

$$\begin{aligned}\dot{\rho}^{qp}_{DL1,u_ju_i} &\equiv \dot{\rho}^{q}_{DL1,u_ju_i} - \dot{\rho}^{p}_{DL1,u_ju_i} \\ &\cong (g^{\hat{q}}_{\hat{u}_j})^{\mathrm{T}}\dot{u}_j - (g^{\hat{q}}_{\hat{u}_i})^{\mathrm{T}}\dot{u}_i - \left((g^{\hat{p}}_{\hat{u}_j})^{\mathrm{T}}\dot{u}_j - (g^{\hat{p}}_{\hat{u}_i})^{\mathrm{T}}\dot{u}_i\right) \\ &\quad +(g^{\hat{q}}_{\hat{u}_j})^{\mathrm{T}}(-\dot{s}^q) - (g^{\hat{q}}_{\hat{u}_i})^{\mathrm{T}}(-\dot{s}^q) - \left((g^{\hat{p}}_{\hat{u}_j})^{\mathrm{T}}(-\dot{s}^p) - (g^{\hat{p}}_{\hat{u}_i})^{\mathrm{T}}(-\dot{s}^p)\right) \\ &\quad +\lambda_1\varepsilon^{q}_{DL1,u_j} - \lambda_1\varepsilon^{q}_{DL1,u_i} - \left(\lambda_1\varepsilon^{p}_{DL1,u_j} - \lambda_1\varepsilon^{p}_{DL1,u_i}\right) \\ &= (g^{\hat{q}\hat{p}}_{\hat{u}_j})^{\mathrm{T}}\dot{u}_j - (g^{\hat{q}\hat{p}}_{\hat{u}_i})^{\mathrm{T}}\dot{u}_i - (g^{\hat{q}}_{\hat{u}_j\hat{u}_i})^{\mathrm{T}}s^q + (g^{\hat{p}}_{\hat{u}_j\hat{u}_i})^{\mathrm{T}}s^p + \lambda_1\varepsilon^{qp}_{DL1,u_ju_i}, \end{aligned} \tag{2.69}$$

where

$$\lambda_1\varepsilon^{qp}_{DL1,u_i} \equiv \lambda_1\varepsilon^{q}_{DL1,u_i} - \lambda_1\varepsilon^{p}_{DL1,u_i} \quad \lambda_1\varepsilon^{qp}_{DL1,u_j} \equiv \lambda_1\varepsilon^{q}_{DL1,u_j} - \lambda_1\varepsilon^{p}_{DL1,u_j}$$

$$\lambda_1\varepsilon^{qp}_{DL1,u_ju_i} \equiv \lambda_1\varepsilon^{qp}_{DL1,u_j} - \lambda_1\varepsilon^{qp}_{DL1,u_i}.$$

Single-difference GR models (SD-PPP)

Let us write again the final results of the single-difference measurement equations from Eqs. (2.53), (2.60), and (2.67) as follows.

$$\begin{aligned}\rho^p_{CA,u_ju_i} &\cong (g^{\hat{p}}_{\hat{u}_j})^{\mathrm{T}}u_j - (g^{\hat{p}}_{\hat{u}_i})^{\mathrm{T}}u_i - (g^{\hat{p}}_{\hat{u}_j\hat{u}_i})^{\mathrm{T}}s^p + c(\delta t_{u_j} - \delta t_{u_i}) + \delta b_{CA,u_j} - \delta b_{CA,u_i} \\ &\quad + e^p_{CA,u_ju_i}, \end{aligned} \tag{2.70}$$

$$\begin{aligned}\Phi^p_{L1,u_ju_i} &\cong (g^{\hat{p}}_{\hat{u}_j})^{\mathrm{T}}u_j - (g^{\hat{p}}_{\hat{u}_i})^{\mathrm{T}}u_i - (g^{\hat{p}}_{\hat{u}_j\hat{u}_i})^{\mathrm{T}}s^p + c(\delta t_{u_j} - \delta t_{u_i}) + \delta b_{L1,u_j} - \delta b_{L1,u_i} \\ &\quad + \lambda_1 N^p_{L_1,u_ju_i} + \lambda_1 \varepsilon^p_{L_1,u_ju_i}, \end{aligned} \tag{2.71}$$

$$\begin{aligned}\dot{\rho}^p_{DL1,u_ju_i} &\cong (g^{\hat{p}}_{\hat{u}_j})^{\mathrm{T}}\dot{u}_j - (g^{\hat{p}}_{\hat{u}_i})^{\mathrm{T}}\dot{u}_i - (g^{\hat{p}}_{\hat{u}_j\hat{u}_i})^{\mathrm{T}}\dot{s}^p + c(\delta t_{u_j} - \delta t_{u_i}) + \delta b_{DL1,u_j} - \delta b_{DL1,u_i} \\ &\quad + \lambda_1 \varepsilon^p_{DL1,u_ju_i}. \end{aligned} \tag{2.72}$$

Now let us assume that the estimated values: $\hat{s}^p, \hat{\dot{s}}^p, p = 1, \ldots n_s$, of the satellite positions: s^p and velocities $\dot{s}^p$, are available as follows [15]–[20]. The $\hat{s}^p$ and $\hat{\dot{s}}^p$ come from the navigation messages of satellites:

$$\hat{s}^p = s^p + e_{s^p}, \quad \hat{\dot{s}}^p = \dot{s}^p + e_{\dot{s}^p}, \quad p = 1, \ldots, n_s, \tag{2.73}$$

where we assume e_{s^p}, $e_{\dot{s}^p}$ are Gaussian white noises. Then substituting Eq. (2.73) to Eqs. (2.71), (2.72), and (2.72), we have

$$\begin{aligned}\tilde{\rho}^{\hat{p}}_{CA,\hat{u}_j\hat{u}_i} &\equiv \rho^p_{CA,u_ju_i} + (g^{\hat{p}}_{\hat{u}_j\hat{u}_i})^{\mathrm{T}}\hat{s}^p \\ &\cong (g^{\hat{p}}_{\hat{u}_j})^{\mathrm{T}}u_j - (g^{\hat{p}}_{\hat{u}_i})^{\mathrm{T}}u_i + (g^{\hat{p}}_{\hat{u}_j\hat{u}_i})^{\mathrm{T}}e_{s^p} + c(\delta t_{u_j} - \delta t_{u_i}) + \delta b_{CA,u_j} - \delta b_{CA,u_i} \\ &\quad + e^p_{CA,u_ju_i}, \end{aligned} \tag{2.74}$$

$$\begin{aligned}\tilde{\Phi}^{\hat{p}}_{L_1,\hat{u}_j\hat{u}_i} &\equiv \Phi^p_{L_1,u_ju_i} + (g^{\hat{p}}_{\hat{u}_j\hat{u}_i})^{\mathrm{T}}\hat{s}^p \\ &\cong (g^{\hat{p}}_{\hat{u}_j})^{\mathrm{T}}u_j - (g^{\hat{p}}_{\hat{u}_i})^{\mathrm{T}}u_i + (g^{\hat{p}}_{\hat{u}_j\hat{u}_i})^{\mathrm{T}}e_{s^p} + c(\delta t_{u_j} - \delta t_{u_i}) + \delta b_{CA,u_j} - \delta b_{CA,u_i} \\ &\quad + \lambda_1 N^p_{L_1,u_ju_i} + \lambda_1 \varepsilon^p_{L_1,u_ju_i}, \end{aligned} \tag{2.75}$$

$$\begin{aligned}\tilde{\dot{\rho}}^{\hat{p}}_{DL1,\hat{u}_j\hat{u}_i} &\equiv \dot{\rho}^{p}_{DL1,u_ju_i} + (g^{\hat{p}}_{\hat{u}_j\hat{u}_i})^{\mathrm{T}}\hat{\dot{s}}^{p} \\ &\cong (g^{\hat{p}}_{\hat{u}_j})^{\mathrm{T}}u_j - (g^{\hat{p}}_{\hat{u}_i})^{\mathrm{T}}u_i + (g^{\hat{p}}_{\hat{u}_j\hat{u}_i})^{\mathrm{T}}e_{\dot{s}^p} + c(\delta t_{u_j} - \delta t_{u_i}) + \delta b_{CA,u_j} - \delta b_{CA,u_i} \\ &\quad + \lambda_1 \varepsilon^{p}_{DL1,u_ju_i}. \end{aligned} \tag{2.76}$$

For the case of $p = 1, \ldots, n_s$ and $u_i = u_1, u_j = u_2$, we have the following measurement equation for antennas of u_1 and u_2 and for n_s satellites:

$$y^{p}_{u_2u_1} = C^{p}_{u_2u_1}\eta^{p}_{u_2u_1} + v^{p}_{u_2u_1}, \tag{2.77}$$

where

$$y^{p}_{u_2u_1} \equiv \begin{bmatrix} \tilde{\rho}^{\hat{1}}_{CA,\hat{u}_2\hat{u}_1} \\ \tilde{\rho}^{\hat{2}}_{CA,\hat{u}_2\hat{u}_1} \\ \vdots \\ \tilde{\rho}^{\hat{n}_s}_{CA,\hat{u}_2\hat{u}_1} \\ \tilde{\Phi}^{\hat{1}}_{L1,\hat{u}_2\hat{u}_1} \\ \tilde{\Phi}^{\hat{2}}_{L1,\hat{u}_2\hat{u}_1} \\ \vdots \\ \tilde{\Phi}^{\hat{n}_s}_{L1,\hat{u}_2\hat{u}_1} \\ \tilde{\dot{\rho}}^{\hat{1}}_{DL1,\hat{u}_2\hat{u}_1} \\ \tilde{\dot{\rho}}^{\hat{2}}_{DL1,\hat{u}_2\hat{u}_1} \\ \vdots \\ \tilde{\dot{\rho}}^{\hat{n}_s}_{DL1,\hat{u}_2\hat{u}_1} \end{bmatrix}, \quad \eta^{p}_{u_2u_1} \equiv \begin{bmatrix} u_1 \\ \dot{u}_1 \\ u_2 \\ \dot{u}_2 \\ c(\delta t_{u_2} - \delta t_{u_1}) \\ c(\delta \dot{t}_{u_2} - \delta \dot{t}_{u_1}) \\ \delta b_{u_2} - \delta b_{u_1} \\ N^{1}_{L1,u_2u_1} \\ N^{2}_{L1,u_2u_1} \\ \vdots \\ \vdots \\ \vdots \\ N^{n_s}_{L1,u_2u_1} \end{bmatrix}, \tag{2.78}$$

$$
C^{p}_{u_2u_1} \equiv \begin{bmatrix}
-(g^{\hat{1}}_{\hat{u}_1})^{\mathrm{T}} & \mathbf{0} & (g^{\hat{1}}_{\hat{u}_2})^{\mathrm{T}} & \mathbf{0} & 1 & 0 & 1 & 0 & \cdots & \cdots & 0 \\
\vdots & \vdots & \vdots & \vdots & \vdots & \vdots & \vdots & \vdots & \ddots & & \vdots \\
\vdots & \vdots & \vdots & \vdots & \vdots & \vdots & \vdots & \vdots & & \ddots & \vdots \\
-(g^{\hat{n}_s}_{\hat{u}_1})^{\mathrm{T}} & \mathbf{0} & (g^{\hat{n}_s}_{\hat{u}_2})^{\mathrm{T}} & \mathbf{0} & 1 & 0 & 1 & 0 & \cdots & \cdots & 0 \\
-(g^{\hat{1}}_{\hat{u}_1})^{\mathrm{T}} & \mathbf{0} & (g^{\hat{1}}_{\hat{u}_2})^{\mathrm{T}} & \mathbf{0} & 1 & 0 & 1 & \lambda_1 & & & \\
\vdots & \vdots & \vdots & \vdots & \vdots & \vdots & \vdots & & \ddots & & \\
\vdots & \vdots & \vdots & \vdots & \vdots & \vdots & \vdots & & & \ddots & \\
-(g^{\hat{n}_s}_{\hat{u}_1})^{\mathrm{T}} & \mathbf{0} & (g^{\hat{n}_s}_{\hat{u}_2})^{\mathrm{T}} & \mathbf{0} & 1 & 0 & 1 & & & & \lambda_1 \\
\mathbf{0} & -(g^{\hat{1}}_{\hat{u}_1})^{\mathrm{T}} & \mathbf{0} & (g^{\hat{1}}_{\hat{u}_2})^{\mathrm{T}} & 0 & 1 & 1 & 0 & \cdots & \cdots & 0 \\
\vdots & \vdots & \vdots & \vdots & \vdots & \vdots & \vdots & \vdots & \ddots & & \vdots \\
\vdots & \vdots & \vdots & \vdots & \vdots & \vdots & \vdots & \vdots & & \ddots & \vdots \\
\mathbf{0} & -(g^{\hat{n}_s}_{\hat{u}_1})^{\mathrm{T}} & \mathbf{0} & (g^{\hat{n}_s}_{\hat{u}_2})^{\mathrm{T}} & 0 & 1 & 1 & 0 & \cdots & \cdots & 0
\end{bmatrix}
$$

$$
= \begin{bmatrix}
-G^{\hat{p}}_{\hat{u}_1} & \mathbf{0} & G^{\hat{p}}_{\hat{u}_2} & \mathbf{0} & \mathbf{1} & \mathbf{0} & \mathbf{1} & \boldsymbol{O} \\
-G^{\hat{p}}_{\hat{u}_1} & \mathbf{0} & G^{\hat{p}}_{\hat{u}_2} & \mathbf{0} & \mathbf{1} & \mathbf{0} & \mathbf{1} & \lambda_1\boldsymbol{I} \\
\mathbf{0} & -G^{\hat{p}}_{\hat{u}_1} & \mathbf{0} & G^{\hat{p}}_{\hat{u}_2} & \mathbf{0} & \mathbf{1} & \mathbf{1} & \boldsymbol{O}
\end{bmatrix}, \tag{2.79}
$$

where

$$
G^{\hat{p}\hat{1}}_{\hat{u}_1} \equiv \begin{bmatrix}
(g^{\hat{1}}_{\hat{u}_1})^{\mathrm{T}} \\
(g^{\hat{2}}_{\hat{u}_1})^{\mathrm{T}} \\
\vdots \\
(g^{\hat{n_s}}_{\hat{u}_1})^{\mathrm{T}}
\end{bmatrix}, \quad
G^{\hat{p}\hat{1}}_{\hat{u}_2} \equiv \begin{bmatrix}
(g^{\hat{1}}_{\hat{u}_2})^{\mathrm{T}} \\
(g^{\hat{2}}_{\hat{u}_2})^{\mathrm{T}} \\
\vdots \\
(g^{\hat{n_s}}_{\hat{u}_2})^{\mathrm{T}}
\end{bmatrix}, \tag{2.80}
$$

and $\mathbf{0}$ is a row or column vector, and $\mathbf{1}$ is a row or column vector, and $\boldsymbol{O}$ is a $(n_s \times n_s)$

zero matrix, and $\boldsymbol{I}$ is the $(n_s \times n_s)$ identity matrix, and

$$v^p_{u_2u_1} \equiv \begin{bmatrix} -(g^{\hat{1}}_{\hat{u}_2\hat{u}_1})^{\mathrm{T}} e_{s^1} + e^1_{CA,u_2u_1} \\ -(g^{\hat{2}}_{\hat{u}_2\hat{u}_1})^{\mathrm{T}} e_{s^2} + e^2_{CA,u_2u_1} \\ \vdots \\ -(g^{\hat{n_s}}_{\hat{u}_2\hat{u}_1})^{\mathrm{T}} e_{s^{n_s}} + e^{n_s}_{CA,u_2u_1} \\ -(g^{\hat{1}}_{\hat{u}_2\hat{u}_1})^{\mathrm{T}} e_{s^1} + \lambda_1 \varepsilon^1_{L_1,u_2u_1} \\ -(g^{\hat{2}}_{\hat{u}_2\hat{u}_1})^{\mathrm{T}} e_{s^2} + \lambda_1 \varepsilon^2_{L_1,u_2u_1} \\ \vdots \\ -(g^{\hat{n_s}}_{\hat{u}_2\hat{u}_1})^{\mathrm{T}} e_{s^{n_s}} + \lambda_1 \varepsilon^{n_s}_{L_1,u_2u_1} \\ -(g^{\hat{1}}_{\hat{u}_2\hat{u}_1})^{\mathrm{T}} e_{\dot{s}^1} + \lambda_1 \varepsilon^1_{DL1,u_2u_1} \\ -(g^{\hat{2}}_{\hat{u}_2\hat{u}_1})^{\mathrm{T}} e_{\dot{s}^2} + \lambda_1 \varepsilon^2_{DL1,u_2u_1} \\ \vdots \\ -(g^{\hat{n_s}}_{\hat{u}_2\hat{u}_1})^{\mathrm{T}} e_{\dot{s}^{n_s}} + \lambda_1 \varepsilon^{n_s}_{DL1,u_2u_1} \end{bmatrix}. \tag{2.81}$$

We assume that all noises:

$$e_{s^p},\ e_{\dot{s}^p},\ e^p_{CA,u_i},\ \varepsilon^p_{L_1,u_i},\ \varepsilon^p_{DL1,u_i},\ (i \neq j),$$

are mutually independent white Gaussian random processes with zero mean and their variances are $\mathrm{Var}(e_{s^p}) = \sigma^2_{e_s}$, $\mathrm{Var}(e_{\dot{s}^p}) = \sigma^2_{e_{\dot{s}}}$, $\mathrm{Var}(e^p_{CA,u_i}) = \sigma^2_{e_{CA}}$, $\mathrm{Var}(\varepsilon^p_{L_1,u_i}) = \sigma^2_{\varepsilon_{L1}}$, and $\mathrm{Var}(\varepsilon^p_{DL_1,u_i}) = \sigma^2_{\varepsilon_{DL1}}$. Then the covariance matrix of $v^p_{u_2u_1}$ is given by

$$\begin{aligned} R_{v^p_{u_2u_1}} &\equiv \mathrm{Cov}\big[v^p_{u_2u_1}\big] \\ &= \begin{bmatrix} -(g^{\hat{n}_s}_{\hat{u}_2\hat{u}_1})^{\mathrm{T}} e_{s^{n_s}} + e^{n_s}_{CA,u_2u_1} \\ -(g^{\hat{n}_s}_{\hat{u}_2\hat{u}_1})^{\mathrm{T}} e_{s^{n_s}} + \lambda_1 \varepsilon^{n_s}_{L_1,u_2u_1} \\ -(g^{\hat{n}_s}_{\hat{u}_2\hat{u}_1})^{\mathrm{T}} e_{\dot{s}^{n_s}} + \lambda_1 \varepsilon^{n_s}_{DL1,u_2u_1} \end{bmatrix} \begin{bmatrix} -(g^{\hat{n}_s}_{\hat{u}_2\hat{u}_1})^{\mathrm{T}} e_{s^{n_s}} + e^{n_s}_{CA,u_2u_1} \\ -(g^{\hat{n}_s}_{\hat{u}_2\hat{u}_1})^{\mathrm{T}} e_{s^{n_s}} + \lambda_1 \varepsilon^{n_s}_{L_1,u_2u_1} \\ -(g^{\hat{n}_s}_{\hat{u}_2\hat{u}_1})^{\mathrm{T}} e_{\dot{s}^{n_s}} + \lambda_1 \varepsilon^{n_s}_{DL1,u_2u_1} \end{bmatrix}^{\mathrm{T}} \\ &= R^{(SD)}_{\hat{s}} + 2R^{(SD)}_{CA,L1.DL1}, \end{aligned} \tag{2.82}$$

where $R_{\hat{s}}^{(SD)}$ is the following matrix for the $n_s \times 1$ vector; $g_{\hat{u}_2\hat{u}_1}^{\hat{p}}$, we define

$$\gamma_{\hat{u}_2\hat{u}_1}^{\hat{p}} \equiv (g_{\hat{u}_2\hat{u}_1}^{\hat{p}})^{\mathrm{T}}(g_{\hat{u}_2\hat{u}_1}^{\hat{p}}), \tag{2.83}$$

$$R_{\hat{p}}^{(SD)} \equiv \begin{bmatrix} \gamma_{\hat{u}_2\hat{u}_1}^{\hat{1}} & & & \\ & \gamma_{\hat{u}_2\hat{u}_1}^{\hat{2}} & & \\ & & \ddots & \\ & & & \gamma_{\hat{u}_2\hat{u}_1}^{\hat{n}_s} \end{bmatrix}, \quad R_{\hat{s}}^{(SD)} \equiv \begin{bmatrix} \sigma_{e_s}^2 R_{\hat{p}}^{(SD)} & \sigma_{e_s}^2 R_{\hat{p}}^{(SD)} & O \\ \sigma_{e_s}^2 R_{\hat{p}}^{(SD)} & \sigma_{e_s}^2 R_{\hat{p}}^{(SD)} & O \\ O & O & \sigma_{e_{\dot{s}}}^2 R_{\hat{p}}^{(SD)} \end{bmatrix}. \tag{2.84}$$

Also $R_{CA,L1,DL1}^{(SD)}$ is a block diagonal matrix as

$$R_{CA,L1,DL1}^{(SD)} \equiv \begin{bmatrix} R_{CA}^{(SD)} & O & O \\ O & R_{L1}^{(SD)} & O \\ O & O & R_{DL1}^{(SD)} \end{bmatrix}, \tag{2.85}$$

where

$$R_{CA}^{(SD)} \equiv \begin{bmatrix} \sigma_{e_{CA}}^2 & 0 & \cdots & 0 \\ 0 & \sigma_{e_{CA}}^2 & & \vdots \\ \vdots & & \ddots & 0 \\ 0 & \cdots & 0 & \sigma_{e_{CA}}^2 \end{bmatrix}, \quad R_{L1}^{(SD)} \equiv \begin{bmatrix} \lambda_1^2\sigma_{\varepsilon_{L1}}^2 & 0 & \cdots & 0 \\ 0 & \lambda_1^2\sigma_{\varepsilon_{L1}}^2 & & \vdots \\ \vdots & & \ddots & 0 \\ 0 & \cdots & 0 & \lambda_1^2\sigma_{\varepsilon_{L1}}^2 \end{bmatrix},$$

$$R_{DL1}^{(SD)} \equiv \begin{bmatrix} \lambda_1^2\sigma_{\varepsilon_{DL1}}^2 & 0 & \cdots & 0 \\ 0 & \lambda_1^2\sigma_{\varepsilon_{DL1}}^2 & & \vdots \\ \vdots & & \ddots & 0 \\ 0 & \cdots & 0 & \lambda_1^2\sigma_{\varepsilon_{DL1}}^2 \end{bmatrix}. \tag{2.86}$$

Double-difference GR models (DD-PPP)

Let us write again the final results of the double-difference measurement equations from Eqs. (2.55), (2.62), and (2.69) as follows.

$$\rho^{qp}_{CA,u_ju_i} = (g^{\hat{q}\hat{p}}_{\hat{u}_j})^{\mathrm{T}}u_j - (g^{\hat{q}\hat{p}}_{\hat{u}_i})^{\mathrm{T}}u_i - (g^{\hat{q}}_{\hat{u}_j\hat{u}_i})^{\mathrm{T}}s^q + (g^{\hat{p}}_{\hat{u}_j\hat{u}_i})^{\mathrm{T}}s^p + e^{qp}_{CA,u_ju_i}, \tag{2.87}$$

$$\Phi^{qp}_{L_1,u_ju_i} = (g^{\hat{q}\hat{p}}_{\hat{u}_j})^{\mathrm{T}}u_j - (g^{\hat{q}\hat{p}}_{\hat{u}_i})^{\mathrm{T}}u_i - (g^{\hat{q}}_{\hat{u}_j\hat{u}_i})^{\mathrm{T}}s^q + (g^{\hat{p}}_{\hat{u}_j\hat{u}_i})^{\mathrm{T}}s^p + \lambda_1 N^{qp}_{L_1,u_ju_i} + \lambda_1\varepsilon^{qp}_{L_1,u_ju_i}, \tag{2.88}$$

$$\dot{\rho}^{qp}_{DL1,u_ju_i} = (g^{\hat{q}\hat{p}}_{\hat{u}_j})^{\mathrm{T}}\dot{u}_j - (g^{\hat{q}\hat{p}}_{\hat{u}_i})^{\mathrm{T}}\dot{u}_i - (g^{\hat{q}}_{\hat{u}_j\hat{u}_i})^{\mathrm{T}}\dot{s}^q + (g^{\hat{p}}_{\hat{u}_j\hat{u}_i})^{\mathrm{T}}\dot{s}^p + \lambda_1\varepsilon^{qp}_{DL1,u_ju_i}. \tag{2.89}$$

Then substituting Eq. (2.73) to Eqs. (2.88), (2.89), and (2.89), we have

$$\begin{aligned}\tilde{\rho}^{\hat{q}\hat{p}}_{CA,\hat{u}_j\hat{u}_i} &\equiv \rho^{qp}_{CA,u_ju_i} + (g^{\hat{q}}_{\hat{u}_j\hat{u}_i})^{\mathrm{T}}\hat{s}^q - (g^{\hat{p}}_{\hat{u}_j\hat{u}_i})^{\mathrm{T}}\hat{s}^p \\ &\cong (g^{\hat{q}\hat{p}}_{\hat{u}_j})^{\mathrm{T}}u_j - (g^{\hat{q}\hat{p}}_{\hat{u}_i})^{\mathrm{T}}u_i + (g^{\hat{q}}_{\hat{u}_j\hat{u}_i})^{\mathrm{T}}e_{s^q} - (g^{\hat{p}}_{\hat{u}_j\hat{u}_i})^{\mathrm{T}}e_{s^p} + e^{qp}_{CA,u_ju_i},\end{aligned} \tag{2.90}$$

$$\begin{aligned}\tilde{\Phi}^{\hat{q}\hat{p}}_{L_1,\hat{u}_j\hat{u}_i} &\equiv \Phi^{qp}_{L_1,u_ju_i} + (g^{\hat{q}}_{\hat{u}_j\hat{u}_i})^{\mathrm{T}}\hat{s}^q - (g^{\hat{p}}_{\hat{u}_j\hat{u}_i})^{\mathrm{T}}\hat{s}^p \\ &\cong (g^{\hat{q}\hat{p}}_{\hat{u}_j})^{\mathrm{T}}u_j - (g^{\hat{q}\hat{p}}_{\hat{u}_i})^{\mathrm{T}}u_i + (g^{\hat{q}}_{\hat{u}_j\hat{u}_i})^{\mathrm{T}}e_{s^q} - (g^{\hat{p}}_{\hat{u}_j\hat{u}_i})^{\mathrm{T}}e_{s^p} + \lambda_1 N^{qp}_{L_1,u_ju_i} + \lambda_1\varepsilon^{qp}_{L_1,u_ju_i},\end{aligned} \tag{2.91}$$

$$\begin{aligned}\tilde{\dot{\rho}}^{\hat{q}\hat{p}}_{DL1,\hat{u}_j\hat{u}_i} &\equiv \dot{\rho}^{qp}_{DL1,u_ju_i} + (g^{\hat{q}}_{\hat{u}_j\hat{u}_i})^{\mathrm{T}}\hat{\dot{s}}^q - (g^{\hat{p}}_{\hat{u}_j\hat{u}_i})^{\mathrm{T}}\hat{\dot{s}}^p \\ &\cong (g^{\hat{q}\hat{p}}_{\hat{u}_j})^{\mathrm{T}}u_j - (g^{\hat{q}\hat{p}}_{\hat{u}_i})^{\mathrm{T}}u_i + (g^{\hat{q}}_{\hat{\dot{u}}_j\hat{\dot{u}}_i})^{\mathrm{T}}e_{\dot{s}^q} - (g^{\hat{p}}_{\hat{u}_j\hat{u}_i})^{\mathrm{T}}e_{\dot{s}^p} + \lambda_1\varepsilon^{qp}_{DL1,u_ju_i}.\end{aligned} \tag{2.92}$$

For the case of $p = 1$, $q = 2, \ldots, n_s$ and $u_i = u_1, u_j = u_2$, we have the following measurement equation for antennas of u_1 and u_2 and for n_s satellites:

$$y^{qp}_{u_2u_1} = C^{qp}_{u_2u_1}\eta^{qp}_{u_2u_1} + v^{qp}_{u_2u_1}, \tag{2.93}$$

where

$$y^{qp}_{u_2u_1} \equiv \begin{bmatrix} \tilde{\rho}^{\hat{2}\hat{1}}_{CA,\hat{u}_2\hat{u}_1} \\ \tilde{\rho}^{\hat{3}\hat{1}}_{CA,\hat{u}_2\hat{u}_1} \\ \vdots \\ \tilde{\rho}^{\hat{n}_s\hat{1}}_{CA,\hat{u}_2\hat{u}_1} \\ \tilde{\Phi}^{\hat{2}\hat{1}}_{L1,\hat{u}_2\hat{u}_1} \\ \tilde{\Phi}^{\hat{3}\hat{1}}_{L1,\hat{u}_2\hat{u}_1} \\ \vdots \\ \tilde{\Phi}^{\hat{n}_s\hat{1}}_{L1,\hat{u}_2\hat{u}_1} \\ \tilde{\rho}^{\hat{2}\hat{1}}_{DL1,\hat{u}_2\hat{u}_1} \\ \tilde{\rho}^{\hat{3}\hat{1}}_{DL1,\hat{u}_2\hat{u}_1} \\ \vdots \\ \tilde{\rho}^{\hat{n}_s\hat{1}}_{DL1,\hat{u}_2\hat{u}_1} \end{bmatrix}, \quad \eta^{qp}_{u_2u_1} \equiv \begin{bmatrix} u_1 \\ \dot{u}_1 \\ u_2 \\ \dot{u}_2 \\ N^{21}_{L1,u_2u_1} \\ N^{31}_{L1,u_2u_1} \\ \vdots \\ \vdots \\ \vdots \\ N^{n_s1}_{L1,u_2u_1} \end{bmatrix}, \tag{2.94}$$

$$
C^{qp}_{u_2u_1} \equiv \begin{bmatrix}
-(g^{\hat{2}\hat{1}}_{\hat{u}_1})^{\mathrm{T}} & \mathbf{0} & (g^{\hat{2}\hat{1}}_{\hat{u}_2})^{\mathrm{T}} & \mathbf{0} & 0 & \cdots & \cdots & 0 \\
\vdots & \vdots & \vdots & \vdots & \vdots & \ddots & & \vdots \\
\vdots & \vdots & \vdots & \vdots & \vdots & & \ddots & \vdots \\
-(g^{\hat{n}_s\hat{1}}_{\hat{u}_1})^{\mathrm{T}} & \mathbf{0} & (g^{\hat{n}_s\hat{1}}_{\hat{u}_2})^{\mathrm{T}} & \mathbf{0} & 0 & \cdots & \cdots & 0 \\
-(g^{\hat{2}\hat{1}}_{\hat{u}_1})^{\mathrm{T}} & \mathbf{0} & (g^{\hat{2}\hat{1}}_{\hat{u}_2})^{\mathrm{T}} & \mathbf{0} & \lambda_1 & & & \\
\vdots & \vdots & \vdots & \vdots & & \ddots & & \\
\vdots & \vdots & \vdots & \vdots & & & \ddots & \\
-(g^{\hat{n}_s\hat{1}}_{\hat{u}_1})^{\mathrm{T}} & \mathbf{0} & (g^{\hat{n}_s\hat{1}}_{\hat{u}_2})^{\mathrm{T}} & \mathbf{0} & & & & \lambda_1 \\
\mathbf{0} & -(g^{\hat{2}\hat{1}}_{\hat{u}_1})^{\mathrm{T}} & \mathbf{0} & (g^{\hat{2}\hat{1}}_{\hat{u}_2})^{\mathrm{T}} & 0 & \cdots & \cdots & 0 \\
\vdots & \vdots & \vdots & \vdots & \vdots & \ddots & & \vdots \\
\vdots & \vdots & \vdots & \vdots & \vdots & & \ddots & \vdots \\
\mathbf{0} & -(g^{\hat{n}_s\hat{1}}_{\hat{u}_1})^{\mathrm{T}} & \mathbf{0} & (g^{\hat{n}_s\hat{1}}_{\hat{u}_2})^{\mathrm{T}} & 0 & \cdots & \cdots & 0
\end{bmatrix}
$$

$$
= \begin{bmatrix}
-G^{\hat{p}\hat{1}}_{\hat{u}_1} & \mathbf{0} & G^{\hat{p}\hat{1}}_{\hat{u}_2} & \mathbf{0} & \boldsymbol{O} \\
-G^{\hat{p}\hat{1}}_{\hat{u}_1} & \mathbf{0} & G^{\hat{p}\hat{1}}_{\hat{u}_2} & \mathbf{0} & \lambda_1\boldsymbol{I} \\
\mathbf{0} & -G^{\hat{p}\hat{1}}_{\hat{u}_1} & \mathbf{0} & G^{\hat{p}\hat{1}}_{\hat{u}_2} & \boldsymbol{O}
\end{bmatrix}, \tag{2.95}
$$

where

$$
G^{\hat{p}\hat{1}}_{\hat{u}_1} \equiv \begin{bmatrix}
(g^{\hat{2}\hat{1}}_{\hat{u}_1})^{\mathrm{T}} \\
(g^{\hat{3}\hat{1}}_{\hat{u}_1})^{\mathrm{T}} \\
\vdots \\
(g^{\hat{n}_s\hat{1}}_{\hat{u}_1})^{\mathrm{T}}
\end{bmatrix}, \quad
G^{\hat{p}\hat{1}}_{\hat{u}_2} \equiv \begin{bmatrix}
(g^{\hat{2}\hat{1}}_{\hat{u}_2})^{\mathrm{T}} \\
(g^{\hat{3}\hat{1}}_{\hat{u}_2})^{\mathrm{T}} \\
\vdots \\
(g^{\hat{n}_s\hat{1}}_{\hat{u}_2})^{\mathrm{T}}
\end{bmatrix}, \tag{2.96}
$$

and $\mathbf{0}$ is a row or column vector, and $\boldsymbol{O}$ is a $(n_s-1)\times(n_s-1)$ zero matrix, and $\boldsymbol{I}$ is the

$(n_s-1)\times(n_s-1)$ identity matrix, and

$$v_{u_2u_1}^{qp} \equiv \begin{bmatrix} (g_{\hat{u}_2\hat{u}_1}^{\hat{2}})^{\mathrm{T}} e_{s^2} - (g_{\hat{u}_2\hat{u}_1}^{\hat{1}})^{\mathrm{T}} e_{s^1} + e_{CA,u_2u_1}^{21} \\ (g_{\hat{u}_2\hat{u}_1}^{\hat{3}})^{\mathrm{T}} e_{s^3} - (g_{\hat{u}_2\hat{u}_1}^{\hat{1}})^{\mathrm{T}} e_{s^1} + e_{CA,u_2u_1}^{31} \\ \vdots \\ (g_{\hat{u}_2\hat{u}_1}^{\hat{n_s}})^{\mathrm{T}} e_{s^{n_s}} - (g_{\hat{u}_2\hat{u}_1}^{\hat{1}})^{\mathrm{T}} e_{s^1} + e_{CA,u_2u_1}^{n_s1} \\ (g_{\hat{u}_2\hat{u}_1}^{\hat{2}})^{\mathrm{T}} e_{s^2} - (g_{\hat{u}_2\hat{u}_1}^{\hat{1}})^{\mathrm{T}} e_{s^1} + \lambda_1 \varepsilon_{L_1,u_2u_1}^{21} \\ (g_{\hat{u}_2\hat{u}_1}^{\hat{3}})^{\mathrm{T}} e_{s^3} - (g_{\hat{u}_2\hat{u}_1}^{\hat{1}})^{\mathrm{T}} e_{s^1} + \lambda_1 \varepsilon_{L_1,u_2u_1}^{31} \\ \vdots \\ (g_{\hat{u}_2\hat{u}_1}^{\hat{n_s}})^{\mathrm{T}} e_{s^{n_s}} - (g_{\hat{u}_2\hat{u}_1}^{\hat{1}})^{\mathrm{T}} e_{s^1} + \lambda_1 \varepsilon_{L_1,u_2u_1}^{n_s1} \\ (g_{\hat{u}_2\hat{u}_1}^{\hat{2}})^{\mathrm{T}} e_{\dot{s}^2} - (g_{\hat{u}_2\hat{u}_1}^{\hat{1}})^{\mathrm{T}} e_{\dot{s}^1} + \lambda_1 \varepsilon_{DL1,u_2u_1}^{21} \\ (g_{\hat{u}_2\hat{u}_1}^{\hat{3}})^{\mathrm{T}} e_{\dot{s}^3} - (g_{\hat{u}_2\hat{u}_1}^{\hat{1}})^{\mathrm{T}} e_{\dot{s}^1} + \lambda_1 \varepsilon_{DL1,u_2u_1}^{31} \\ \vdots \\ (g_{\hat{u}_2\hat{u}_1}^{\hat{n_s}})^{\mathrm{T}} e_{\dot{s}^{n_s}} - (g_{\hat{u}_2\hat{u}_1}^{\hat{1}})^{\mathrm{T}} e_{\dot{s}^1} + \lambda_1 \varepsilon_{DL1,u_2u_1}^{n_s1} \end{bmatrix}. \tag{2.97}$$

We assume that all noises:

$$e_{s^p}, e_{s^q}, e_{\dot{s}^p}, e_{\dot{s}^q},\ e_{CA,u_i}^{p}, e_{CA,u_j}^{q},\ \varepsilon_{L_1,u_i}^{p},\ \varepsilon_{L_1,u_j}^{q},\ \varepsilon_{DL1,u_i}^{p},\ \varepsilon_{DL1,u_j}^{q};\ (i\neq j, p\neq q),$$

are mutually independent white Gaussian random processes with zero mean and their variances are $\mathrm{Var}(e_{s^p})=\sigma_{e_s}^2$, $\mathrm{Var}(e_{\dot{s}^p})=\sigma_{e_{\dot{s}}}^2$, $\mathrm{Var}(e_{CA,u_i}^{p})=\sigma_{e_{CA}}^2$, $\mathrm{Var}(\varepsilon_{L_1,u_i}^{p})=\sigma_{\varepsilon_{L1}}^2$, and $\mathrm{Var}(\varepsilon_{DL_1,u_i}^{p})=\sigma_{\varepsilon_{DL1}}^2$. Then the covariance matrix of $v_{u_2u_1}^{qp}$ is given by

$$\begin{aligned} R_{v_{u_2u_1}^{qp}}^{(DD)} &\equiv \mathrm{Cov}\big[v_{u_2u_1}^{qp}\big] \\ &= \begin{bmatrix} (g_{\hat{u}_2\hat{u}_1}^{\hat{n}_s})^{\mathrm{T}} e_{s^{n_s}} - (g_{\hat{u}_2\hat{u}_1}^{\hat{1}})^{\mathrm{T}} e_{s^1} + e_{CA,u_2u_1}^{n_s1} \\ (g_{\hat{u}_2\hat{u}_1}^{\hat{n}_s})^{\mathrm{T}} e_{s^{n_s}} - (g_{\hat{u}_2\hat{u}_1}^{\hat{1}})^{\mathrm{T}} e_{s^1} + \lambda_1 \varepsilon_{L_1,u_2u_1}^{n_s1} \\ (g_{\hat{u}_2\hat{u}_1}^{\hat{n}_s})^{\mathrm{T}} e_{\dot{s}^{n_s}} - (g_{\hat{u}_2\hat{u}_1}^{\hat{1}})^{\mathrm{T}} e_{\dot{s}^1} + \lambda_1 \varepsilon_{DL1,u_2u_1}^{n_s1} \end{bmatrix} \begin{bmatrix} (g_{\hat{u}_2\hat{u}_1}^{\hat{n}_s})^{\mathrm{T}} e_{s^{n_s}} - (g_{\hat{u}_2\hat{u}_1}^{\hat{1}})^{\mathrm{T}} e_{s^1} + e_{CA,u_2u_1}^{n_s1} \\ (g_{\hat{u}_2\hat{u}_1}^{\hat{n}_s})^{\mathrm{T}} e_{s^{n_s}} - (g_{\hat{u}_2\hat{u}_1}^{\hat{1}})^{\mathrm{T}} e_{s^1} + \lambda_1 \varepsilon_{L_1,u_2u_1}^{n_s1} \\ (g_{\hat{u}_2\hat{u}_1}^{\hat{n}_s})^{\mathrm{T}} e_{\dot{s}^{n_s}} - (g_{\hat{u}_2\hat{u}_1}^{\hat{1}})^{\mathrm{T}} e_{\dot{s}^1} + \lambda_1 \varepsilon_{DL1,u_2u_1}^{n_s1} \end{bmatrix}^{\mathrm{T}} \\ &= (g_{\hat{u}_2\hat{u}_1}^{\hat{1}})^{\mathrm{T}} (g_{\hat{u}_2\hat{u}_1}^{\hat{1}}) \sigma_{e_s}^2 U_{\hat{s}} + R_{\hat{s}}^{(DD)} + 2R_{CA,L1.DL1}^{(DD)}, \end{aligned} \tag{2.98}$$

where $U_{\hat{s}}$ is the $2(n_s-1)\times 2(n_s-1)$ matrix whose elements are all one, namely

$$U_{\hat{s}} \equiv \left[\begin{array}{ccc|ccc|ccc} 1 & \cdots & 1 & 1 & \cdots & 1 & 0 & \cdots & 0 \\ \vdots & \ddots & \vdots & \vdots & \ddots & \vdots & \vdots & \ddots & \vdots \\ 1 & \cdots & 1 & 1 & \cdots & 1 & 0 & \cdots & 0 \\ \hline 1 & \cdots & 1 & 1 & \cdots & 1 & 0 & \cdots & 0 \\ \vdots & \ddots & \vdots & \vdots & \ddots & \vdots & \vdots & \ddots & \vdots \\ 1 & \cdots & 1 & 1 & \cdots & 1 & 0 & \cdots & 0 \\ \hline 0 & \cdots & 0 & 0 & \cdots & 0 & 1 & \cdots & 1 \\ \vdots & \ddots & \vdots & \vdots & \ddots & \vdots & \vdots & \ddots & \vdots \\ 0 & \cdots & 0 & 0 & \cdots & 0 & 1 & \cdots & 1 \end{array}\right], \tag{2.99}$$

and $R_{\hat{s}}^{(DD)}$ is the following matrix, where for the $(n_s-1)\times 1$ vector; $g_{\hat{u}_2\hat{u}_1}^{\hat{p}}$, we define

$$\gamma_{\hat{u}_2\hat{u}_1}^{\hat{p}} \equiv (g_{\hat{u}_2\hat{u}_1}^{\hat{p}})^{\mathrm{T}}(g_{\hat{u}_2\hat{u}_1}^{\hat{p}}), \tag{2.100}$$

$$R_{\hat{p}}^{(DD)} \equiv \left[\begin{array}{cccc} \gamma_{\hat{u}_2\hat{u}_1}^{\hat{2}} & & & \\ & \gamma_{\hat{u}_2\hat{u}_1}^{\hat{3}} & & \\ & & \ddots & \\ & & & \gamma_{\hat{u}_2\hat{u}_1}^{\hat{n}_s} \end{array}\right], \quad R_{\hat{s}}^{(DD)} \equiv \left[\begin{array}{ccc} \sigma_{e_s}^2 R_{\hat{p}}^{(DD)} & \sigma_{e_s}^2 R_{\hat{p}}^{(DD)} & O \\ \sigma_{e_s}^2 R_{\hat{p}}^{(DD)} & \sigma_{e_s}^2 R_{\hat{p}}^{(DD)} & O \\ O & O & \sigma_{e_{\hat{s}}}^2 R_{\hat{p}}^{(DD)} \end{array}\right]. \tag{2.101}$$

Also $R_{CA,L1,DL1}^{(DD)}$ is a block diagonal matrix as

$$R_{CA,L1,DL1}^{(DD)} \equiv \left[\begin{array}{ccc} R_{CA}^{(DD)} & O & O \\ O & R_{L1}^{(DD)} & O \\ O & O & R_{DL1}^{(DD)} \end{array}\right], \tag{2.102}$$

where

$$R_{CA}^{(DD)} \equiv \begin{bmatrix} 2\sigma_{e_{CA}}^2 & \sigma_{e_{CA}}^2 & \cdots & \sigma_{e_{CA}}^2 \\ \sigma_{e_{CA}}^2 & 2\sigma_{e_{CA}}^2 & & \vdots \\ \vdots & & \ddots & \sigma_{e_{CA}}^2 \\ \sigma_{e_{CA}}^2 & \cdots & \sigma_{e_{CA}}^2 & 2\sigma_{e_{CA}}^2 \end{bmatrix}, \; R_{L1}^{(DD)} \equiv \begin{bmatrix} 2\lambda_1^2\sigma_{\varepsilon_{L1}}^2 & \lambda_1^2\sigma_{\varepsilon_{L1}}^2 & \cdots & \lambda_1^2\sigma_{\varepsilon_{L1}}^2 \\ \lambda_1^2\sigma_{\varepsilon_{L1}}^2 & 2\lambda_1^2\sigma_{\varepsilon_{L1}}^2 & & \vdots \\ \vdots & & \ddots & \lambda_1^2\sigma_{\varepsilon_{L1}}^2 \\ \lambda_1^2\sigma_{\varepsilon_{L1}}^2 & \cdots & \lambda_1^2\sigma_{\varepsilon_{L1}}^2 & 2\lambda_1^2\sigma_{\varepsilon_{L1}}^2 \end{bmatrix},$$

$$R_{DL1}^{(DD)} \equiv \begin{bmatrix} 2\lambda_1^2\sigma_{\varepsilon_{DL1}}^2 & \lambda_1^2\sigma_{\varepsilon_{DL1}}^2 & \cdots & \lambda_1^2\sigma_{\varepsilon_{DL1}}^2 \\ \lambda_1^2\sigma_{\varepsilon_{DL1}}^2 & 2\lambda_1^2\sigma_{\varepsilon_{DL1}}^2 & & \vdots \\ \vdots & & \ddots & \lambda_1^2\sigma_{\varepsilon_{DL1}}^2 \\ \lambda_1^2\sigma_{\varepsilon_{DL1}}^2 & \cdots & \lambda_1^2\sigma_{\varepsilon_{DL1}}^2 & 2\lambda_1^2\sigma_{\varepsilon_{DL1}}^2 \end{bmatrix}. \tag{2.103}$$

In the cases of $n_r = 3$ and $n_r = 4$, see Appendix A.

Individuating satellite positions

The mathematical models of C/A code pseudorange observables in Eqs. (2.49)-(2.52) suppose that the GNSS satellite positions obtained from the navigation messages at the antennas u_i and u_j are approximately the same. However, the positions s_i^p and s_j^p of the satellite p from the u_i and u_j are strictly different, and applied as follows:

$$\rho_{CA,u_i}^p \cong (g_{\hat{u}_i}^{\hat{p}})^{\mathrm{T}}(u_i - s_i^p) + \delta I_{u_i}^p + \delta T_{u_i}^p + c(\delta t_{u_i} - \delta t^p) + \delta b_{CA,u_i} - \delta b_{CA}^p + e_{CA,u_i}^p, \tag{2.104}$$

$$\rho_{CA,u_j}^p \cong (g_{\hat{u}_j}^{\hat{p}})^{\mathrm{T}}(u_j - s_j^p) + \delta I_{u_j}^p + \delta T_{u_j}^p + c(\delta t_{u_j} - \delta t^p) + \delta b_{CA,u_j} - \delta b_{CA}^p + e_{CA,u_j}^p, \tag{2.105}$$

The DD-based measurement equation for C/A code pseudorange observables based on

Eqs. (2.104), (2.104) is as follows:

$$
\begin{aligned}
&\rho^{qp}_{CA,u_ju_i} \equiv \rho^{q}_{CA,u_ju_i} - \rho^{p}_{CA,u_ju_i} \\
\cong\ & (g^{\hat{q}}_{\hat{u}_j})^{\mathrm{T}} u_j - (g^{\hat{q}}_{\hat{u}_i})^{\mathrm{T}} u_i - \left[(g^{\hat{p}}_{\hat{u}_j})^{\mathrm{T}} u_j - (g^{\hat{p}}_{\hat{u}_i})^{\mathrm{T}} u_i\right] \\
&+(g^{\hat{q}}_{\hat{u}_j})^{\mathrm{T}}(-s^q_j) - (g^{\hat{q}}_{\hat{u}_i})^{\mathrm{T}}(-s^q_i) - \left[(g^{\hat{p}}_{\hat{u}_j})^{\mathrm{T}}(-s^p_j) - (g^{\hat{p}}_{\hat{u}_i})^{\mathrm{T}}(-s^p_i)\right] \\
&+e^q_{CA,u_j} - e^q_{CA,u_i} - (e^p_{CA,u_j} - e^p_{CA,u_i}) \\
=\ & (g^{\hat{q}\hat{p}}_{\hat{u}_j})^{\mathrm{T}} u_j - (g^{\hat{q}\hat{p}}_{\hat{u}_i})^{\mathrm{T}} u_i - (g^{\hat{q}}_{\hat{u}_j})^{\mathrm{T}} s^q_j + (g^{\hat{q}}_{\hat{u}_i})^{\mathrm{T}} s^q_i + \left[(g^{\hat{p}}_{\hat{u}_j})^{\mathrm{T}} s^p_j - (g^{\hat{p}}_{\hat{u}_i})^{\mathrm{T}} s^p_i\right] + e^{qp}_{CA,u_ju_i}, \quad (2.106)
\end{aligned}
$$

Now let us assume that the estimated values: $\hat{s}^p_i, p = 1, \ldots, n_s$, of the satellite positions: $s^p_i, p = 1, \ldots, n_s$, are available as follows [15]–[20]. $\hat{s}^p_i$ come from the navigation messages of satellites:

$$
\hat{s}^p_i = s^p_i + e_{s^p_i}, \quad p = 1, \ldots, n_s, \tag{2.107}
$$

where we assume $e_{s^p_i}$ are Gaussian white noises. Then the DD-based estimates for the C/A code pseudorange and carrier-phase observables in Eqs. (2.90) and (2.91) are modified as follows:

$$
\begin{aligned}
&\tilde{\rho}^{\hat{q}\hat{p}}_{CA,\hat{u}_j\hat{u}_i} \equiv \rho^{qp}_{CA,u_ju_i} + (g^{\hat{q}}_{\hat{u}_j})^{\mathrm{T}} \hat{s}^q_j - (g^{\hat{q}}_{\hat{u}_i})^{\mathrm{T}} \hat{s}^q_i - \left[(g^{\hat{p}}_{\hat{u}_j})^{\mathrm{T}} \hat{s}^p_j - (g^{\hat{p}}_{\hat{u}_i})^{\mathrm{T}} \hat{s}^p_i\right] \\
\cong\ & (g^{\hat{q}\hat{p}}_{\hat{u}_j})^{\mathrm{T}} u_j - (g^{\hat{q}\hat{p}}_{\hat{u}_i})^{\mathrm{T}} u_i + (g^{\hat{q}}_{\hat{u}_j})^{\mathrm{T}} e_{s^q_j} - (g^{\hat{q}}_{\hat{u}_i})^{\mathrm{T}} e_{s^q_i} - \left[(g^{\hat{p}}_{\hat{u}_j})^{\mathrm{T}} e_{s^p_j} + (g^{\hat{p}}_{\hat{u}_i})^{\mathrm{T}} e_{s^p_i}\right] + e^{qp}_{CA,u_ju_i}, \quad (2.108) \\
&\tilde{\Phi}^{\hat{q}\hat{p}}_{L_1,\hat{u}_j\hat{u}_i} \equiv \Phi^{qp}_{L_1,u_ju_i} + (g^{\hat{q}}_{\hat{u}_j})^{\mathrm{T}} \hat{s}^q_j - (g^{\hat{q}}_{\hat{u}_i})^{\mathrm{T}} \hat{s}^q_i - \left[(g^{\hat{p}}_{\hat{u}_j})^{\mathrm{T}} \hat{s}^p_j - (g^{\hat{p}}_{\hat{u}_i})^{\mathrm{T}} \hat{s}^p_i\right] \\
\cong\ & (g^{\hat{q}\hat{p}}_{\hat{u}_j})^{\mathrm{T}} u_j - (g^{\hat{q}\hat{p}}_{\hat{u}_i})^{\mathrm{T}} u_i + (g^{\hat{q}}_{\hat{u}_j})^{\mathrm{T}} e_{s^q_j} - (g^{\hat{q}}_{\hat{u}_i})^{\mathrm{T}} e_{s^q_i} \\
&- \left[(g^{\hat{p}}_{\hat{u}_j})^{\mathrm{T}} e_{s^p_j} - (g^{\hat{p}}_{\hat{u}_i})^{\mathrm{T}} e_{s^p_i}\right] + \lambda_1 N^{qp}_{L_1,u_ju_i} + \lambda_1 \varepsilon^{qp}_{L_1,u_ju_i}, \quad (2.109)
\end{aligned}
$$

and the observation noises in Eq. (2.97) of the DD-PPP measurement equation are modified

as follows:

$$v_{u_2u_1}^{n_s} \equiv \begin{bmatrix} \xi_{\hat{u}_2\hat{u}_1}^{\hat{2}\hat{1}} + e_{CA,u_2u_1}^{21} \\ \xi_{\hat{u}_2\hat{u}_1}^{\hat{3}\hat{1}} + e_{CA,u_2u_1}^{31} \\ \vdots \\ \xi_{\hat{u}_2\hat{u}_1}^{\hat{n}_s\hat{1}} + e_{CA,u_2u_1}^{n_s1} \\ \xi_{\hat{u}_2\hat{u}_1}^{\hat{2}\hat{1}} + \lambda_1 \varepsilon_{L_1,u_2u_1}^{21} \\ \xi_{\hat{u}_2\hat{u}_1}^{\hat{3}\hat{1}} + \lambda_1 \varepsilon_{L_1,u_2u_1}^{31} \\ \vdots \\ \xi_{\hat{u}_2\hat{u}_1}^{\hat{n}_s\hat{1}} + \lambda_1 \varepsilon_{L_1,u_2u_1}^{n_s1} \end{bmatrix}, \tag{2.110}$$

$$\xi_{\hat{u}_2\hat{u}_1}^{\hat{q}\hat{1}} = (g_{\hat{u}_2}^{\hat{q}})^{\mathrm{T}} e_{s_2^q} - (g_{\hat{u}_1}^{\hat{q}})^{\mathrm{T}} e_{s_1^q} - \left[(g_{\hat{u}_2}^{\hat{1}})^{\mathrm{T}} e_{s_2^1} - (g_{\hat{u}_1}^{\hat{1}})^{\mathrm{T}} e_{s_1^1} \right], \tag{2.111}$$

also the matrix in Eq. (2.101) are modified as follows:

$$R_{\hat{p}}^{(DD)} \equiv \begin{bmatrix} \gamma_{\hat{u}_2}^{\hat{2}} + \gamma_{\hat{u}_1}^{\hat{2}} & & & \\ & \gamma_{\hat{u}_2}^{\hat{3}} + \gamma_{\hat{u}_1}^{\hat{3}} & & \\ & & \ddots & \\ & & & \gamma_{\hat{u}_2}^{\hat{n}_s} + \gamma_{\hat{u}_1}^{\hat{n}_s} \end{bmatrix}, \tag{2.112}$$

$$\gamma_{\hat{u}_i}^{\hat{p}} \equiv (g_{\hat{u}_i}^{\hat{p}})^{\mathrm{T}} g_{\hat{u}_i}^{\hat{p}}. \tag{2.113}$$

State equations for SD/DD-PPP

In the static case for SD-PPP, we utilize the state vector $\eta_{u_2u_1}^p$ without velocity parameters $\dot{u}_1, \dot{u}_2$ related to Doppler observables in Eq. (2.77) for antennas of u_1 and u_2 ($n_r = 2$) and for n_s satellites. In order to simplify the expression, superscripts p and subscripts u_1,u_2 are omitted hereafter.

$$\eta_L(t+1) = \eta_L(t), \quad \eta_L \equiv \left[u_{1,L}^{\mathrm{T}}, u_{2,L}^{\mathrm{T}}, c(\delta t_{u_2} - \delta t_{u_1}), (\delta b_{u_2} - \delta b_{u_1})^{\mathrm{T}}, N^{\mathrm{T}} \right]^{\mathrm{T}}, \tag{2.114}$$

where L stands for the coordinates in the local frame (or the local-level system (LLS), or east-north-up (ENU) system) [20], [26]. And the observation equation $y(t)$ is based on a local position as a origin and derived from the relation between Eq. (2.93) and the transformation by T_W^L as follows:

$$y(t) = C_{\eta_L}(t)\eta_L(t) + v(t), \tag{2.115}$$

$$C_{\eta_L}(t) = \begin{bmatrix} -G_{\hat{u}_1}^{\hat{p}}(T_W^L)^{\mathrm{T}} & G_{\hat{u}_2}^{\hat{p}}(T_W^L)^{\mathrm{T}} & \mathbf{1} & \mathbf{1} & \boldsymbol{O} \\ -G_{\hat{u}_1}^{\hat{p}}(T_W^L)^{\mathrm{T}} & G_{\hat{u}_2}^{\hat{p}}(T_W^L)^{\mathrm{T}} & \mathbf{1} & \mathbf{1} & \lambda_1 \boldsymbol{I} \end{bmatrix}, \tag{2.116}$$

where $G_{\hat{u}_j}^{\hat{p}}(T_W^L)^{\mathrm{T}}$ is a $(n_s \times 3)$ matrix, and $\mathbf{1}$ is a column vector, and $\boldsymbol{O}$ is a $(n_s \times n_s)$ zero matrix, and $\boldsymbol{I}$ is the $(n_s \times n_s)$ identity matrix. They are related to the corresponding values in WGS-84 coordinate frame through the linear transformation defined by 3×3 transformation matrix T_W^L which transforms WGS-84 coordinates into ENU coordinates [34].

In the static case for DD-PPP, we utilize the state vector $\eta_{u_2u_1}^{qp}$ without velocity parameters $\dot{u}_1, \dot{u}_2$ related to Doppler observables in Eq. (2.94) for antennas of u_1 and u_2 ($n_r = 2$) and for n_s satellites. In order to simplify the expression, superscripts p, q and subscripts u_1,u_2 are omitted hereafter.

$$\eta_L(t+1) = \eta_L(t), \quad \eta_L \equiv \left[u_{1,L}^{\mathrm{T}}, u_{2,L}^{\mathrm{T}}, N^{\mathrm{T}}\right]^{\mathrm{T}}, \tag{2.117}$$

where L stands for the coordinates in the local frame. The observation equation $y(t)$ is based on a local position as a origin and derived from the relation between Eq. (2.93) and the transformation by T_W^L as follows:

$$y(t) = C_{\eta_L}(t)\eta_L(t) + v(t), \tag{2.118}$$

$$C_{\eta_L}(t) = \begin{bmatrix} -G_{\hat{u}_1}^{\hat{p}\hat{1}}(T_W^L)^{\mathrm{T}} & G_{\hat{u}_2}^{\hat{p}\hat{1}}(T_W^L)^{\mathrm{T}} & \boldsymbol{O} \\ -G_{\hat{u}_1}^{\hat{p}\hat{1}}(T_W^L)^{\mathrm{T}} & G_{\hat{u}_2}^{\hat{p}\hat{1}}(T_W^L)^{\mathrm{T}} & \lambda_1 \boldsymbol{I} \end{bmatrix}, \tag{2.119}$$

where $G_{\hat{u}_j}^{\hat{p}\hat{1}}(T_W^L)^{\mathrm{T}}$ is a $(n_s-1)\times 3$ matrix. They are related to the corresponding values in WGS-84 coordinate frame through the linear transformation defined by 3×3 transformation matrix T_W^L.

The positioning estimation algorithms based on the Kalman filter [35], [36] (See Appendix B) for Eqs. (2.114) and (2.115), or Eqs. (2.117) and (2.118) are given as follows:

$$\hat{\eta}_L(t+1|t) = \hat{\eta}_L(t|t) \tag{2.120}$$

$$\hat{\eta}_L(t|t) = \hat{\eta}_L(t|t-1) + K(t)\nu(t) \tag{2.121}$$

$$\nu(t) \equiv y(t) - C_{\eta_L}(t)\hat{\eta}_L(t|t-1) \tag{2.122}$$

(: Innovation Process)

$$K(t) = \Sigma_{\eta_L}(t|t-1)C_{\eta_L}(t)^{\mathrm{T}}\Big[C_{\eta_L}(t)\Sigma_{\eta_L}(t|t-1)C_{\eta_L}(t)^{\mathrm{T}} + R(t)\Big]^{-1} \tag{2.123}$$

(: Kalman Gain)

$$\Sigma_{\eta_L}(t+1|t) = \Sigma_{\eta_L}(t|t) \tag{2.124}$$

$$\Sigma_{\eta_L}(t|t) = \Sigma_{\eta_L}(t|t-1) - K(t)C_{\eta_L}(t)\Sigma_{\eta_L}(t|t-1) \tag{2.125}$$

$$\text{Initial condition:} \quad \begin{cases} \hat{\eta}_L(0|-1) = \bar{\eta}_L(0) \\ \Sigma_{\eta_L}(0|-1) = \Sigma_{\eta_L}(0) \end{cases}$$

Chapter 3

Detection and Correction of Observable Outliers

3.1 Introduction

In order to improve the accuracy of C/A code pseudoranges for positioning, the method of carrier-smoothed code pseudoranges has been proposed [37]. The carrier-smoothed code pseudoranges are the measurements generated by combining code pseudoranges with low-noise carrier-phase observables, and can contribute to improve the positioning accuracy. However, in general, carrier-phase observables are mainly utilized by high-end multi-frequency receivers for surveyors, geophysical researchers, etc., and such receivers cannot be applied for the civilian navigation. Instead of the carrier-phase observables, the positioning method by Doppler-smoothed code pseudoranges has been proposed as the so-called Doppler-aided positioning [27], [38].

Doppler-shift frequencies are measured by the relative motion of satellites and receivers, i.e. the variations of the distance between satellites and receivers, and Doppler observables can be measured even by low-end receivers. Doppler shift observables are utilized on a priority basis even in urban areas because of immunity to cycle-slip and continuous availability. In [27], [38], Doppler-smoothed pseudoranges are introduced based on the

similar technique of the carrier-smoothed pseudoranges at the preprocessing stage of the position calculation, and the improved positioning accuracy is reported. The applicability of Doppler observables for precise positioning at high cost receivers is also reported [34]. The positioning algorithm is based on the multi-frequency pseudorange, Doppler and carrier-phase measurements, and the Kalman filter is applied to estimate vehicle positions, velocity and acceleration with the appropriate dynamics model of the vehicle.

By using the modified algorithm of [34], we analyze the test drives which were mainly conducted in Japan and the United States in 2014. Doppler range-rates are more stable than code delta-ranges even under multipath environments, and has the same quality level as carrier-phase delta-ranges, however, unexpected Doppler outliers prone to cause positioning errors. As a practical matter, we had a vehicle positioning error by Doppler bias in real test drives under open-sky environment [39]. By using the bias of real observables, the positioning errors are reproduced by the GR models based on Doppler-aided positioning method.

Although there are a lot of literature about detection of the outlier or the robust Kalman filter [9],[10] to overcome these problems, In this chapter, we propose the following two methods: 1) statistical tests on the innovation processes of the Kalman filter, 2) statistical test on the difference between C/A code delta-range and Doppler range-rate measurement. Method-1 is derived by modifying the cycle slip detection algorithm in [11], [12], and Method-2 is a novel method. In addition, two correction methods, namely the Doppler outlier exclusion, or the Doppler outlier estimation, for detected anomalies are proposed.

Chi-squared tests based on Method-1,2 are applied for the Doppler outlier detection. The tests are expanded to consecutive number of epochs, and appropriate bias-detection

periods are selected for Method-1,2. The upper probability of the tests is 5 % for the both methods. Method-2 can be also applied to the difference between carrier-phase delta-range and Doppler range-rate measurement. These detection and correction methods are applied to the positioning errors caused by Doppler bias of automotive single-frequency receivers. The experimental results by the combinations of these methods are shown.

3.2 GR Models for Automotive Kinematic Positioning

Let us derive the state equation for kinematic positioning. Since the kinematic case requires mathematical models of the automobiles, we often apply one of the dynamical models which are assumed as first-order Markov processes of, the velocity of u (: v), of the acceleration of u (: a) (the so-called Singer's moving model [40]). The Singer's models are adopted for the east-west (E) coordinate and the north-south (N) coordinate, and a first-order Markov model of the velocity for the up-down (U) coordinate [34]. The state vector therefore is defined as follows:

$$\eta \equiv \left[u^{\mathrm{T}}, \dot{u}^{\mathrm{T}}, a^{\mathrm{T}}, c\delta t_u, c\dot{\delta} t_u\right]^{\mathrm{T}}, \tag{3.1}$$

The PPP observable equations in Eq. (2.36) which utilize for a single antenna u and the discrete-time state equations are as follows:

$$y_{\hat{u},t} = C^{\hat{p}}_{\hat{u},t}\theta_{u,t} + v_{u,t}, \quad \theta_{u,t+1} = A_{u,t}\theta_{u,t} + w_{u,t}, \tag{3.2}$$

$$y_{\hat{u},t} \equiv \begin{bmatrix} y_{CA,\hat{u}} \\ \\ y_{DL1,\hat{u}} \end{bmatrix}, \; C^{\hat{p}}_{\hat{u},t} \equiv \begin{bmatrix} G^{\hat{p}}_{\hat{u}} & \mathbf{0} & \mathbf{1} & \\ & G^{\hat{p}}_{\hat{u}} & \mathbf{0} & \mathbf{1} \end{bmatrix}, \; \theta_{u,t} \equiv \begin{bmatrix} u \\ \dot{u} \\ a \\ c\delta t_u \\ c\dot{\delta} t_u \end{bmatrix}. \tag{3.3}$$

The carrier-phase related obsrvables $y^{\hat{p}}_{L1,\hat{u}}$ and unknown parameters $N_{L1,u}$ are excluded in Eq. (2.36)-(2.37), and the receiver's biases δb_u are negligible for the positioning without carrier-phase observables. The $A(t)$ is the 10×10 known matrix defined from Singer's models, and details are summarized in [34].

3.3 Detection of Anomalous Observables

We apply two methods of detecting Doppler observable outliers. First method is the innovation based detection in Kalman filtering (IBD-method), which is a existing method [41] for more accurate positioning by using carrier-phase observables and utilized for detecting cycle slips of RTK positioning [11]. Second method is a novel method and the measurement based detection (MBD-method) which focuses on the difference between C/A code pseudoranges and Doppler shift range-rates. The Both methods are based on the chi-squared tests, and applied for Doppler observables of low-end GNSS receivers to keep the vehicle positioning accuracy high.

3.3.1 IBD-method

Since the innovation process in Eq. (2.122) is a white Gaussian with 0 mean and covariance matrix $M(t)(= [M_{ij}(t)]; i, j = 1, \cdots, 2n_s)$ under the hypothesis H_0 such that there are no Doppler outliers. $M(t)$ is formulated as follows [12]:

$$\begin{aligned} M(t) &\equiv \mathrm{E}[\nu(t)\nu^{\mathrm{T}}(t)] \\ &= [C(t)\Sigma_\eta(t|t-1)C^{\mathrm{T}}(t) + R(t)], \end{aligned} \tag{3.4}$$

where $\Sigma_\eta(t|t-1)$ is the error covariance matrix of $\hat{\eta}_L(t|t-1)$. Under hypothesis H_0, the j-th element of innovation vector ν which is expressed by ν_j would be the normal

distribution with zero mean and variance M_{jj}. Then ν_j can be normalized as follows:

$$\nu_{n,j}(t) \equiv \sqrt{\frac{1}{M_{jj}(t)}}\nu_j(t), \quad j = 1, \ldots, 2n_s \tag{3.5}$$

$$\mathrm{E}[\nu_{n,j}(t)] = 0, \quad \mathrm{Var}[\nu_{n,j}(t)] = 1. \tag{3.6}$$

Based on Eq. (3.5), the anomaly of Doppler frequency observables can be detected by monitoring the normalized innovation processes corresponding to the Doppler shift observables, i.e. $\nu_{n,j}$ for $j = n_s + 1, \ldots, 2n_s$. Each element of $\nu_{n,j}(t)$ is a Gaussian process. The test statistics $T_j(t)$ of the squared value of $\nu_{n,j}(t)$ follows the chi-squared distribution with 1 degree of freedom, namely,

$$T_j(t) = (\nu_{n,j}(t))^2. \tag{3.7}$$

Statistical tests of innovation processes can be easily extended to the tests based on multiple epochs or observables. $\nu_{n,j,k}$ is the j-th innovation vector in Eq. (3.5) for k consecutive epochs. The consecutive $\nu_{n,j}$ are independent, the mean vector therefore is zero and the covariance matrix I,

$$\begin{aligned} \nu_{n,j,k}(t) &= [\nu_{n,j}(t), \nu_{n,j}(t-1), ..., \nu_{n,j}(t-k+1)]^{\mathrm{T}} \\ &\sim N([0, 0, ..., 0]^{\mathrm{T}}, I). \end{aligned} \tag{3.8}$$

Statistics $T_{j,k}(t)$ of the sum of k consecutive $\nu_{n,j}$ follows the chi-squared distribution with k degrees of freedom,

$$T_{j,k}(t) \equiv (\nu_{n,j,k}(t))^{\mathrm{T}}(\nu_{n,j,k}(t)). \tag{3.9}$$

In order to effectively detect the Doppler anomaly, we focus on chi-squared test of each Doppler shift observable. If Doppler outliers occur, the covariance matrix of the innovation

process changes. Therefore, we formulate two hypotheses such as,

$$H_0: \text{ the anomal outlier does not occur}$$

$$H_1: \text{ the anomal outlier occurs}$$

Our decision rule of accepting or rejecting the hypothesis is as follows; If $T_{j,k}(t)$ is larger than the upper percent point $\chi^2_\alpha(k)$ whose α is upper probability (α=0.05) and k is degrees of freedom, then the observed data of Doppler shift contain an outlier (accept H_1).

3.3.2 MBD-method

Let us rewrite the mathmatical measurement models in Eqs. (2.11) -(2.13).

$$\rho^p_{CA,u}(t) = r^p_u(t) + \delta I^p_u(t) + \delta T^p_u(t) + c\left[\delta t_u(t) - \delta t^p(t)\right] + B^p_{CA,u}(t) + e^p_{CA,u}(t), \quad (3.10)$$

$$\Phi^p_{L1,u}(t) = r^p_u(t) - \delta I^p_u(t) + \delta T^p_u(t) + c\left[\delta t_u(t) - \delta t^p(t)\right] + B^p_{L1,u}(t) + \lambda_1 N^p_u + \lambda_1 \varepsilon^p_{L1,u}(t), \quad (3.11)$$

$$\dot{\rho}^p_{DL1,u}(t) = \dot{r}^p_u(t) + \delta \dot{I}^p_u(t) + \delta \dot{T}^p_u(t) + c\left[\delta \dot{t}_u(t) - \delta \dot{t}^p(t)\right] + b^p_{DL1,u}(t) + \varepsilon^p_{DL1,u}(t) \quad (3.12)$$

where $B^p_{CA,u}(t)$, $B^p_{L1,u}(t)$, $b^p_{DL1,u}(t)$ contain anomalous measurements based on L1-C/A code pseudoranges, carrier-phases, Doppler shift frequencies, respectively.

In the case of normal state we can assume as follows:

$$\dot{r}^p_u(t) \cong r^p_u(t) - r^p_u(t-1),$$

$$\delta \dot{I}^p_u(t) \cong \delta I^p_u(t) - \delta I^p_u(t-1), \quad \delta \dot{T}^p_u(t) \cong \delta T^p_u(t) - \delta T^p_u(t-1),$$

$$\delta \dot{t}_u(t) \cong \delta t_u(t) - \delta t_u(t-1), \quad \delta \dot{t}^p(t) \cong \delta t^p(t) - \delta t^p(t-1),$$

then the $q^p_{m_1}(t)$ which denotes difference measurement between the C/A code derived

delta-range and the range-rate from the satellite p at the epoch t is formulated as follows:

$$\begin{aligned} q^p_{m_1}(t) &= [\rho^p_{CA}(t) - \rho^p_{CA}(t-1)] - \dot{\rho}^p_{DL1}(t) \\ &= [B^p_{CA}(t) - B^p_{CA}(t-1) - b^p_{DL1}(t)] + [e^p_{CA}(t) - e^p_{CA}(t-1) - \varepsilon^p(t)_{DL1}] \\ &= \mu^p_{m_1}(t) + d^p_{m_1}(t), \end{aligned} \tag{3.13}$$

$$\mu^p_{m_1}(t) = [B^p_{CA}(t) - B^p_{CA}(t-1) - b^p_{DL1}(t)], \tag{3.14}$$

$$d^p_{m_1}(t) = [e^p_{CA}(t) - e^p_{CA}(t-1) - \varepsilon^p_{DL1}(t)]. \tag{3.15}$$

In order to simplify the expression, the sub script "u" which indicates the receiver is dropped. The $q^p_{m_2}(t)$ which denotes difference measurement between the carrier-phase derived delta-range and the range-rate from the satellite p at the epoch t is formulated as follows:

$$\begin{aligned} q^p_{m_2}(t) &= [\Phi^p_{L1}(t) - \Phi^p_{L1}(t-1)] - \dot{\rho}^p_{DL1}(t) \\ &= [B^p_{L1}(t) - B^p_{L1}(t-1) - b^p_{DL1}(t)] + [\varepsilon^p_{L1}(t) - \varepsilon^p_{L1}(t-1) - \varepsilon^p(t)_{DL1}] \\ &= \mu^p_{m_2}(t) + d^p_{m_2}(t), \end{aligned} \tag{3.16}$$

$$\mu^p_{m_2}(t) = [B^p_{L1}(t) - B^p_{L1}(t-1) - b^p_{DL1}(t)], \tag{3.17}$$

$$d^p_{m_2}(t) = [\varepsilon^p_{L1}(t) - \varepsilon^p_{L1}(t-1) - \varepsilon^p_{DL1}(t)]. \tag{3.18}$$

The difference of geometric distance $r^p(t) - r^p(t-1)$ in Eqs. (3.10), (3.11) and the velocity $\dot{r}^p(t)$ in Eq. (3.12) are almost the same value and canceled, and the values related to δI^p, δT^p, δt_u, and δt^p are also canceled. The bias $\mu^p_{m_1}(t)$ and $\mu^p_{m_2}(t)$ based on anomalous measurements B^p_{CA},B^p_{L1},and b^p_{DL1}, and the noise $d^p_{m_1}(t)$ and $d^p_{m_2}(t)$ based on the measurement noises e^p_{CA},ε^p_{L1}, and ε^p_{DL1} are left. When there are no anomalous measurements in the observables of C/A code pseudoranges, carrier-phases and Doppler shifts, the $q^p_{m_1}(t)$ and $q^p_{m_2}(t)$ are nearly zero, and $\mu^p(t)_{m_1}$ and $\mu^p(t)_{m_2}$ are zero, and $q^p_{m_1}(t) = d^p_{m_1}(t)$,

$q^p_{m_2}(t) = d^p_{m_2}(t)$.

The noises e^p_{CA}, ε^p_{L1}, and ε^p_{DL1} are independent white Gaussian with zero mean, and their variance are supposed to be σ^2_ρ, σ^2_Φ, and σ^2_D, respectively. The mean and variance of $d^p_{m_1}(t)$, $d^p_{m_2}(t)$ and $q^p_{m_1}(t)$, $q^p_{m_2}(t)$ measured at single epoch are as follows:

$$e^p_{CA}(t) \sim N(0, \sigma^2_\rho), \quad \varepsilon^p_{L1}(t) \sim N(0, \sigma^2_\Phi), \quad \varepsilon^p_{DL1}(t) \sim N(0, \sigma^2_D), \tag{3.19}$$

$$d^p_{m_1}(t) \sim N(0, 2\sigma^2_\rho + \sigma^2_D), \quad d^p_{m_2}(t) \sim N(0, 2\sigma^2_\Phi + \sigma^2_D), \tag{3.20}$$

$$q^p_{m_1}(t) \sim N(\mu^p_{m_1}(t), 2\sigma^2_\rho + \sigma^2_D), \quad q^p_{m_2}(t) \sim N(\mu^p_{m_2}(t), 2\sigma^2_\Phi + \sigma^2_D). \tag{3.21}$$

The variance matrix of the noise $d^p_{m_1,t,j}$ between two different epochs t, j is as follows:

$$\begin{aligned}
\mathrm{E}\begin{bmatrix} d^p_{m_1}(t) \\ d^p_{m_1}(j) \end{bmatrix}\begin{bmatrix} d^p_{m_1}(t) \\ d^p_{m_1}(j) \end{bmatrix}^{\mathrm{T}} &= \mathrm{E}\begin{bmatrix} d^p_{m_1}(t)d^p_{m_1}(t) & d^p_{m_1}(t)d^p_{m_1}(j) \\ d^p_{m_1}(j)d^p_{m_1}(t) & d^p_{m_1}(j)d^p_{m_1}(j) \end{bmatrix} \\
&= \begin{bmatrix} 2\sigma^2_\rho + \sigma^2_D & -\sigma^2_\rho \\ -\sigma^2_\rho & 2\sigma^2_\rho + \sigma^2_D \end{bmatrix}, \quad (j = t \pm 1) \\
&= \begin{bmatrix} 2\sigma^2_\rho + \sigma^2_D & 0 \\ 0 & 2\sigma^2_\rho + \sigma^2_D \end{bmatrix}, \quad (j \neq t \pm 1)
\end{aligned} \tag{3.22}$$

where the covariance value of two consecutive epochs is -σ^2_ρ when $j = t \pm 1$, and zero when $j \neq t \pm 1$. The variance matrix of the noise $d^p_{m_2,t,j}$ between two different epochs t, j is as follows:

$$\begin{aligned}
\mathrm{E}\begin{bmatrix} d^p_{m_2}(t) \\ d^p_{m_2}(j) \end{bmatrix}\begin{bmatrix} d^p_{m_2}(t) \\ d^p_{m_2}(j) \end{bmatrix}^{\mathrm{T}} &= \mathrm{E}\begin{bmatrix} d^p_{m_2}(t)d^p_{m_2}(t) & d^p_{m_2}(t)d^p_{m_2}(j) \\ d^p_{m_2}(j)d^p_{m_2}(t) & d^p_{m_2}(j)d^p_{m_2}(j) \end{bmatrix} \\
&= \begin{bmatrix} 2\sigma^2_\Phi + \sigma^2_D & -\sigma^2_\Phi \\ -\sigma^2_\Phi & 2\sigma^2_\Phi + \sigma^2_D \end{bmatrix}, \quad (j = t \pm 1) \\
&= \begin{bmatrix} 2\sigma^2_\Phi + \sigma^2_D & 0 \\ 0 & 2\sigma^2_\Phi + \sigma^2_D \end{bmatrix}, \quad (j \neq t \pm 1)
\end{aligned} \tag{3.23}$$

where the covariance value of two consecutive epochs is -σ_{Φ}^2 when $j = t \pm 1$, and zero when $j \neq t \pm 1$.

$d^p_{m_1,k}$ and $d^p_{m_2,k}$ are the measurement noise vectors in Eqs. (3.15) and (3.18), respectively, which uses k consecutive epochs. The mean vectors are zero and the covariance matrixes Σ_{m_1},Σ_{m_2} of $d^p_{m_1,k}$ and $d^p_{m_2,k}$ are not diagonal matrixes, namely,

$$d^p_{m_1,k}(t) = [d^p_{m_1}(t), d^p_{m_1}(t-1), ..., d^p_{m_1}(t-k+1)]^{\mathrm{T}} \sim N([0,0,...,0]^{\mathrm{T}}, \Sigma_{m_1}), \quad (3.24)$$

$$d^p_{m_2,k}(t) = [d^p_{m_2}(t), d^p_{m_2}(t-1), ..., d^p_{m_2}(t-k+1)]^{\mathrm{T}} \sim N([0,0,...,0]^{\mathrm{T}}, \Sigma_{m_2}), \quad (3.25)$$

where

$$\Sigma_{m_1} \equiv \begin{bmatrix} 2\sigma_\rho^2 + \sigma_D^2 & -\sigma_\rho^2 & 0 & \cdots & \cdots & 0 \\ -\sigma_\rho^2 & 2\sigma_\rho^2 + \sigma_D^2 & -\sigma_\rho^2 & & & \vdots \\ 0 & -\sigma_\rho^2 & 2\sigma_\rho^2 + \sigma_D^2 & & & \vdots \\ \vdots & & & \ddots & & 0 \\ \vdots & & & & 2\sigma_\rho^2 + \sigma_D^2 & -\sigma_\rho^2 \\ 0 & \cdots & \cdots & 0 & -\sigma_\rho^2 & 2\sigma_\rho^2 + \sigma_D^2 \end{bmatrix}, \quad (3.26)$$

$$\Sigma_{m_2} \equiv \begin{bmatrix} 2\sigma_\Phi^2 + \sigma_D^2 & -\sigma_\Phi^2 & 0 & \cdots & \cdots & 0 \\ -\sigma_\Phi^2 & 2\sigma_\Phi^2 + \sigma_D^2 & -\sigma_\Phi^2 & & & \vdots \\ 0 & -\sigma_\Phi^2 & 2\sigma_\Phi^2 + \sigma_D^2 & & & \vdots \\ \vdots & & & \ddots & & 0 \\ \vdots & & & & 2\sigma_\Phi^2 + \sigma_D^2 & -\sigma_\Phi^2 \\ 0 & \cdots & \cdots & 0 & -\sigma_\Phi^2 & 2\sigma_\Phi^2 + \sigma_D^2 \end{bmatrix}. \quad (3.27)$$

In order to normalize the measurement noise vectors $d^p_{m_1,k}$ and $d^p_{m_2,k}$, the zero covariance matrixes Σ_{m_1} and Σ_{m_2} are decomposed to generate the unitary matrixes U_{m_1} and

U_{m_2} by the Cholesky decomposition method, respectively, as follows:

$$\Sigma_{m_1} = d^p_{m_1,k} d^{p\,\mathrm{T}}_{m_1,k} = U^{-1}_{m_1} U^{-\mathrm{T}}_{m_1}, \quad \Sigma_{m_2} = d^p_{m_2,k} d^{p\,\mathrm{T}}_{m_2,k} = U^{-1}_{m_2} U^{-\mathrm{T}}_{m_2}. \tag{3.28}$$

The mean value of $U_{m_1} d^p_{m_1,k}$ becomes an identity matrix as follows:

$$\begin{aligned} \mathrm{E}\left[(U_{m_1} d^p_{m_1,k})(U_{m_1} d^p_{m_1,k})^{\mathrm{T}}\right] &= \mathrm{E}\left[U_{m_1} d^p_{m_1,k} d^{p\,\mathrm{T}}_{m_1,k} U^{\mathrm{T}}_{m_1}\right] \\ &= \mathrm{E}\left[U_{m_1} U^{-1}_{m_1} U^{-\mathrm{T}}_{m_1} U^{\mathrm{T}}_{m_1}\right] \\ &= \mathrm{E}\left[I_k\right]. \quad (I_k : k \times k \text{ identity matrix}) \end{aligned} \tag{3.29}$$

Therefore the $U_{m_1} d^p_{m_1,k}$ becomes a normalized noise vector, namely $d^p_{m_1,n,k}$. The $d^p_{m_2,n,k}$ is also generated in the same manner by using the unitary matrix U_{m_2}.

The $q^p_{m_1,k}$ and $q^p_{m_2,k}$ are the measurement difference vectors in Eqs. (3.13) and (3.16), respectively, which use k consecutive epochs. The normalized vectors $q^p_{m_1,n,k}$ and $q^p_{m_2,n,k}$ are generated by the unitary matrixes U_{m_1} and U_{m_2} in the same manner of the noise vectors $d^p_{m_1,k}$ and $d^p_{m_2,k}$, respectively. The statistics $T^p_{m_1,k}(t)$ and $T^p_{m_2,k}(t)$ of the sum of squared $q^p_{m_1,n,k}$ and $q^p_{m_2,n,k}$, respectively, follow the chi-squared distribution with k degree of freedom, namely,

$$q^p_{m_1,k}(t) = [q^p_{m_1}(t), q^p_{m_1}(t-1), ..., q^p_{m_1}(t-k+1)]^{\mathrm{T}},$$

$$q^p_{m_2,k}(t) = [q^p_{m_2}(t), q^p_{m_2}(t-1), ..., q^p_{m_2}(t-k+1)]^{\mathrm{T}}, \tag{3.30}$$

$$q^p_{m_1,n,k}(t) \equiv U_{m_1} q^p_{m_1,k}(t), \;\; q^p_{m_2,n,k}(t) \equiv U_{m_2} q^p_{m_2,k}(t), \tag{3.31}$$

$$T^p_{m_1,k}(t) \equiv (q^p_{m_1,n,k}(t))^{\mathrm{T}} (q^p_{m_1,n,k}(t)), \;\; T^p_{m_2,k}(t) \equiv (q^p_{m_2,n,k}(t))^{\mathrm{T}} (q^p_{m_2,n,k}(t)). \tag{3.32}$$

If Doppler outliers occur, the measurement difference vector $q^p_{m_1}(t)$ changes. We therefore formulate two hypotheses such as,

$$H_0(\text{normal}) : \; T^p_{m_1,k} < \chi^2_\alpha(k), \quad T^p_{m_2,k} < \chi^2_\alpha(k)$$

$$H_\alpha(\text{abnormal}) : \; T^p_{m_1,k} \geq \chi^2_\alpha(k), \quad T^p_{m_2,k} \geq \chi^2_\alpha(k)$$

Our decision rule of accepting or rejecting the hypothesis is as follows; If $T^p_{m_1,k}(t)$ is larger than the upper percent point $\chi^2_\alpha(k)$ whose α is upper probability (α=0.05) and k is degrees of freedom, then the observed data of Doppler shift contain an outlier (accept H_α). The α shows the probability of false alarm P_{FA}.

Table 3.1: Detection of observable outliers

$\mathrm{T}^p_{m_1,k}$	$\mathrm{T}^p_{m_2,k}$	B^p_{CA}	B^p_{L1}	b^p_{DL1}
H_0	H_0	O(Normal)	O	O
H_α	H_0	A(Abnormal)	O	O
H_0	H_α	O	A	O
H_α	H_α	O	O	A

If Doppler observables have a outlier, the statistics $T^p_{m_1,k}(t)$ follows the non-central chi-squared distribution with non-central parameter λ as follows:

$$H_1(\text{abnormal}): \; T^p_{m_1,k} \approx \chi^2(k,\lambda)$$
$$(\lambda \equiv (U_{m_1}\mu^p_{m_1})^{\mathrm{T}}(U_{m_1}\mu^p_{m_1})),$$

and the detectable minimum bias $T_{m_1,bias}$ of Doppler observables is derived from the λ as follows:

$$T_{m_1,bias} = \sigma_D\sqrt{\lambda}, \tag{3.33}$$

and when the probability of missed detection P_{MD} is defined as the lower probability β of non-central $\chi^2(k,\lambda)$ distribution, and the lower percent point $\chi^2_\beta(k,\lambda)$ is equal to the upper percent point $\chi^2_\alpha(k)$ of normal $\chi^2(k)$ distribution, the λ is decided and the $T_{m_1,bias}$ is derived from Eq. (3.33). The protection levels of RAIM(Receiver Autonomous Integrity Monitoring) are defined by P_{FA}, P_{MD}, and $T_{m_1,bias}$ [42].

3.4 Correction of Doppler Biases

We focus on the correction of Doppler outliers b^p_{DL1} in Eq. (2.13), because we had a positioning error data of the real test drive whose Doppler-aided positioning was affected by a Doppler bias. The biased Doppler shift observables are detected by the IBD or MBD-methods, and then the bias impacts are removed by the following two methods which are Doppler bias exclusion, or Doppler bias estimation.

In the case of Doppler bias exclusion, if the Doppler bias is detected in the j-th satellite, then the related observable, i.e. the j-th component of $y^{\hat{p}}_{DL1,\hat{u}}$ and the related row of observation matrix $C(t)$ in Eqs. (2.122-2.123) are excluded. The observation noises related to $y^{\hat{p}}_{DL1,\hat{u}}$ are similarly excluded from the covariance matrix $R(t)$ in Eq. (2.123). For example, if $j = 2$, the 2nd Doppler observable and the related row components with brackets are excluded as follows:

$$\begin{bmatrix} y^{\hat{1}}_{CA,\hat{u}} \\ \vdots \\ y^{\hat{n}_s}_{CA,\hat{u}} \\ y^{\hat{1}}_{DL1,\hat{u}} \\ (y^{\hat{2}}_{DL1,\hat{u}}) \\ \vdots \\ y^{\hat{n}_s}_{DL2,\hat{u}} \end{bmatrix} = \begin{bmatrix} G^{\hat{1}}_{\hat{u}} & \mathbf{0} & 1 & 0 \\ & \vdots & & \\ G^{\hat{n}_s}_{\hat{u}} & \mathbf{0} & 1 & 0 \\ \mathbf{0} & G^{\hat{1}}_{\hat{u}} & 0 & 1 \\ \mathbf{(0)} & (G^{\hat{2}}_{\hat{u}}) & (0) & (1) \\ & \vdots & & \\ \mathbf{0} & G^{\hat{n}_s}_{\hat{u}} & 0 & 1 \end{bmatrix} \begin{bmatrix} u \\ \dot{u} \\ c\delta t_u \\ c\dot{\delta} t_u \end{bmatrix} + v. \tag{3.34}$$

In the case of Doppler bias estimation, if the Doppler bias is detected in the j-th satellite, then Doppler bias will be augmented as unknown parameter b^j_{DL1} for the j-th component of $y^{\hat{p}}_{DL1,\hat{u}}$ to the state vector η_L in Eq. (2.120), and the related column is added to the last column of observation matrix $C(t)$ in Eqs. (2.122-2.123). The initial values of the unknown parameters b^j_{DL1} are set to the difference values between Doppler range-rates

and code delta-ranges. The initial variance 0.1 related to b^j_{DL1} are added into estimation error covariance matrix $\Sigma_\eta(t|t)$ in Eq. (2.124). The model of Doppler bias b^j_{DL1} is defined by the state transition matrix $A(t)$ in Eqs. (2.120) and (2.124) is as follows:

$$b^j_{DL1}(t+1) = b^j_{DL1}(t) + w_b(t). \tag{3.35}$$

The system noise 0.01 related to the b^j_{DL1} are added into covariance matrix $Q(t)$ in Eq. (2.124).

For example, if $j = 2$, the unknown parameter for 2nd Doppler observable and the related column with brackets are added into the state vector and the observation matrix, respectively as follows:

$$\begin{bmatrix} y^{\hat{1}}_{CA,\hat{u}} \\ \vdots \\ y^{\hat{n}_s}_{CA,\hat{u}} \\ y^{\hat{1}}_{DL1,\hat{u}} \\ y^{\hat{2}}_{DL1,\hat{u}} \\ \vdots \\ y^{\hat{n}_s}_{DL1,\hat{u}} \end{bmatrix} = \begin{bmatrix} G^{\hat{1}}_{\hat{u}} & \mathbf{0} & 1 & 0 & (0) \\ & \vdots & & & \\ G^{\hat{n}_s}_{\hat{u}} & \mathbf{0} & 1 & 0 & (0) \\ \mathbf{0} & G^{\hat{1}}_{\hat{u}} & 0 & 1 & (0) \\ \mathbf{0} & G^{\hat{2}}_{\hat{u}} & 0 & 1 & (1) \\ & \vdots & & & \\ \mathbf{0} & G^{\hat{n}_s}_{\hat{u}} & 0 & 1 & (0) \end{bmatrix} \begin{bmatrix} u \\ \dot{u} \\ c\delta t_u \\ c\dot{\delta} t_u \\ (b^2_{DL1}) \end{bmatrix} + v. \tag{3.36}$$

3.5 Experiments

3.5.1 Doppler Bias Sample and the Simulating Positioning Error

In order to verify the detection and correction methods, we use a real observable outlier, namely Doppler bias, which causes a vehicle positioning error in real test drives under open sky environment. The conditions when the error occurred are shown in Table 3.2. Fig. 3.1 shows the Doppler range-rate bias of SBAS (Satellite-Based Augmentation System) satellite (black line) which causes the error. The bias is extracted by subtracting the

Table 3.2: Positioning error conditions

Date	April 15, 2014
GPS-Time	17:14:41〜17:32:05
Location	Streets in State of Maryland, US
Antenna(ANT)	Patch antenna for automobile
Receiver	u-blox GPS-module NEO-7N
Epoch interval	1 [s]
Elevation angle mask	5 [deg.]
C/No mask	20 [dB/Hz]
Measurement Data	C/A-L1 Code, Doppler shifts

delta-ranges from the range-rates of the satellite, and has the rectangular shape whose length is from epoch 60 to 280 and size is approximately 10 m/s. The delta-ranges and the range-rates are independent observables, and the subtracted values, namely the extracted bias, is also independent.

In order to reproduce the positioning error by the GR model which is the GPS and Doppler-based Kalman filter positioning, the extracted Doppler range-rate bias is injected to the original range-rate of PRN6 as a experimental sample (green line). The delta-ranges of PRN6 (red line) are almost the same values as the original range-rates of PRN6 (blue line) because of open sky environment. The PRN6 is the closest GPS satellite to the SBAS satellite. The observables of the SBAS and the PRN6 GPS are independent, and the injected values, namely the PRN6 range-rate with the extracted bias, is independent.

We confirmed that Doppler dominant positioning causes positioning errors even under open sky environments due to the Doppler bias sample [39]. In general, Doppler shift frequency observable is derived from the change of the frequency of the received signal caused by the relative motion of the GNSS satellite and the receiver. The GNSS signals are

affected by not only the motions but also the fluctuation on the travel path, and various geomorphic environments such as scintillation, interference, multipath, and so on.

Generally speaking, standard error model says that one-sigma error of pseudoranges is approximately 5 m [1]. As Doppler shifts are more accurate, one-sigma error of the shifts is supposed to be approximately one tenth of pseudorange errors that is approximately 0.5 m/s. We have the Kalman filter positioning with 5 m and 0.5 m/s as typical positioning for C/A code and Doppler shift observables, respectively (see Table 3.3). For comparison, we use two other different simulation conditions as Code-based positioning or Doppler based positioning.

Table 3.3: Noise variance for R(t)

Noise variance	C/A code pseudoranges $[m^2]$	Doppler shift frequencies $[(m/s)^2]$
Code-based positioning	0.3^2	3^2
Typical positioning	5.0^2	0.5^2
Doppler-based positioning	10.0^2	0.3^2

As for typical positioning, the positioning errors from the vehicle position is gradually getting bigger according to the vehicle movement. The continuous Doppler bias causes abnormal velocity vector, and then the continuous abnormal velocity vector finally causes the bigger positioning errors. In the case of Doppler-based positioning with bigger C/A code noise and less Doppler noise variance, the amount of positioning errors are the biggest among three cases. As for Code-based positioning, the positioning errors are smaller than other two cases, although the biased Doppler is used for the positioning (see Fig. 3.2). The C/A code pseudoranges are utilized for the positioning on a priority basis.

Fig. 3.3 shows the ENU errors of simulation results. The positioning results by orig-

inal log data which include no Doppler bias are regarded as the reference trajectory for evaluating positioning errors. In the case of typical positioning, the positioning error is simulated even under open sky environment, and has approximately 50-m error to the direction of east and north. Doppler-based positioning is more affected by the Doppler bias, and causes the errors after epoch 280 which includes no Doppler bias.

3.5.2 Detection and Correction Results

The experiment of Kalman filter-based positioning has been carried out to detect and correct the Doppler biases. Table 3.4 shows the conditions of experiments (a)-(c) combined of the IBD or MBD-methods, the exclusion or estimation correction methods, and a square or a slope bias wave. C/A code pseudorange and Doppler shift noise variances are supposed to be 5^2 m and 0.5^2 m/s for all experiments. The variances are decided by the one-sigma standard deviation error model of pseudoranges [1], and the measurement analysis of the fixed point positioning of NEO-7N receiver under open sky environments [39]. MBD-

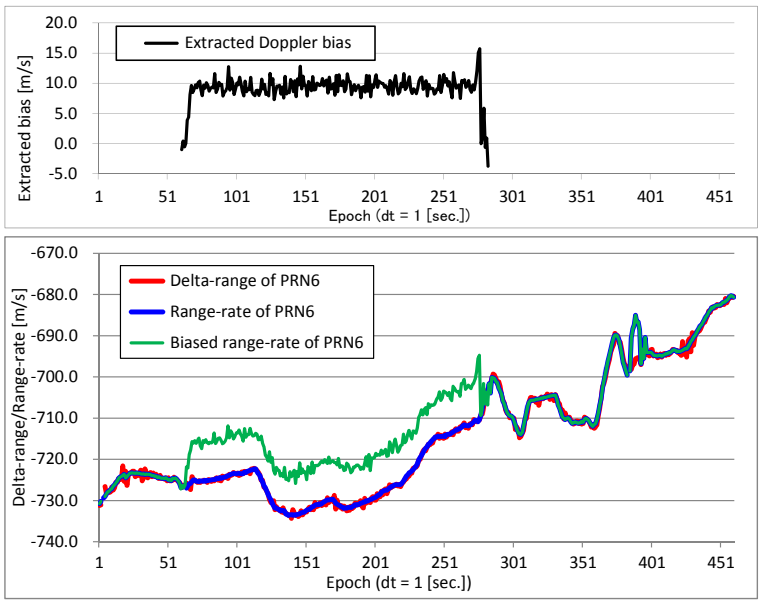

Figure 3.1: Extracted Doppler bias and Experimental sample

method also uses $\sigma_\rho^2 = 5\,\mathrm{m}$ and $\sigma_D^2 = 0.5\,\mathrm{m/s}$ as the noise variances for pseudoranges and range-rates, respectively.

The IBD or MBD-methods are applied for experiments (a),(b), or experiments (c), respectively. The bias exclusion or estimation methods are applied for experiments (a),(c),

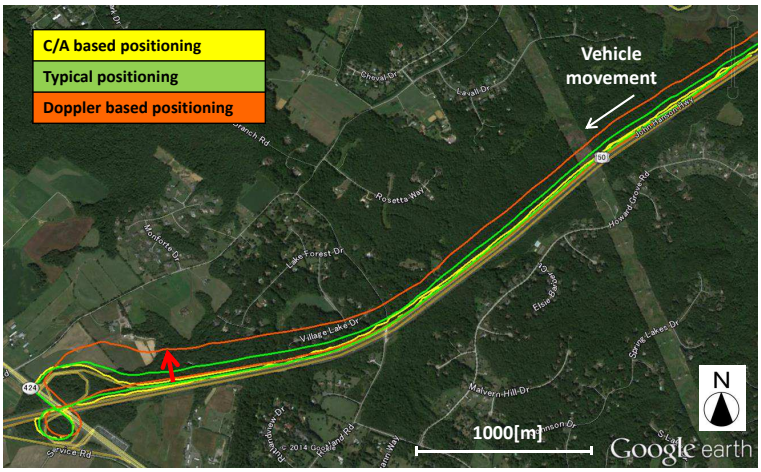

Figure 3.2: Vehicle trajectories simulated by (a) Code-based, (b) Typical,(c) Doppler-based positioning

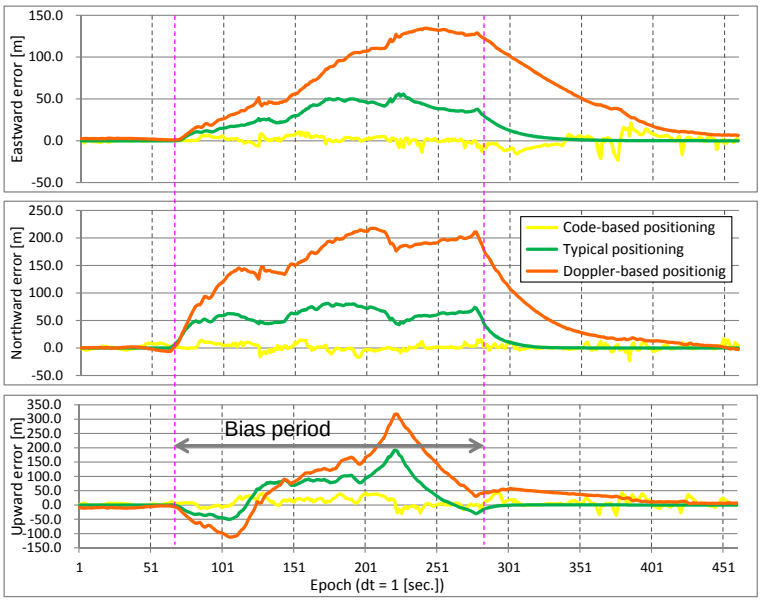

Figure 3.3: ENU errors of (a) Code-based, (b) Typical,(c) Doppler-based positioning

or experiment (b), respectively. The same upper probability $\alpha = 0.05$ of chi-squared tests are used for the both IBD and MBD-methods. The k degrees of freedom for the chi-squared tests are decided by the number of consecutive epochs for testing which is window width k. The window width is decided to achieve the better detection performance.

Table 3.4: Experimental conditions

		(a)	(b)	(c)
C/A code pseudorange noise variance		5^2 [m^2]		
Doppler shift noise variance		0.5^2 [(m/s)^2]		
Detection	IBD (Innovation based)	O	O	–
	MBD (Measurement based)	–	–	O
Correction	Exclusion method	O	–	O
	Estimation method	–	O	–
Upper probability α of χ^2 tests		0.05		

Fig. 3.4 shows the comparison of two correction methods. They are experiment (a) by the exclusion method and experiment (b) by the estimation method at the same IBD-method whose window width is 1 epoch. In experiment (a), during the bias-injected period (black line), the Doppler observable of the target satellite PRN6 which includes the Doppler bias sample is synchronously excluded (blue line), and the exclusion method almost can have no response delays at the start and end points of the bias. However, approximately 30 percent normal Doppler observables (green line) are excluded with the PRN6 Doppler observable, because the normal observables include spikes which are sudden fluctuation in one or two epochs. The spikes cause some detection errors, and the number of normal Doppler shift observables for positioning are decreased. In experiment (b), during the bias-injected period, the estimated bias values (yellow line) are almost the

same as the extracted bias. Few other satellites' Doppler biases are estimated (green line), because the start condition for the bias estimation is that H_1 acceptances by Hypothesis testing of IBD-method continue for 3 consecutive epochs. The bias estimations are stopped after several epochs when the estimation value is less than specific threshold level 1.5 m/s. Although the start condition can mask spikes of Doppler innovation values and be effective to avoid type-I errors for normal Doppler shifts, the condition causes the response delay of estimation process for several epochs.

Fig. 3.5 shows the comparison of two detection methods. They are experiments (a1-7) by IBD and experiments (c1-7) by MBD using the same exclusion correction methods. (a1) denotes the experiment (a) by using Doppler bias model (1). The same square or slope biases are used for experiments (a1-3), (c1-3), or experiments (a4-7),(c4-7), respectively.

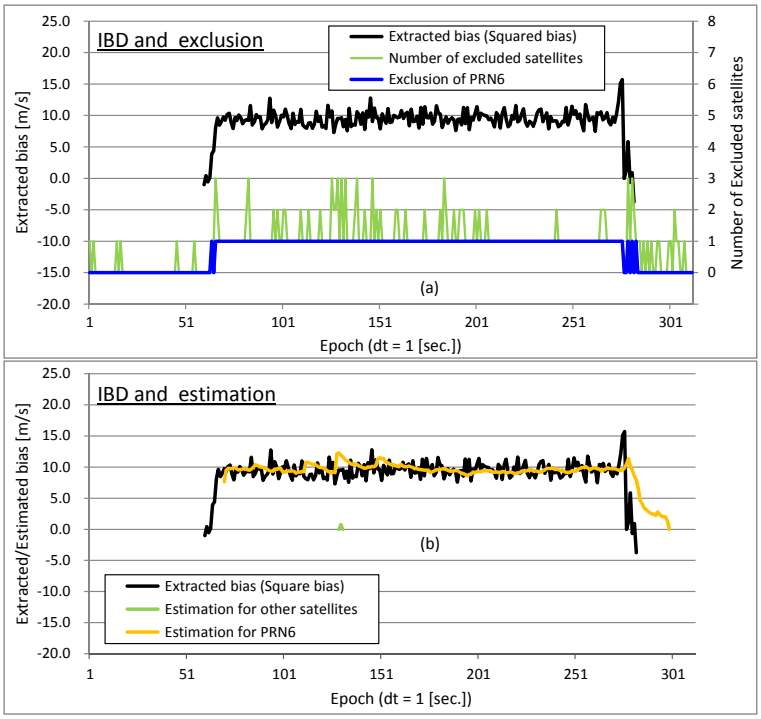

Figure 3.4: Doppler bias correction by (a) IBD and exclusion, (b) IBD and estimation

The square bias waves (1) is the original extracted bias range-rates, and we prepare for the square (2),(3) or slope biases (4),(5),(6),(7) to evaluate the detection response according to the bias size. The bias waves are formed by multiplying coefficients to the square bias wave (1). The coefficients for (2)-(7) are doubled, halved, ascent slope 1, ascent slope 2, descent slope 1, and descent slope 2, respectively.

The IBD-method chooses 1 epoch as the window width, because the statistics $T_{j,k}$ in equation (3.9) can be more widely affected by spikes of Doppler observables when $k \geq 2$ than $k = 1$, and normal Doppler observables are unintentionally excluded for several consecutive epochs. The excess exclusions degrade the detection capability of the IBD-method. While the MBD-method chooses 4 epochs as the window width, because the statistics T_k^p in equation (3.32) doesn't surpass the upper percent point even during the

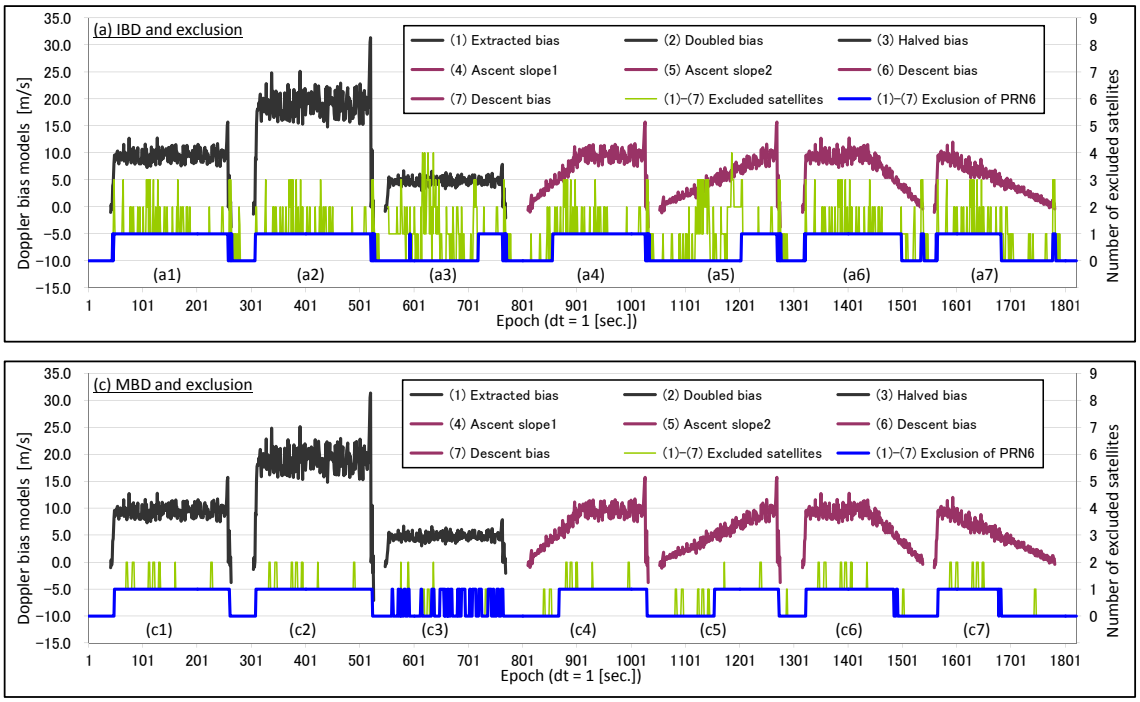

Figure 3.5: Square/Slope Doppler bias correction by (a) IBD and exclusion, (c) MBD and exclusion

bias-injected period when $k = 1$. $k = 4$ can effectively detect the Doppler bias and keep the smaller response delay of correction processes.

In the comparison between experiments (a1-2) and (c1-2) using square biases (black line), the both detection methods synchronously exclude the target satellite PRN6 (blue line) during the bias-injected period. There are no critical response delays by the detection processes at the start and end points of the period. In the comparison between experiments (a3) and (c3) using halved square bias (black line), the both methods cannot fully detect the PRN6. MBD-method has intermissive detections.

In the case of experiments (a4-7) and (c4-7) using slope bias (brown line), the both detection methods have the response delays (blue line). The exclusion of PRN6 is earlier started by experiment (c5) than experiment (a5). Experiments (c1-7) have less number of excluded satellites with normal Doppler observable (green line) compared with experiments (a1-7). We consider that the innovation process in Kalman filter is easily affected by spikes in Doppler observables obtained by low-end single frequency receivers. On the other hand, the difference values by the MBD-method are less affected by spike-like noises. because the noises can be lowered by the subtraction between the delta-ranges and the range-rates. Also The MBD-method can effectively detect Doppler biases when C/A code pseudorange observables do not have anomalies caused by noises or multipath. The MBD-method therefore is required to combine with the quality monitoring process of the C/A code pseudoranges.

Fig. 3.6 shows the comparison of the positioning results with no correction (green line) or with three corrections (a),(b),(c) of the square Doppler bias. The gaps between the green trajectory with no correction and the road gradually get wider due to the abnormal vehicle speed vectors caused by the Doppler bias. The deviated green trajectory is corrected by

three correction experiments (a),(b),(c), and the corrected trajectories come close to the road.

Fig. 3.7 shows the ENU errors of correction results. The positioning results by original

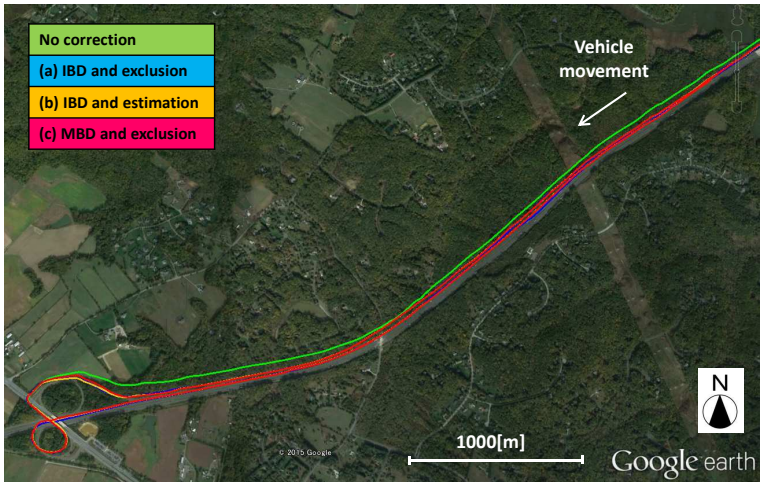

Figure 3.6: Vehicle trajectories corrected by (a) IBD and exclusion, (b) IBD and estimation,(c) MBD and exclusion

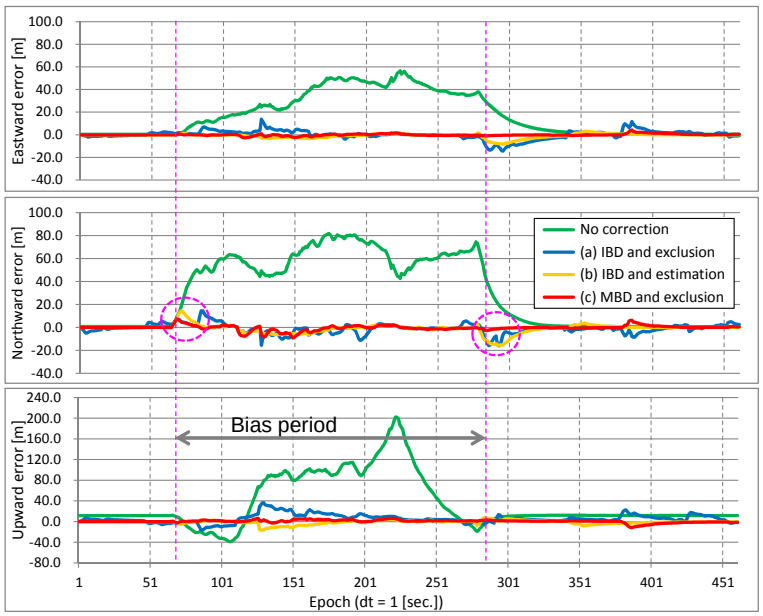

Figure 3.7: ENU errors of (a) IBD and exclusion,(b) IBD and estimation, (c) MBD and exclusion

data which include no Doppler bias are regarded as the reference trajectory for evaluating positioning errors. No correction (green line) causes that the ENU errors are more than 20 m in the Doppler bias-injected period. Contrarily, three correction experiments result in almost less than 20-m errors. Experiment (a),(blue line) results in that there are some small positioning errors even when no Doppler bias injection because of the excess exclusion of normal observables. Experiment (b),(yellow line) results in that positioning errors are bigger than experiment (a) at the start and end points (pink dotted circle) of the bias-injected period because of some response delays of estimation process. Experiment (c),(red line) results in that positioning errors are smaller than experiments (a) and (b) from the start to the end. The positioning misalignments from the reference positioning are almost less than approximately 10 m.

3.6 Concluding Remarks

In this chapter, we have formulated a Doppler-aided Kalman filter positioning from the PPP GR models. Instead of carrier-phase pseudoranges, Doppler range-rates are utilized with C/A code pseudoranges in the GR model. Experiments of the detection and correction methods have been done by using the Doppler outlier (bias) from the real receiver data, and artificially simulated the positioning errors by the bias under open sky environments. The existing innovation based detection (IBD) method and a novel measurement based detection (MBD) method combined with the exclusion or the estimation correction methods has been proposed for the injected Doppler bias of PRN6 range-rates, and been able to remove the impacts of the Doppler bias to keep the vehicle position accuracy high. We have shown that the both IBD and MBD-methods can properly detect the Doppler bias by the chi-squared tests. The window widths k of the bias detection

tests by the IBD or MBD-methods are decided to achieve better detection performance under the same upper probability of chi-squared tests, namely $k = 1$ for IBD-method and $k = 4$ for MBD-method. The IBD-method can be widely affected by the spikes included in the normal Doppler observables of automotive single-frequency receivers than the MBD-method, and provide the false detections of the observables. The exclusion method can be easier implemented because of the smaller response delays at the start and end points of the bias-injected period than the estimation method. The MBD and exclusion method provides the best performance compared with the IBD and exclusion method, and the IBD and estimation method.

We also consider that Robust Kalman Filter methods can be applied for GNSS observable outliers at a next step, because it is reported to be effective to reduce the impacts of observable spike noises [9], [10]. The number of satellite signals for C/A code pseudoranges and Doppler shift observables increases more and more by the operation start of multi-frequency and multi-GNSS systems. Our proposal can achieve the selective utilization of the better signals and have the possibility to be effective for more precise positioning.

Chapter 4

DD-PPP/VPPP Algorithms by using Multiple Antennas

4.1 Introduction

In general, so-called SPP (standard point positioning) utilizes C/A code pseudoranges of low-end single-frequency receivers solving the nonlinear equations, and has several tens of meter positioning errors caused by the error sources [43]. On the other hand, relative positioning additionally utilizes carrier-phase observables which provide more precise pseudoranges, and augmentation data obtained from reference stations through communication means. The data are based on multi-GNSS observables at reference stations, and utilized for cancelling common bias-related error sources by single difference (SD) or double difference (DD) methods [2] applied to the observables at receivers and the reference stations. The relative positioning therefore has millimeter-level positioning for topographic surveying.

PPP also utilizes carrier-phase observables, and is an ultimately desirable technology in the GPS/GNSS positioning community [29]. According to [15]–[20], the PPP GR models achieved the positioning accuracy in decimeter-level without any external transmitted information such as WAAS by the high-end receivers for topographic surveying. Then we

had derived the VPPP (very precise point positioning) algorithm with multiple antennas and with common receivers' clock errors by applying the multiple GR models and Kalman filtering [21]–[25].

We have advanced our previous PPP algorithms, and applied DD-based observables among multiple antennas to the algorithms and derived the DD-based GR models (DD-PPP). The DD-PPP GR models are based on the relative positioning GR models, however, all antennas' positions are unknown. Furthermore, VPPP algorithm has been applied to the DD-PPP by geometrical distance constraints among antennas' position. Although other methods utilize the distance constraints to fix integer ambiguity of carrier-phase observables [44], our proposed VPPP algorithms update PPP estimates every epoch by the minimum mean square (MMS) methods based on the constraints to improve the positioning accuracy. In these derivations, we had discovered the simplest derivation of Kalman's measurement update equations shown in [23], as a byproduct.

The GR models for PPP algorithm by applying the DD-based GNSS observables among multiple antennas (receivers) are shown in Chapter 2. The Kalman filtering algorithms for recursive estimation of all antennas' positions and the DD-based integer ambiguity of all carrier-phase observables are derived.

In this chapter, we show the advantages of VPPP method which utilizes the DD-based observables and the geometric distance constraints among multiple antennas' positions. The MMS estimation method based on the constraints are applied for every epoch in conjunction with the DD-PPP Kalman filtering algorithms.

We have carried out the experiments of static positioning by four antennas located on a square area. The experimental results of our proposed DD-PPP/VPPP algorithms comparing with the previous PPP/VPPP algorithms are shown. Then we show the DD-

PPP/VPPP root-mean-square (RMS) error comparison results between two and four antennas through 24-hour static positioning.

4.2 DD-PPP/VPPP Algorithms and Updating by Constraints

For the case of $p = 1$, $q = 2, \ldots, n_s$ and $u_i = u_1, u_j = u_2$ $(n_r = 2)$, we have the following measurement equations for antennas of u_1 and u_2 and for n_s satellites. In the static case, Doppler shift observables are not necessary in the GR equations for PPP/VPPP positioning, because the antennas are located at the fixed positions, and the speed parameters related to Doppler observables are zero.

PPP GR Equations for Two Antennas

The PPP observable equations in Eq. (2.36) are individually utilized for antennas of u_1 and u_2. The Doppler-related observables $y^{\hat{p}}_{DL1,\hat{u}_i}$ and unknown parameters $\dot{u}_i$, $c\dot{\delta}t_{u_i}$ are excluded in Eq. (2.36)-(2.37).

$$y_{\hat{u}_1}(t) = C^{\hat{p}_1}_{\hat{u}_1}(t)\theta_{u_1}(t) + v_{u_1}(t), \quad \theta_{u_1}(t+1) = \theta_{u_1}(t), \tag{4.1}$$

$$y_{\hat{u}_2}(t) = C^{\hat{p}_2}_{\hat{u}_2}(t)\theta_{u_2}(t) + v_{u_2}(t), \quad \theta_{u_2}(t+1) = \theta_{u_2}(t), \tag{4.2}$$

$$y_{\hat{u}_i} \equiv \begin{bmatrix} y_{CA,\hat{u}_i} \\ \\ y_{L1,\hat{u}_i} \end{bmatrix}, \; C^{\hat{p}_i}_{\hat{u}_i} \equiv \begin{bmatrix} G^{\hat{p}}_{\hat{u}_i} & \mathbf{1} & \mathbf{1} & \mathbf{0} \\ G^{\hat{p}}_{\hat{u}_i} & \mathbf{1} & \mathbf{1} & \lambda_1 \boldsymbol{I} \end{bmatrix}, \; \theta_{u_i} \equiv \begin{bmatrix} u_i \\ c\delta t_{u_i} \\ \delta b_{u_i} \\ N_{L1,u_i} \end{bmatrix}, \; i = 1, 2. \tag{4.3}$$

SD-PPP GR Equations for Two Antennas

The SD-PPP observable equations in Eq. (2.77) are utilized for antennas of u_1 and u_2. The Doppler-related SD-based observables $\tilde{\dot{\rho}}^{\hat{p}}_{DL1,\hat{u}_2\hat{u}_1}$ $(p = 1, \ldots, n_s)$ and unknown parameters $\dot{u}_1$, $\dot{u}_2$, $c\delta\dot{t}_{u_2u_1}$ are excluded in Eq. (2.77)-(2.81).

$$y_{\hat{u}_2\hat{u}_1}(t) = C_{\hat{u}}(t)\eta_{u_2u_1}(t) + v_{u_2u_1}(t), \quad \eta_{u_2u_1}(t+1) = \eta_{u_2u_1}(t), \tag{4.4}$$

$$y_{\hat{u}_2\hat{u}_1} \equiv \begin{bmatrix} y_{CA,\hat{u}_2\hat{u}_1} \\ y_{L1,\hat{u}_2\hat{u}_1} \end{bmatrix},\ C_{\hat{u}}^{\hat{p}} \equiv \begin{bmatrix} -G_{\hat{u}_1}^{\hat{p}} & G_{\hat{u}_2}^{\hat{p}} & \mathbf{1} & \mathbf{1} & \mathbf{0} \\ -G_{\hat{u}_1}^{\hat{p}} & G_{\hat{u}_2}^{\hat{p}} & \mathbf{1} & \mathbf{1} & \lambda_1 \boldsymbol{I} \end{bmatrix},\ \eta_{u_2u_1} \equiv \begin{bmatrix} u_1 \\ u_2 \\ c\delta t_{u_2u_1} \\ \delta b_{u_2u_1} \\ N_{L1,u_2u_1} \end{bmatrix}. \quad (4.5)$$

DD-PPP GR Equations for Two Antennas

The DD-PPP observable equations in Eq. (2.93) are utilized for antennas of u_1 and u_2. The Doppler-related DD-based observables $\tilde{\rho}_{DL1,\hat{u}_2\hat{u}_1}^{\hat{q}\hat{p}}$ ($p = 1$, $q = 2, \ldots, n_s$) and unknown parameters $\dot{u}_1$, $\dot{u}_2$ are excluded in Eq. (2.93)-(2.97).

$$y_{\hat{u}_2\hat{u}_1}^{\hat{p}\hat{1}}(t) = C_{\hat{u}}^{\hat{p}\hat{1}}(t)\eta_{u_2u_1}^{p1}(t) + v_{u_2u_1}^{p1}(t), \quad \eta_{u_2u_1}^{p1}(t+1) = \eta_{u_2u_1}^{p1}(t), \quad (4.6)$$

$$y_{\hat{u}_2\hat{u}_1}^{\hat{p}\hat{1}} \equiv \begin{bmatrix} y_{CA,\hat{u}_2\hat{u}_1}^{\hat{p}\hat{1}} \\ y_{L1,\hat{u}_2\hat{u}_1}^{\hat{p}\hat{1}} \end{bmatrix},\ C_{\hat{u}}^{\hat{p}\hat{1}} \equiv \begin{bmatrix} -G_{\hat{u}_1}^{\hat{p}_1\hat{1}_1} & G_{\hat{u}_2}^{\hat{p}_2\hat{1}_2} & \mathbf{0} \\ -G_{\hat{u}_1}^{\hat{p}_1\hat{1}_1} & G_{\hat{u}_2}^{\hat{p}_2\hat{1}_2} & \lambda_1 \boldsymbol{I} \end{bmatrix},\ \eta_{u_2u_1}^{p1} \equiv \begin{bmatrix} u_1 \\ u_2 \\ N_{L1,u_2u_1}^{n_s1} \end{bmatrix}. \quad (4.7)$$

Updating by Constraint Conditions

The constraint conditions are applied to update PPP/DD-PPP estimates as follows. Namely, when we obtain the filtering estimates $\hat{\eta}_{t|t}$ and the error covariance matrix $\Sigma_{\eta_t|t}$, we apply the geometric distance and clock constraint conditions. The PPP algorithms with constraint updating is hereinafter called VPPP ("Very" Precise Point Positioning):

$$d_{ji} = ||u_j - u_i|| + e_{d_{ji}}, \quad (4.8)$$

$$c\delta t_j - c\delta t_i = e_{c\delta t_{ji}}, \quad (4.9)$$

where the measurement error $e_{d_{ji}}$ is assumed as a Gaussian white noise with $e_{d_{ji}} \sim \mathrm{N}(0, r_{d_{ji}})$. We should note that the electrical phase center of an antenna is generally not identically to its geometric center. The phase center can also vary with the direction

of arrival (azimuth and elevation) of the signal and such variation can range from under a millimeter to 1 cm∼2 cm, depending upon antenna design. Usually the phase center variation is treated as measurement noise [26], and $e_{d_{ji}}$ and $e_{c\delta_{ji}}$ are mutually independent Gaussian white noises with

$$e_{d_{ji}} \sim \mathrm{N}(0, r_{d_{ji}}), \quad e_{c\delta t_{ji}} \sim \mathrm{N}(0, r_{c\delta t_{ji}}). \tag{4.10}$$

In the case of $n_r = 2$, define the constraint conditions at time t:

$$\gamma_{21,t} \equiv \begin{bmatrix} d_{21} \\ c\delta t_1 \end{bmatrix}, \tag{4.11}$$

and consider the following relations of the conditional probability density function (CPDF):

$$\begin{aligned} p(\eta_t|Y^t, \gamma_{21,t}) &= \frac{p(\eta_t, Y^t, \gamma_{21,t})}{p(Y^t, \gamma_{21,t})} = \frac{p(\eta_t, \gamma_{21,t}|Y^t)p(Y^t)}{p(Y^t, \gamma_{21,t})} \\ &= \frac{p(\gamma_{21,t}|\eta_t, Y^t)p(\eta_t|Y^t)p(Y^t)}{p(Y^t, \gamma_{21,t})} \\ &= \frac{p(Y^t)}{p(Y^t, \gamma_{21,t})} p(\eta_t|Y^t)p(\gamma_{21,t}|\eta_t, Y^t) \\ &\equiv K_0(Y^t, \gamma_{21,t})p(\eta_t|Y^t)p(\gamma_{21,t}|\eta_t), \end{aligned} \tag{4.12}$$

$$Y^t \equiv \{y_0, y_1, \cdots, y_t\}, \; K_0(Y^t, \gamma_{21,t}) \equiv \frac{p(Y^t)}{p(Y^t, \gamma_{21,t})}.$$

Then we have relations:

$$p(\eta_t|Y^t) = \frac{1}{(2\pi)^{n'/2}|\Sigma_{\eta,t|t}|^{1/2}} \exp\Big\{ -\frac{1}{2}[\eta_t - \hat{\eta}_{t|t}]^{\mathrm{T}} \Sigma_{\eta,t|t}^{-1} [\eta_t - \hat{\eta}_{t|t}] \Big\}, \tag{4.13}$$

$$\begin{aligned} p(\gamma_{21,t}|\eta_t) &= \frac{1}{\sqrt{2\pi r_{d_{21}}}} \exp\Big\{ -\frac{[d_{21} - ||u_2 - u_1||]^2}{2r_{d_{21}}} \Big\} \\ &\quad \times \frac{1}{\sqrt{2\pi r_{c\delta t_{21}}}} \exp\Big\{ -\frac{(c\delta t_2 - c\delta t_1)^2}{2r_{c\delta t_{21}}} \Big\}. \end{aligned} \tag{4.14}$$

Therefore, $p(\eta_t|Y^t, \gamma_{21,t})$ in Eq. (4.12) is expressed as follows:

$$\begin{aligned} p(\eta_t|Y^t, \gamma_{21,t}) = K_0(Y^t, \gamma_{21,t}) & \frac{1}{(2\pi)^{n'/2}|\Sigma_{\eta,t|t}|} \\ & \times \exp\Big\{ -\frac{1}{2}[\eta_t - \hat{\eta}_{t|t}]^{\mathrm{T}} \Sigma^{-1}_{\eta,t|t}[\eta_t - \hat{\eta}_{t|t}]\Big\} \\ & \times \frac{1}{\sqrt{2\pi r_{d_{21}}}} \exp\Big\{ -\frac{[d_{21} - ||u_2 - u_1||]^2}{2r_{d_{21}}}\Big\} \\ & \times \frac{1}{\sqrt{2\pi r_{c\delta t_{21}}}} \exp\Big\{ -\frac{(c\delta t_2 - c\delta t_1)^2}{2r_{c\delta t_{21}}}\Big\}. \end{aligned} \tag{4.15}$$

Then we remark that the constraints is expressed by the quadratic form of η as follows:

$$\begin{aligned} \frac{[d_{21} - ||u_2 - u_1||]^2}{2r_{d_{21}}} &= \frac{1}{2r_{d_{21}}}\Big\{ d_{21}^2 + ||u_2 - u_1||^2 - 2d_{21}||u_2 - u_1||\Big\} \\ &= \frac{1}{2r_{d_{21}}}\Big\{ d_{21}^2 + (u_2 - u_1)^{\mathrm{T}}(u_2 - u_1) - 2d_{21}||u_2 - u_1||\Big\} \\ &\cong \frac{1}{2}\Big\{ \frac{d_{21}^2}{r_{d_{21}}} + \frac{1}{r_{d_{21}}}u_2^{\mathrm{T}}u_2 - \frac{1}{r_{d_{21}}}u_2^{\mathrm{T}}u_1 - \frac{1}{r_{d_{21}}}u_1^{\mathrm{T}}u_2 + \frac{1}{r_{d_{21}}}u_1^{\mathrm{T}}u_1 - c_{21}^{\mathrm{T}}u_2 + c_{21}^{\mathrm{T}}u_1\Big\}, \end{aligned} \tag{4.16}$$

where

$$||u_2 - u_1|| \cong \frac{(\hat{u}_2 - \hat{u}_1)^{\mathrm{T}}}{||\hat{u}_2 - \hat{u}_1||^2}(u_2 - u_1) \equiv \kappa_{21}^{\mathrm{T}}(u_2 - u_1), \tag{4.17}$$

and

$$d_{\kappa 21}^{\mathrm{T}} \equiv \frac{2d_{21}\kappa_{21}^{\mathrm{T}}}{r_{d_{21}}}. \tag{4.18}$$

Also we have

$$\frac{(c\delta t_2 - c\delta t_1)^2}{2r_{c\delta t_{21}}} = \frac{1}{2}[c_{r21}(c\delta t_2)^2 + c_{r21}(c\delta t_1)^2 - 2c_{r21}(c\delta t_2)(c\delta t_1)], \tag{4.19}$$

where

$$c_{r21} \equiv \frac{1}{r_{c\delta t_{21}}}.$$

Finally, we have the expression of the quadratic form:

$$\frac{1}{2}\frac{[d_{21}-||u_2-u_1||]^2}{r_{d_{21}}}+\frac{1}{2}\frac{(c\delta t_2-c\delta t_1)^2}{r_{c\delta t_{21}}}\cong\frac{1}{2}\{\eta^{\mathrm{T}}M_{\eta_{21}}\eta+c_{\eta_{21}}^{\mathrm{T}}\eta+\frac{d_{21}^2}{r_{d_{21}}}\},\qquad(4.20)$$

where therefore, we have the following quadratic form for the power term of the CPDF (4.15):

$$\begin{aligned}
&\frac{1}{2}(\eta-\ \hat{\eta}\ )\Sigma_\eta^{-1}(\eta-\hat{\eta})+\frac{1}{2}\frac{[d_{21}-||u_2-u_1||]^2}{r_{d_{21}}}+\frac{1}{2}\frac{(c\delta t_2-c\delta t_1)^2}{2rc\delta t_{21}}\\
&\quad\cong\frac{1}{2}\Big\{\eta^{\mathrm{T}}\Sigma_\eta^{-1}\eta-\eta^{\mathrm{T}}\Sigma_\eta^{-1}\hat{\eta}-\hat{\eta}^{\mathrm{T}}\Sigma_\eta^{-1}\eta+\hat{\eta}^{\mathrm{T}}\Sigma_\eta^{-1}\hat{\eta}+\eta^{\mathrm{T}}M_{\eta_{21}}\eta+c_{\eta_{21}}^{\mathrm{T}}\eta+\frac{d_{21}^2}{r_{d_{21}}}\Big\}\\
&\quad=\frac{1}{2}\Big\{\eta^{\mathrm{T}}(\Sigma_\eta^{-1}+M_{\eta_{21}})\eta-\eta^{\mathrm{T}}(\Sigma_\eta^{-1}\hat{\eta}-\frac{1}{2}c_{\eta_{21}})-(\hat{\eta}^{\mathrm{T}}\Sigma_\eta^{-1}-\frac{1}{2}c_{\eta_{21}})\eta+\hat{\eta}^{\mathrm{T}}\Sigma_\eta^{-1}\hat{\eta}+\frac{d_{21}^2}{r_{d_{21}}}\Big\}\\
&\quad=\frac{1}{2}\Big\{[\eta-(\Sigma_\eta^{-1}+M_{\eta_{21}})^{-1}(\Sigma_\eta^{-1}\hat{\eta}-\frac{1}{2}c_{\eta_{21}})]^{\mathrm{T}}(\Sigma_\eta^{-1}+M_{\eta_{21}})\\
&\qquad\times[\eta-(\Sigma_\eta^{-1}+M_{\eta_{21}})^{-1}(\Sigma_\eta^{-1}\hat{\eta}-\frac{1}{2}c_{\eta_{21}})]-(\Sigma_\eta^{-1}\hat{\eta}-\frac{1}{2}c_{\eta_{21}})^{\mathrm{T}}(\Sigma_\eta^{-1}+M_{\eta_{21}})^{-1}\\
&\qquad(\Sigma_\eta^{-1}\hat{\eta}-\frac{1}{2}c_{\eta_{21}})+\hat{\eta}^{\mathrm{T}}\Sigma^{-1}\hat{\eta}+\frac{d_{21}^2}{r_{d_{21}}}\Big\}.
\end{aligned}$$

Then the update estimated vector $\check{\eta}$ and error covariance matrix $\check{\Sigma}_\eta$ of η based on the minimum mean square estimate are given by

$$\check{\eta}_{21}=\left(\Sigma_{\eta_{21}}^{-1}+M_{\eta_{21}}\right)^{-1}(\Sigma_{\eta_{21}}^{-1}\hat{\eta}_{21}-\frac{1}{2}c_{\eta_{21}}),\qquad(4.21)$$

$$\check{\Sigma}_{\eta_{21}}=\left(\Sigma_{\eta_{21}}^{-1}+M_{\eta_{21}}\right)^{-1}.\qquad(4.22)$$

In the case of VPPP under two independent PPP positioning,

$$M_{\eta_{21}}\equiv\left[\begin{array}{ccc|ccc}
\frac{1}{r_{d_{21}}}I & & & -\frac{1}{r_{d_{21}}}I & & \\
& c_{r21} & & & -c_{r21} & \\
& & O_{n_s+3} & & & O_{n_s+3}\\
\hline
-\frac{1}{r_{d_{21}}}I & & & \frac{1}{r_{d_{21}}}I & & \\
& -c_{r21} & & & c_{r21} & \\
& & O_{n_s+3} & & & O_{n_s+3}
\end{array}\right],\qquad(4.23)$$

$$c_{\eta_{21}}^{\mathrm{T}}\equiv\left[\begin{array}{cc|cc} d_{\kappa 21}^{\mathrm{T}} & 0_{n_r+4}^{\mathrm{T}} & -d_{\kappa 21}^{\mathrm{T}} & 0_{n_r+4}^{\mathrm{T}}\end{array}\right],\qquad(4.24)$$

O_{n_s+3} is the $(n_s+3)\times(n_s+3)$ zero matrix, and 0_{n_s+4} is the (n_s+4) zero vector.

In the case of constraint updating under DD-PPP positioning, the receiver clock errors $c\delta t_2$ and $c\delta t_1$ are canceled. The clock-related constraint c_{r21} therefore is unnecessary.

$$M_{\eta 21} \equiv \left[\begin{array}{ccc|ccc} \frac{1}{r_{d21}}I & & -\frac{1}{r_{d21}}I & 0 & \cdots & 0 \\ -\frac{1}{r_{d21}}I & & \frac{1}{r_{d21}}I & 0 & \cdots & 0 \\ \hline 0 & \cdots & 0 & 0 & \cdots & 0 \\ \vdots & & \vdots & & \vdots & \\ 0 & \cdots & 0 & 0 & \cdots & 0 \end{array}\right], \tag{4.25}$$

$$c_{\eta 21}^{\mathrm{T}} \equiv \left[\begin{array}{ccccc} d_{\kappa 21}^{\mathrm{T}} & -d_{\kappa 21}^{\mathrm{T}} & 0^{\mathrm{T}} & \cdots & 0^{\mathrm{T}} \end{array}\right]. \tag{4.26}$$

In the cases of $n_r = 3$ and $n_r = 4$, see Appendix A.

These updated values are applied to Eqs. (2.120) and (2.124), respectively, as

$$\hat{\eta}_{t|t} \equiv \check{\eta}, \quad \hat{\Sigma}_{\eta,t|t} \equiv \check{\Sigma}_{\eta}.$$

Additional constraints

See Appendix C.

4.3 Experiments

We carried out the comparison of positioning methods by using the GPS data obtained under the experimental conditions (see Table 4.1). Single-frequency and economical u-blox GPS receiver NEO-M8N and patch antennas (ANTs) for automobile were used for the experiments. The antennas ANT-$1, 2, 3, 4$ were located at the corners of a square board (see Fig. 4.1), and the coordinates of their positions in the WGS84 system are listed in Table 4.2. The positioning errors applying the relative positioning method are less than

a few centimeters, and the positions are used to evaluate the proposed positioning as reference positions. Receivers connected to ANT-1 and 2, or receivers connected to ANT-3 and 4 are operated by synchronized clocks, respectively. ANT-1 and 4 are reference antennas for SD/DD-based positioning methods. ANT-X is the antenna for two frequency topographic surveying GNSS receiver, and located on the center of the square board.

Table 4.1: Experimental Conditions

Date	March 8, 2015
GPS-Time	06:00:00〜06:10:00
Location	Biwako Kusatsu Campus, Ritsumeikan Univ.
Antenna(ANT)	INPAQ patch antenna for automobile
Receiver	u-blox GPS-module NEO-M8N (FW2.0)
Epoch interval	1 [s]
Elevation angle mask	15 [deg.]
Measurement Data	C/A Code Pseudorange, L1-Carrier-Phase

Table 4.3 shows the DD-PPP/VPPP positioning conditions. The state variables, namely antenna positions and integer ambiguity, are estimated by Kalman filter as unknown parameters. The initial values of the positions are obtained by SPP, and affect the positioning accuracy. The broadcast ephemeris and Klobucher parameters obtained from navigation messages are utilized as the SPP conditions. The data provided by international GNSS service (IGS) are not effective for improving the SPP. The noise variances for Kalman filtering are decided under the better positioning results.

Table 4.4 shows the positioning methods (a)-(f). The methods (e) and (f) utilize SD-based observables which can cancel the satellite, ionosphere, and troposphere-related errors. The methods (c) and (d) utilize DD-based observables which can additionally cancel the receiver-related errors. On the contrary, the methods (a) and (b) utilize the broadcast messages for satellites and the signal delay models for ionosphere or troposphere, and es-

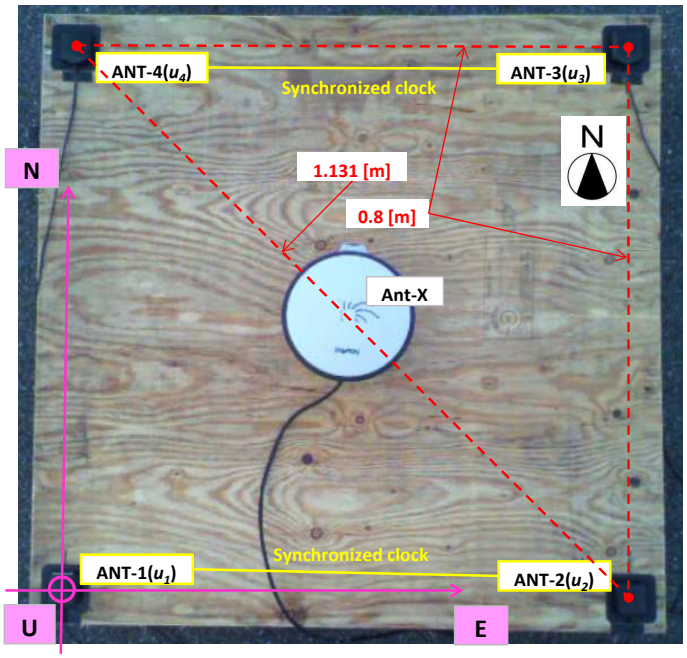

Figure 4.1: GNSS antenna array on a square board

Table 4.2: Real antennas positions by relative positioning

	WGS-84		
	X [m]	Y [m]	Z [m]
ANT-1	-3761236.152	3636879.281	3635962.036
ANT-2	-3761236.711	3636878.709	3635962.020
ANT-3	-3761236.392	3636878.384	3635962.676
ANT-4	-3761235.833	3636878.954	3635962.689

timate the receiver-related errors. All methods (a)-(f) estimate the integer ambiguity of raw, SD, and DD-based carrier-phase, respectively. The constraint of geometric distance among antennas are applied to the methods (b),(d), and (f).

Fig. 4.2 shows the concept of the positioning (a), (b), (c), (d) when two antennas ANT-1 (u_1), 2 (u_2) are used, and the positioning (c2), (d2) when four antennas ANT-1 (u_1), 2 (u_2), 3 (u_3), 4 (u_4) are used. (a)PPP is individually applied for each antenna to estimate each antenna position. (b)VPPP additionally utilizes the updating algorithm by geometric

distance constraint (GDC) on (a). (c)DD-PPP utilizes the DD-based observables (DDO) for a pair of two antennas. (d)DD-VPPP additionally utilizes the updating algorithm by GDC on (c). (c2)DD-PPP utilizes DDOs for six pairs of two antennas. (d2)DD-VPPP additionally utilizes the updating algorithm by GDCs of six pairs of two antennas on (c2).

Table 4.3: DD-PPP/VPPP positioning conditions

State variables	Initial values [m]	Initial variance [m^2]
Antenna positions	SPP	1^2
Integer ambiguity	DD of $(\phi - \rho - 2\tilde{\delta}I)$	10^2
SPP conditions		
Satellite orbits/clocks	Broadcast ephemeris (IGS)	
Ionosphere models	Klobucher (IGS)	
Troposphere models	Saastamoinen	
	Noise variance [m^2]	
C/A code pseudoranges	0.3^2	
Carrier-phase pseudoranges	0.08^2	
Satellite orbits	0.05^2	
Satellite clocks	0.03^2	
Geometric distance	0.01^2	

4.3.1 Comparison of PPP/VPPP/DD-PPP/DD-VPPP

The positioning experiments of (a) PPP and (b) VPPP for two methods; without differences of C/A code and L1 carrier-phase observables in [23],[24] (call WOD-methods), and the presently proposed (c) DD-PPP and (d) DD-VPPP by taking double differences for observables (call DD-methods), are carried out by applying the Kalman filter formulation under static positioning conditions.

Fig. 4.3 shows the positioning errors for the ANT-1 (u_1) and 2 (u_2), respectively, using GPS observables in 06:00:00 - 06:00:59 (60 epochs) by the DD-methods with the local level axes (ENU: East, North, and Height(Up)), where the blue and red lines show the ENU errors of (c) DD-PPP and (d) DD-VPPP results, respectively. The errors are computed

Table 4.4: Positioning methods

	(a)	(b)	(c)	(d)	(e)	(f)
Positioning methods	PPP	VPPP	DD-PPP	DD-VPPP	SD-PPP	SD-VPPP
Satellite orbit	Broadcast					
Satellite clock error	Broadcast					
Satellite H/W bias	Negligible		Canceled by SD			
Ionospheric delay	Klobuchar					
Tropospheric delay	Magnavox					
Estimation method	Kalman filter					
Antenna position	Static					
Receiver H/W bias	1st-order Markov		Canceled by DD		1st-order Markov	
Receiver clock bias	1st-order Markov				1st-order Markov	
Integer ambiguity	Random walk					
Distance constraint	–	O	–	O	–	O

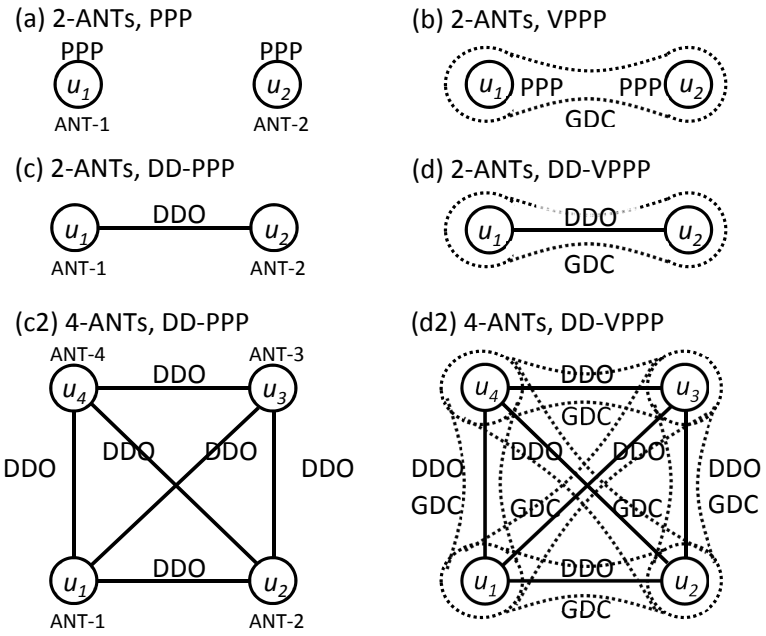

Figure 4.2: Positioning concept for two and four antennas

by difference between each estimated position and the corresponding position shown in Table 4.2. We can observe from Fig. 4.3 that the positioning quality is slightly improved by using VPPP (using the geometric constraints), and (d) DD-VPPP just needs several seconds after the positioning start to reach the fixed position. The RMSE (Root Mean

Square Error) of ENU coordinate is defined as follows:

$$RMSE = \sqrt{\frac{1}{n_r}\frac{1}{n_e}\sum_{i=1}^{n_r}\sum_{t=1}^{n_e}\left((E_{e,i,t}^2 + N_{e,i,t}^2 + U_{e,i,t}^2)/3\right)} \tag{4.27}$$

where n_e denotes the number of epochs. $E_{e,i,t}, N_{e,i,t}, U_{e,i,t}$ means the ENU errors of antenna i at epoch t, respectively. The RMSE of 60 epochs (n_e=60) Eastward, Northward, Upward errors at the individual antenna (n_r=1) in Fig. 4.3 are shown in Table 4.5. The 2 ANTs horizontal ENU RMS errors of (d) DD-VPPP1 is slightly better than that of (c) DD-PPP, and the improvement ratio of the errors from (c) to (d) is approximately 88 %.

Fig. 4.4 shows the RMS errors of PPP and VPPP ENU coordinate by WOD (a),(b) and DD-methods (c),(d) which utilize two antennas, ANT-1 and ANT-2. The vertical axis shows the RMS errors of two antennas (n_r=2) after 10 seconds (tenth epoch) from the positioning start (n_e=1) in Eq. (4.27). The horizontal axis shows sequential numbers of experiments. The experiments for the comparison of four positioning methods (a),(b),(c),(d) are repeated 10 times during 06:00:00 - 06:10:00 (GPST) every 1 minute. The results show the RMS errors of estimated positions after 10 seconds from the positioning starts, which are 60(k-1)+10 (k=1∼10: the sequential number) seconds from 06:00:00. Basically, the RMS errors of u-blox NEO-M8 GPS positioning are approximately 2.5-m CEP (Circular Error Probability) [45], while the errors of the four positioning methods are less than 1.5 m. There are some fluctuations among estimated positions, because the priori initial estimations by SPP (Standard Point Positioning) are used as the antennas' position for Kalman filter, however, (d) DD-VPPP has the smallest RMS errors. The total improvement ratio from (a) PPP to (d) DD-VPPP is approximately 84 %.

(e) SD-PPP and (f) SD-VPPP approximately have the same RMS errors as (c) DD-PPP and (d) DD-VPPP, respectively, because the clock error difference of receivers con-

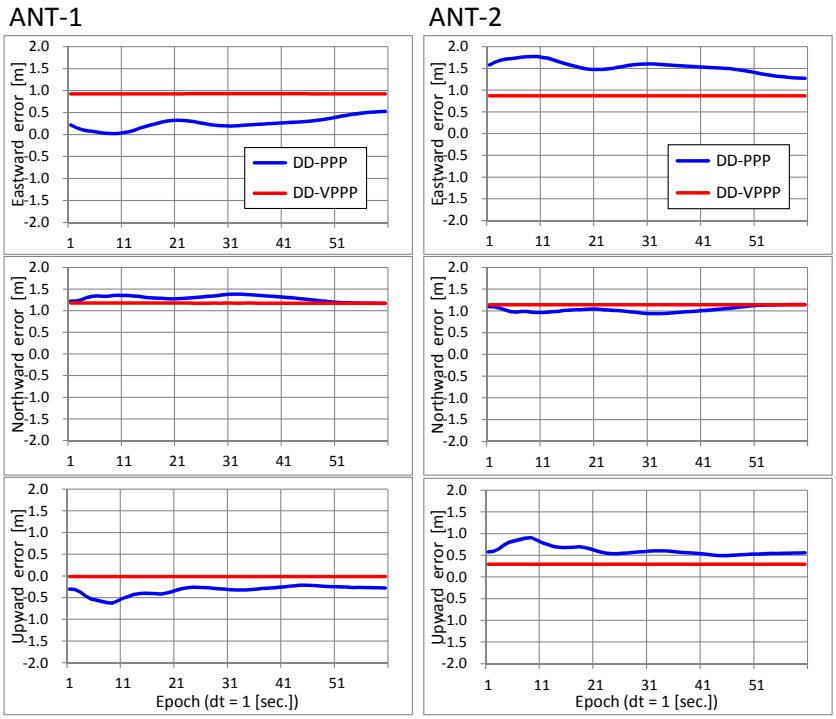

Figure 4.3: ENU errors of ANT-1 and ANT-2

Table 4.5: RMS errors of DD-methods

			[m]	RMS[m]	
				EN	ENU
ANT-1	(c) DD-PPP	E	0.3619	0.9116	0.7801
		N	1.2374		
		U	0.4046		
	(d) DD-VPPP	E	0.9374	1.0550	0.8616
		N	1.1608		
		U	0.0294		
ANT-2	(c) DD-PPP	E	1.4710	1.2933	1.1272
		N	1.0880		
		U	0.6815		
	(d) DD-VPPP	E	0.8643	1.0240	0.8552
		N	1.1619		
		U	0.3116		
Total (2-ANTs)	(c) DD-PPP	-	–	1.1188	0.9693
	(d) DD-VPPP	-	–	1.0396	0.8584

nected to the ANT-1 and 2 operated by synchronized clock has little influence on the SD/DD-based positioning. The DD-based positioning approximately has the same perfor-

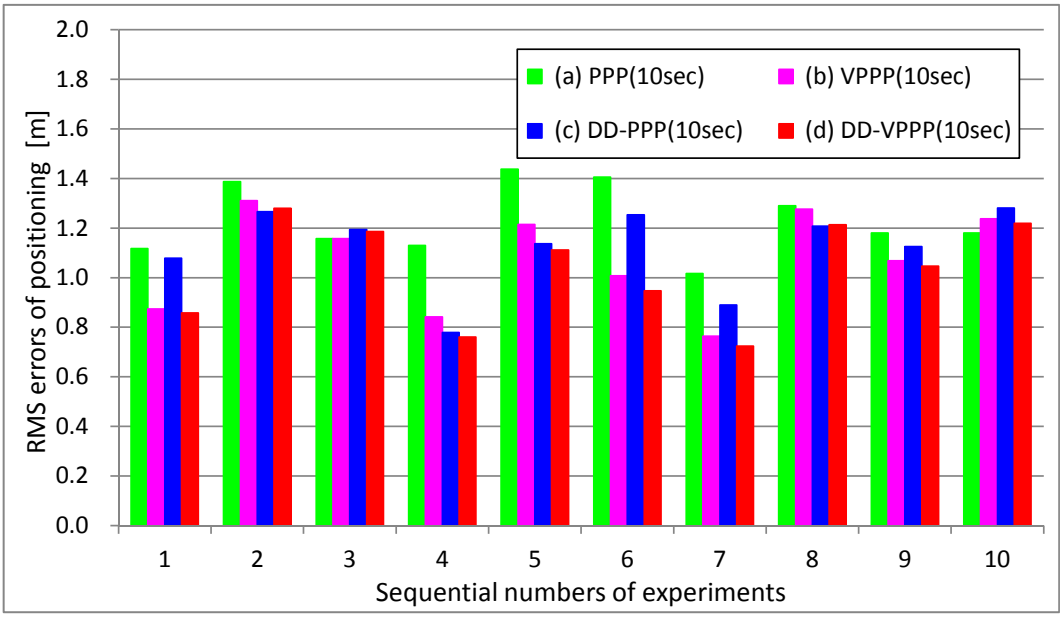

Figure 4.4: RMS errors of four positioning methods

Table 4.6: Improvement ratio of DD-VPPP

			RMS error [m]				Improvement ratio [%]	
	Start time	Sampled time	(a) PPP	(b) VPPP	(c) DD-PPP	(d) DD-VPPP	(d) / (a)	(d) / (b)
1	6:00'00	6:00'10	1.1171	0.8736	1.0783	0.8574	76.7	98.1
2	6:01'00	6:01'10	1.3877	1.3110	1.2658	1.2797	92.2	97.6
3	6:02'00	6:02'10	1.1570	1.1574	1.1941	1.1858	102.5	102.5
4	6:03'00	6:03'10	1.1300	0.8416	0.7789	0.7595	67.2	90.3
5	6:04'00	6:04'10	1.4372	1.2139	1.1363	1.1111	77.3	91.5
6	6:05'00	6:05'10	1.4057	1.0071	1.2537	0.9475	67.4	94.1
7	6:06'00	6:06'10	1.0161	0.7637	0.8899	0.7236	71.2	94.7
8	6:07'00	6:07'10	1.2895	1.2760	1.2075	1.2131	94.1	95.1
9	6:08'00	6:08'10	1.1806	1.0681	1.1253	1.0465	88.6	98.0
10	6:09'00	6:09'10	1.1801	1.2368	1.2812	1.2188	103.3	98.5
	Average		1.230	1.075	1.121	1.034	84.1	96.0

mance even in the case of ANT-1 and 4 operated by desynchronized clock, however, the SD-based positioning has a high probability of performance degradation.

4.3.2 Comparison of the Number of Antennas and Constraints

In order to compare the positioning accuracy by the number of antennas and constraints, we carried out the 24-hours static positioning by using four low-cost single-frequency GPS receivers (four antennas) obtained under the experimental conditions (see

Table 4.7). Compared with the conditions in Table 4.1, the same antennas and receivers NEO-M8N are used, however, the firmware version FW3.1 is different from FW2.0. The antennas ANT-1, 2, 3, 4 were located at the corners of a square, 80 cm on a side on the rooftop of the vehicle, and the coordinates of their positions in the WGS84 system are listed in Table 4.8, and they are also obtained by the relative positioning method. Each receiver is operated by its individual clock because of the receiver clock offset cancellations by the DD-based positioning technique among receivers. Fig. 4.5 shows the GPS satellite

Table 4.7: Experimental Conditions

Date	February 13-14, 2017
GPS-Time	03:00:00〜02:59:59 (24-hours)
Location	Sanda works, Mitsubishi Electric Corp.
Antenna(ANT)	INPAQ patch antenna for automobile
Receiver	u-blox GPS-module NEO-M8N (FW3.1)
Epoch interval	1 [s]
Elevation angle mask	10 [deg.]
Measurement Data	C/A Code Pseudorange, L1-Carrier-Phase

Table 4.8: Real antennas positions by relative positioning

	WGS-84		
	X [m]	Y [m]	Z [m]
ANT-1	-3717933.028	3688815.774	3628264.294
ANT-2	-3717933.658	3688815.561	3628263.855
ANT-3	-3717933.790	3688814.943	3628264.343
ANT-4	-3717933.164	3688815.161	3628264.785

constellations every 2-hours based on the observables obtained by the 24-hours GPS static positioning. In general, the orbits of GPS satellites are nearly circular, and the orbital period is approximately 11 hours and 58 minutes. Each satellite approximately goes around the earth two times a day, and the rotation of the earth is 24-hours. The satellites return again to the first positions after 24-hours. Fig. 4.6 shows the Eastward/Northward (EN)

errors of NEO-M8N positioning every 2-hours during 24-hours. According to the u-blox product catalog [45], the errors of NEO-M8N GPS positioning are approximately 2.5-m CEP (Circular Error Probability). The EN errors of the positioning results in Fig. 4.6 shows approximately less than 2.5 m from the average positioning accuracy, however, the average values tend to have northward offsets. The tendency is generally caused by the GPS satellite constellations. Fig. 4.7 shows the Upward (U) errors of NEO-M8N positioning every 2-hours during 24-hours. In general, the upward errors of the positioning is worse than the EN errors, because the only satellites above the horizon can be acquired by the receivers and utilized for the positioning. Fig. 4.7 shows that the downward errors of more than 4 m frequently occur. Table. 4.9 shows the EN and the ENU RMS errors of SPP for four antennas every 2-hours. The SPP results of the antenna positions are obtained by GR models and utilized as the initial values for the positioning (a)-(f).

Fig. 4.8 shows the RMS errors of (c) DD-PPP and (d) DD-VPPP on ENU and EN coordinate by using the two antennas ANT-$1, 4$ or the four antennas ANT-$1, 2, 3, 4$. In the case of two antennas, the DD-based observables and the distance constraint d_{21} in Eq. (4.8) by one pair of ANT-$1, 4$ are utilized for the positioning. In the case of four antennas, the DD-based observables and the distance constraints d_{21}, d_{31}, d_{41}, d_{32}, d_{42}, d_{43} in Eq. (4.8) by six pairs of ANT-1,-2, ANT-1,-3, ANT-1,-4, ANT-2,-3, ANT-2,-4, ANT-3,-4 are utilized for the positioning. The vertical axis shows the RMS errors of two antennas (n_r=2) or four antennas (n_r=4) after 10 seconds (tenth epoch) from the positioning start (n_e=1) in Eq. (4.27). The horizontal axis shows sequential numbers of experiments. The experiments for the comparison of two positioning methods (c) and (d) are repeated 120 times during 13:00:00 - 14:59:59 (GPST) or during 17:00:00 - 18:59:59 (GPST) every 1 minute, respectively. The former time period has the smallest RMS errors of the total four antennas'

SPP, and the latter time period has the biggest RMS errors of the total four antennas' SPP in Table 4.9. The results show the RMS errors of estimated positions after 10 seconds from the positioning starts, which are 60(k-1)+9 (k=1∼120: the sequential number) seconds from the start time 13:00:00 or 17:00:00.

There are some fluctuations among the RMS positioning errors, because the fluctuations of SPP affect the positioning accuracy as the priori initial estimations of the antennas' position for the Kalman filter. Some of the RMS errors on EN coordinates are approximately less than 20 cm∼30 cm. The 4-ANTs, DD-PPP(blue)/VPPP(red), EN has less fluctuations compared with the 2-ANTs, DD-PPP/VPPP, EN. Table 4.10 shows the average RMS errors and the improvement ratio (120-times) in Fig 4.8. Basically, the errors of u-blox NEO-M8 GPS positioning are approximately 2.5-m CEP (Circular Error Probability) [45], while the average RMS errors in all cases are approximately less than 1.5 m, and 4-ANTs, DD-VPPP, EN has the smallest RMS errors which are approximately 50∼60 cm. Although the time period 17:00:00 - 18:59:59 (GPST) has the bigger ENU RMS errors of SPP, the 4-ANTs, DD-VPPP, EN has almost the same average RMS errors as that of the smallest time period 13:00:00 - 14:59:59 (GPST), because the upward errors of SPP cause the difference of the positioning RMS errors between the both time periods. The improvement ratio of the EN RMS errors in the 4-ANTs case are approximately 68 %.

One of the causes to affect the SPP accuracy is the ionosphere delay parameters of the Klobuchar model [46] in the navigation messages from satellites. The model parameters simulate the changes of the zenith directional ionosphere delays for a day by the cosine curve. The GPS parameters can improve the ionospheric bias errors, 4 m∼5 m, which is the biggest cause of the positioning errors by approximately 50 %. The QZSS also broadcasts the original parameters, the altitude positioning errors can be improved more than

GPS in Japan and the areas surrounding Japan. The difference between GPS and QZSS parameters does not appear during the time period 11:00:00 - 23:00:00 (GPST) in Table 4.9, because the cosine curve of the Klobuchar model does not get involved in the period.

Fig. 4.9 shows an example of the four antennas' DD-PPP(blue) /VPPP(red) EN RMS errors compared with the NEO-M8N positioning results(yellow). The positioning period is 20 minutes, 13:50:00 - 14:09:59 (GPST). The DD-PPP/VPPP have smaller positioning fluctuations than NEO-M8N, and the errors tend to have offsets from the real antennas' positions to the same northeastward directions except for the ANT-2. The baseline vectors, namely the differences between two antenna positions, could have smaller errors by canceling the offsets of the two antennas. Table 4.11 shows the RMS errors of three positioning methods in Fig. 4.9. The EN RMS errors of the DD-VPPP is approximately half compared with that of the NEO-M8N.

4.4 Concluding Remarks

In this chapter, we have presented a novel PPP algorithm based on double difference (DD) observables, and the update equations of an improved VPPP algorithm by minimum mean square (MMS) methods based on geometric distance constraints (GDC) of multiple antennas. The updating process based on the constraints are applied to the positioning estimates every epoch in conjunction with the DD-PPP Kalman filtering algorithms.

The experiments of four antennas (receivers) have been carried out in a static situation. The DD-VPPP needs several seconds to reach a fixed position, and has the smallest root-mean-square (RMS) errors among four positioning methods, namely PPP and VPPP of without DD (WOD) and DD-methods when two antennas are used. The total improvement ratio from the conventional PPP method to our proposed DD-VPPP

is approximately 84 %. Furthermore, the DD-based PPP/VPPP algorithms based on GR models have approximately the same positioning performance under the both synchronous or asynchronous clock operation, and easy to be utilized under multiple antenna system which includes asynchronous clock operation compared with SD-based positioning.

The experiments of the 24-hours static positioning by using four low-end single-frequency GPS antennas (receivers) have been carried out. In the case of the RMS errors of two antenna DD-PPP/VPPP, We have achieved less than 40-cm positioning errors on horizontal east-north (EN) coordinate after ten seconds (epochs) from the positioning starts without any external transmitted information. Our proposed DD-VPPP methods are approximately less than half on EN coordinate, and less than 1/4 on east-north-up (ENU) coordinates compared with the low-cost single-frequency u-blox NEO-M8N positioning. In the case of the improvement ratios of the averaged RMS errors from DD-PPP to DD-VPPP, when the antenna numbers are increased from 2-ANTs to 4-ANTs, the ratios are approximately improved from 82 % to 66 % on EN coordinates. The 4-ANTs DD-VPPP has less fluctuations of the RMS errors caused by SPP, because six GDCs are applied to the MMS estimation method of DD-VPPP.

Compared with the positioning results of u-blox NEO-M8N single-frequency receivers without carrier-phase observables, the improvement ratios of the DD-VPPP positioning errors from the NEO-M8N are approximately 70 % as ENU RMS errors, and approximately 50 % as EN RMS errors. The total EN RMS errors of 1200 epochs and four antennas is less than 40 cm. The errors tend to have offsets from the real antennas' positions to the same directions. The baseline vectors, i.e. the differences between two antenna positions, could have smaller errors by canceling the offsets of two antennas.

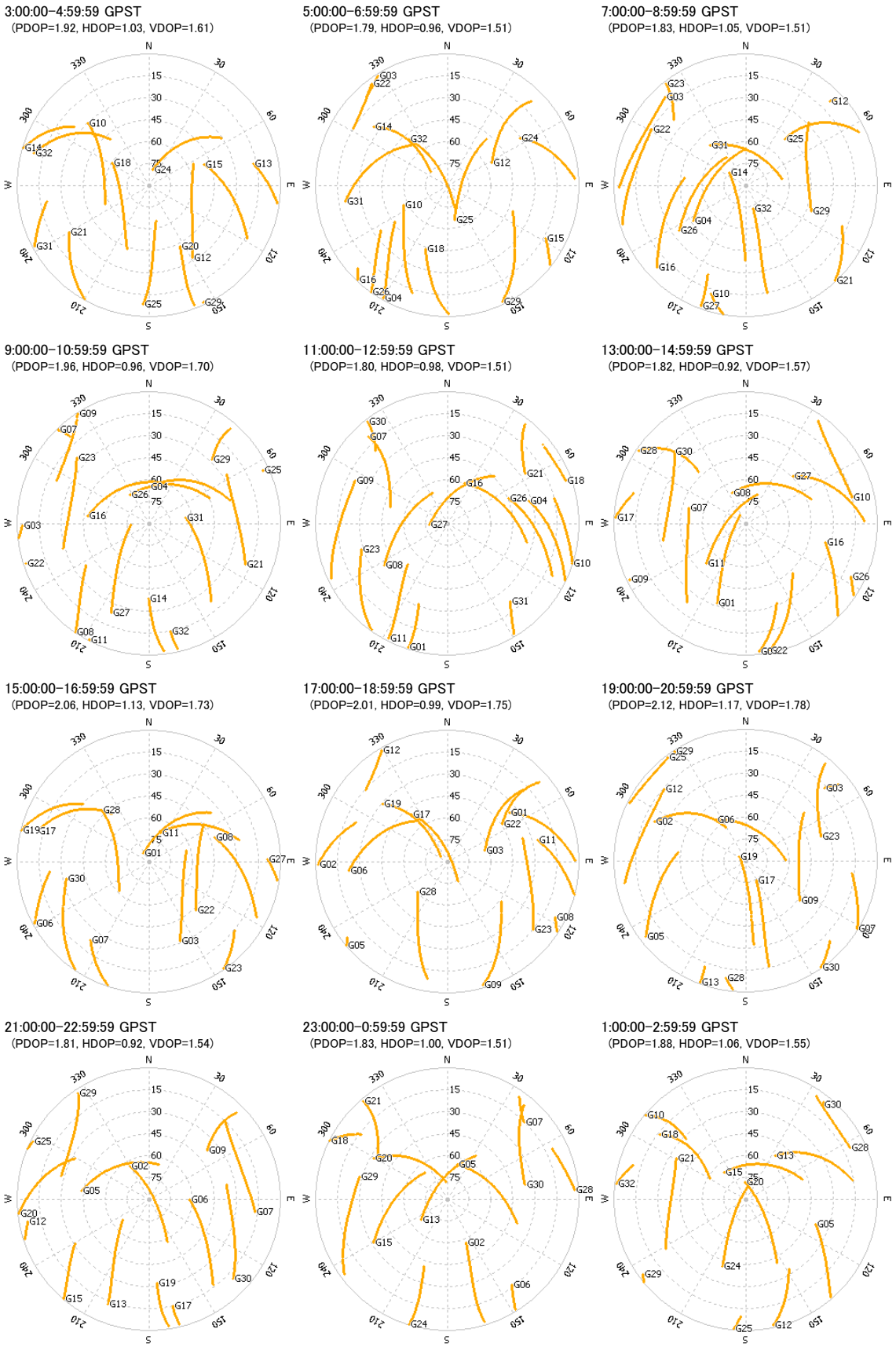

Figure 4.5: GPS satellite constellations during 24-hours

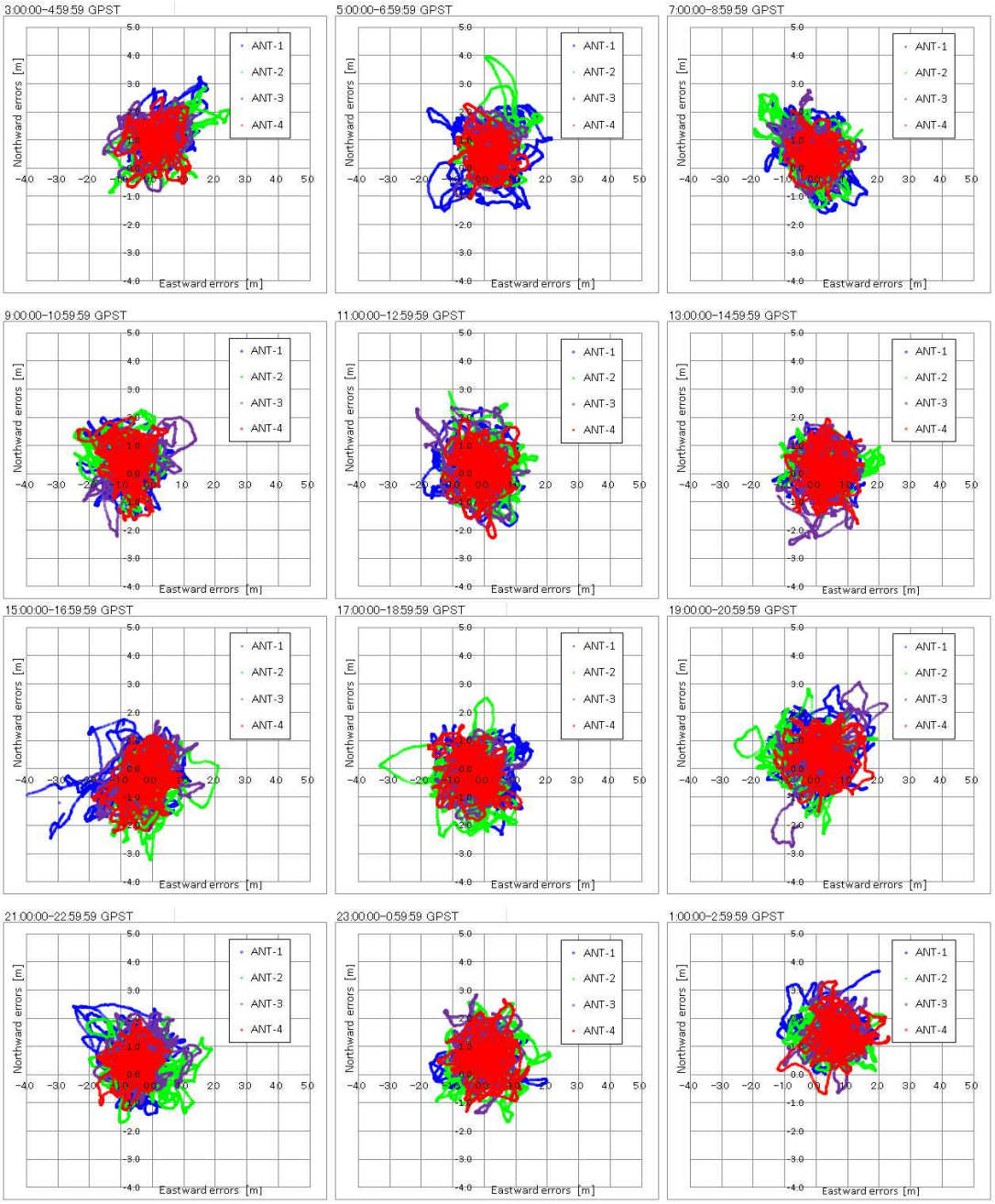

Figure 4.6: Eastward/Northward errors of NEO-M8N positioning during 24-hours

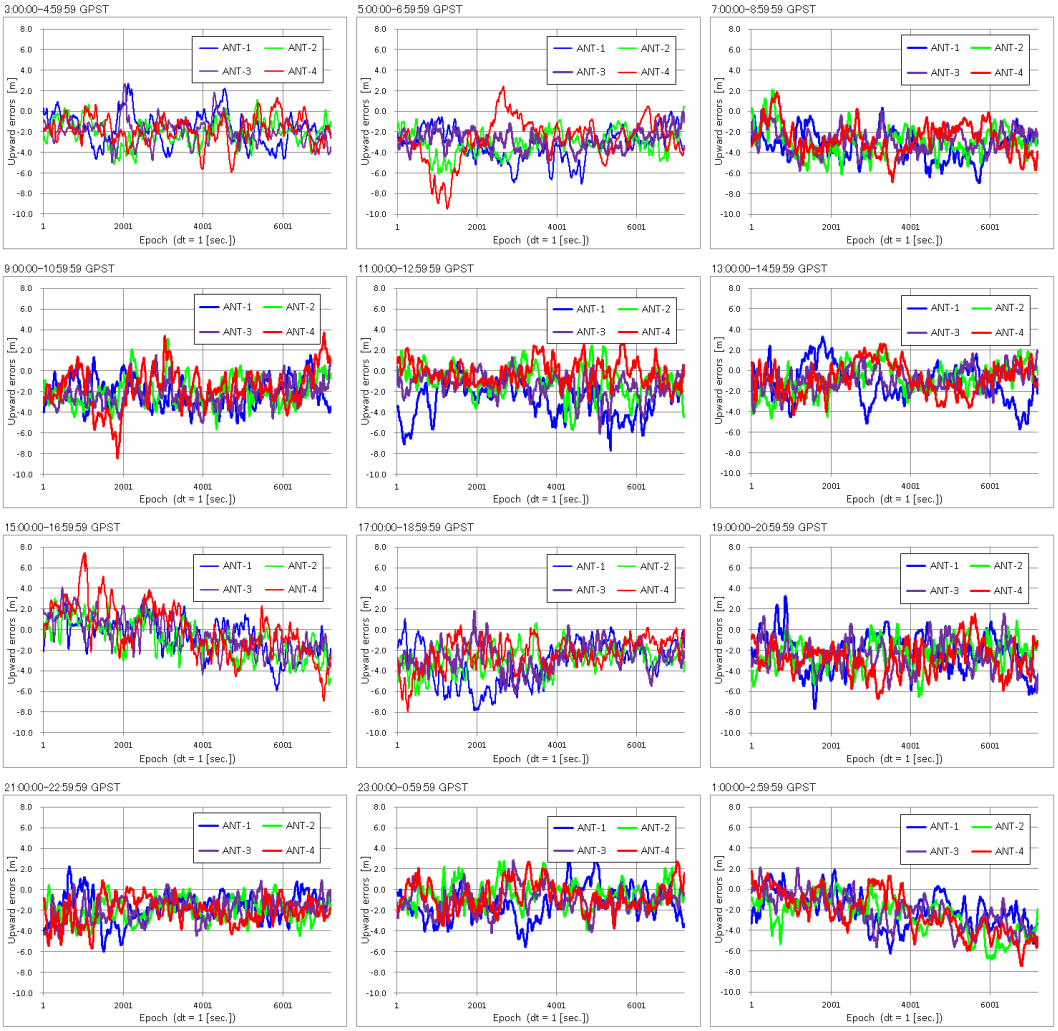

Figure 4.7: Upward errors of NEO-M8N positioning during 24-hours

Table 4.9: EN and ENU RMS errors [m] of SPP for four antennas

Time period (GPST)	ANT-1		ANT-2		ANT-3		ANT-4		Total(4-ANTs)	
	EN	ENU	EN	ENU	EN	ENU	EN	ENU	EN	ENU
03:00:00-05:00:00	1.2348	1.8531	1.1074	1.8779	1.0678	1.7777	0.9493	1.6604	1.0946	1.7943
05:00:00-07:00:00	1.0996	2.3821	0.9701	2.2625	0.8414	2.0950	0.8159	1.9252	0.9386	2.1731
07:00:00-09:00:00	1.0279	2.1424	0.8502	2.3907	0.9195	2.0975	0.7216	2.0057	0.8868	2.1638
09:00:00-11:00:00	1.0486	1.8842	0.9663	1.7747	0.8485	1.5911	0.8207	1.5779	0.9256	1.7118
11:00:00-13:00:00	0.9877	1.3642	0.9008	1.7558	0.9214	1.2651	0.7830	1.2377	0.9013	1.4209
13:00:00-15:00:00	0.7488	1.1816	0.8134	1.2664	0.8433	1.3179	0.7586	1.2254	0.7920	1.2488
15:00:00-17:00:00	1.1336	2.0562	0.9449	1.4207	0.8959	1.5390	0.9272	1.5062	0.9798	1.6495
17:00:00-19:00:00	0.8298	1.9591	0.9448	2.2779	0.7618	1.9974	0.7538	1.9545	0.8261	2.0516
19:00:00-21:00:00	1.0390	2.1567	1.1269	2.0377	1.0447	2.0504	0.9847	2.0176	1.0501	2.0663
21:00:00-23:00:00	1.0774	1.8064	0.9113	1.5961	1.0078	1.7984	0.8721	1.5745	0.9705	1.6973
23:00:00-01:00:00	1.5054	1.8484	1.3202	1.6095	1.4544	1.7142	1.4286	1.5907	1.4288	1.6938
01:00:00-03:00:00	1.4866	2.3697	1.3229	2.0169	1.4721	2.2941	1.4416	2.1319	1.4322	2.2075

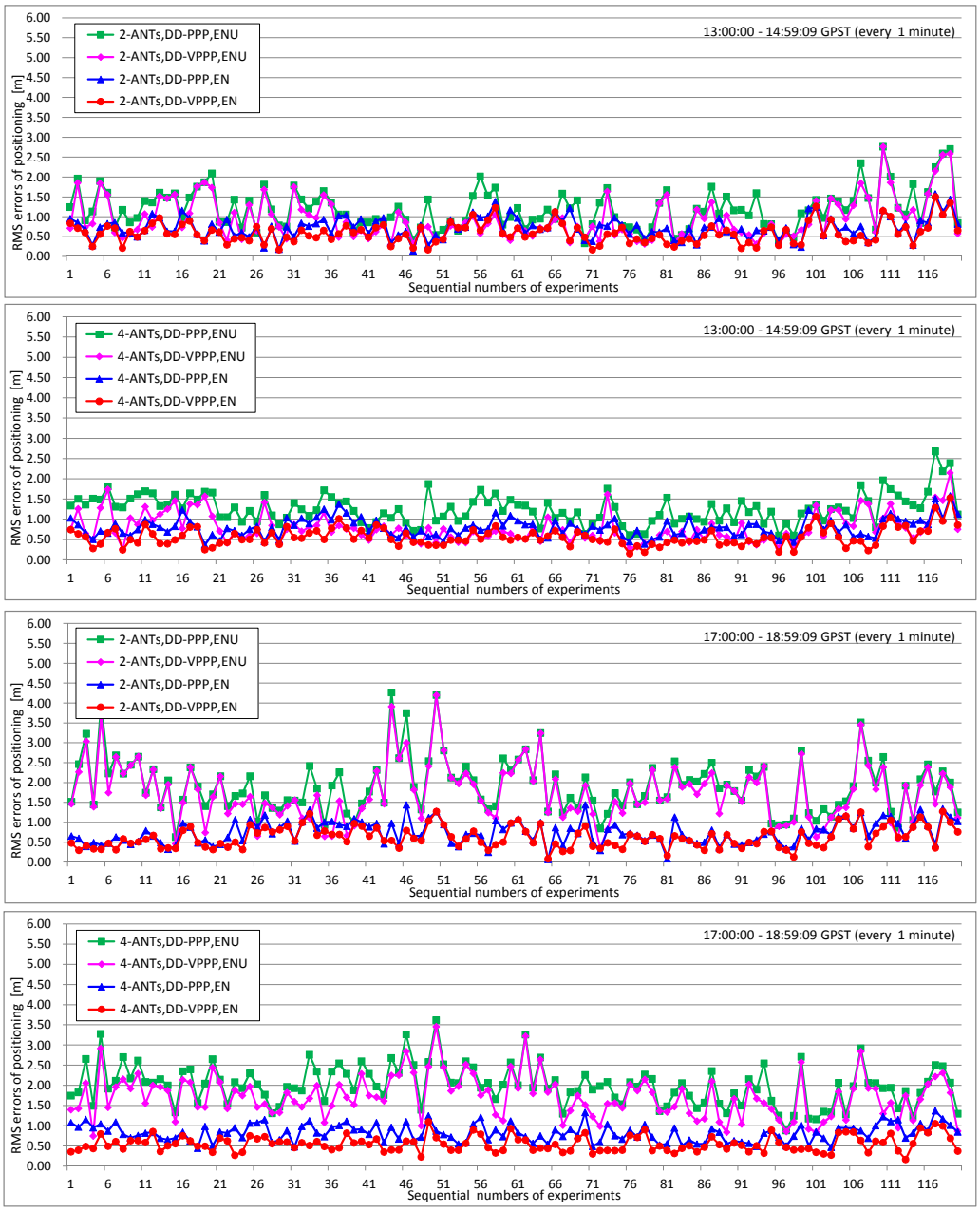

Figure 4.8: ENU and EN RMS errors of two/four antennas' positioning during 2-hours

Table 4.10: Average EN and ENU RMS errors of DD-PPP/VPPP for two/four antennas

Time period (GPST)	Antenna numbers	ENU (RMS)			EN (RMS)		
		(c) DD-PPP (10sec) [m]	(d) DD-VPPP (10sec) [m]	(d)/(c) Improvement ratio [%]	(c) DD-PPP (10sec) [m]	(d) DD-VPPP (10sec) [m]	(d)/(c) Improvement ratio [%]
13:00:00-14:59:09	2-ANTs	1.1998	0.9409	78.42	0.7242	0.5903	81.52
	4-ANTs	1.2582	0.7812	62.09	0.7945	0.5634	70.92
17:00:00-18:59:09	2-ANTs	1.9193	1.7413	90.73	0.7479	0.6200	82.91
	4-ANTs	2.0123	1.7233	85.64	0.8218	0.5496	66.88

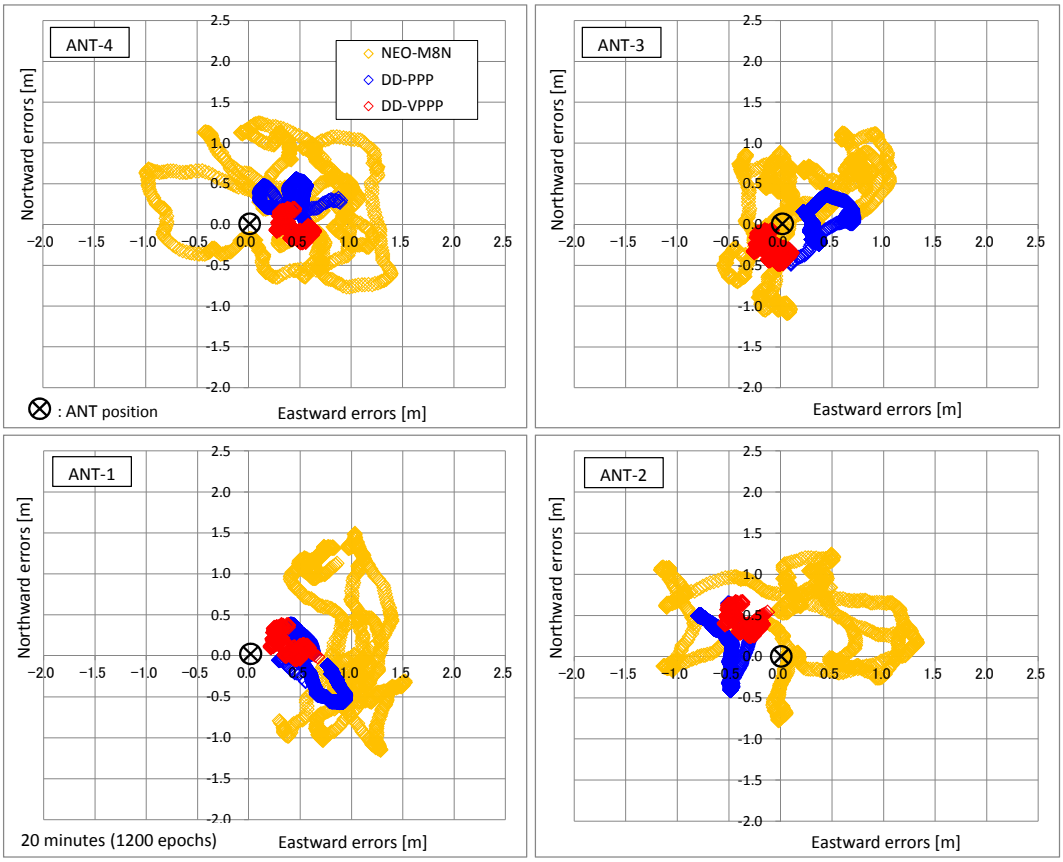

Figure 4.9: EN RMS errors of a sample of four antenna positioning

Table 4.11: EN and ENU RMS errors [m] of a sample of four antennas

Positioning Methods	ANT-1		ANT-2		ANT-3		ANT-4		Total(4-ANTs)	
	EN	ENU	EN	ENU	EN	ENU	EN	ENU	EN	ENU
NEO-M8N	0.8819	1.0596	0.6612	1.3130	0.5397	0.8693	0.6483	0.8898	0.6940	1.0481
DD-PPP	0.5750	0.5219	0.4921	1.5613	0.3065	0.4720	0.3898	0.8572	0.4524	0.9576
DD-VPPP	0.3626	0.4549	0.3657	0.8783	0.2411	0.7709	0.3892	0.7026	0.3445	0.7187

Chapter 5

Euler Angle Estimation by Baseline Vectors

5.1 Introduction

In general, not only positions, velocities, and accelerations but also body attitude of vehicles are important information for the navigation or system control of vehicle mobile applications. Basically the more reliable and higher performed attitude determination system (ADS) are developed by combining Global Navigation Satellite System (GNSS) receiver systems with inertial navigation systems (INS). The ADS performance can be achieved by approximately 0.5 degrees as 1-sigma errors within one minute at three-dimensional performance, however, the several expensive multi-frequency receivers are utilized to solve the attitude accuracy, the reliability, and the output rate. Even any expensive receiver cannot resolve the limitation of non-positioning state under the tunnels and the underground parking and higher output rate, therefore the INS could complement the GNSS receiver for the disadvantages of ADS [47].

Relative positioning equivalent methods by low-cost single frequency GNSS receivers and their patch antennas are applied for the vehicle heading determination [48]. The integer ambiguity resolution of the double-difference (DD) carrier-phase observables are

needed. In order to stably obtain the fixed integer ambiguities, the detection and correction of cycle slips are needed. The inertial measurement units (IMU) with gyro sensors are utilized for the detection and correction.

We propose one approach of the body attitude estimation methods by low-end single-frequency receivers for automotive applications. The baseline-vector estimation algorithms are derived from the DD-based PPP among multiple antennas. The update algorithms by baseline-vector length constraints are derived to improve the accuracy in conjunction with the baseline-vector estimation.

The GR models of DD-PPP/VPPP algorithms based on double-difference (DD) observables are shown in Chapter 2. The DD-PPP/VPPP can cancel the biases or the delays by single-difference (SD) or DD methods [49]. Even when low-cost single-frequency GNSS receivers are used, more precise positioning of DD-PPP/VPPP are shown compared with the conventional PPP/VPPP methods in Chapter 4.

In order to estimate the body attitude by the array-aided PPP comprised of multiple antennas, the observation equations are defined to estimate the baseline vectors between two antennas. The equations for the SD or DD-based observables are derived, and the gradient vectors from two antennas to a same satellite are assumed as approximately the same [50]. We present a novel GR model of the baseline-vector estimation derived from DD-based PPP algorithm. The gradient vectors are precisely estimated by DD-PPP methods, and the vectors for the baseline vectors are the average of two different vectors from two antennas to a same satellite. The baseline-vector lengths can be utilized as constraints by the similar minimum mean square method of VPPP/DD-VPPP [21], [24].

In order to obtain the body attitude angles (Euler angles) using multiple baseline vectors, the rotation matrix based on Euler's principal rotation theorem is considered as a

simpler method. The weighted least-squares method by multiple baseline vectors is applied to obtain the theorem-based parameters. Euler angles are obtained by the components of the rotation matrix in the sequence of Z-Y-X axis.

In order to show the estimation results of the baseline vectors and Euler angles, we analyze the experimental results of static positioning by four antennas located on a square area. The six baseline vectors of four antenna deployment in a plane are utilized for the estimation methods.

5.2 Baseline Vector Estimation and Updating by Constraints

For the case of $p = 1,\ q = 2, \ldots, n_s$ and $u_i = u_1, u_j = u_2\ (n_r = 2)$, we have the DD-based PPP measurement equation for antennas of u_1 and u_2 and for n_s satellites as follows [23], [50]:

$$y^{qp}_{u_2u_1}(t) = C^{qp}_{u_2u_1}(t)\eta^{qp}_{u_2u_1}(t) + v^{qp}_{u_2u_1}(t), \tag{5.1}$$

where

$$y^{qp}_{u_2u_1} \equiv \begin{bmatrix} y^{\hat{p}\hat{1}}_{CA,\hat{u}_2\hat{u}_1} \\ y^{\hat{p}\hat{1}}_{L1,\hat{u}_2\hat{u}_1} \end{bmatrix},\ \eta^{qp}_{u_2u_1} \equiv \begin{bmatrix} u_1 \\ u_2 \\ N^{n_s1}_{L1,u_2u_1} \end{bmatrix},\ C^{qp}_{u_2u_1} \equiv \begin{bmatrix} -G^{\hat{p}\hat{1}}_{\hat{u}_1} & G^{\hat{p}\hat{1}}_{\hat{u}_2} & \mathbf{0} \\ -G^{\hat{p}\hat{1}}_{\hat{u}_1} & G^{\hat{p}\hat{1}}_{\hat{u}_2} & \lambda_1 \boldsymbol{I} \end{bmatrix},$$

$$G^{\hat{p}\hat{1}}_{u_i} \equiv \begin{bmatrix} (g^{\hat{2}\hat{1}}_{\hat{u}_i})^{\mathrm{T}} \\ (g^{\hat{3}\hat{1}}_{\hat{u}_i})^{\mathrm{T}} \\ \vdots \\ (g^{\hat{n}_s\hat{1}}_{\hat{u}_i})^{\mathrm{T}} \end{bmatrix} : (n_s - 1) \times 3. \tag{5.2}$$

$y^{\hat{p}\hat{1}}_{CA,\hat{u}_2\hat{u}_1}$, $y^{\hat{p}\hat{1}}_{L_1,\hat{u}_2\hat{u}_1}$ are observation vector matrixes, and the both matrix sizes are $((n_s - 1) \times 1)$. $v^{qp}_{u_2u_1}$ is an observation noise vector matrix,

In Eqs. (5.1),(5.2) of DD-PPP method, the distance between two antennas u_i, u_j is very small compared with the distance between the satellites and the antennas (receivers),

namely approximately 20,000 kilometers, therefore the gradient vectors $g^{\hat{q}\hat{p}}_{\hat{u}_{ji}}$ of baseline vector u_{ji} are assumed as the average values of $g^{\hat{q}\hat{p}}_{\hat{u}_i}$ and $g^{\hat{q}\hat{p}}_{\hat{u}_j}$ as follows:

$$g^{\hat{q}\hat{p}}_{\hat{u}_i} \cong g^{\hat{q}\hat{p}}_{\hat{u}_j} \cong \frac{1}{2}[g^{\hat{q}\hat{p}}_{\hat{u}_i} + g^{\hat{q}\hat{p}}_{\hat{u}_j}] \equiv g^{\hat{q}\hat{p}}_{\hat{u}_{ji}}, \tag{5.3}$$

Then in the case of the baseline vector u_{21} between two antennas u_1,u_2, the GR equations for Kalman filtering are derived as follows:

$$y^{qp}_{u_2u_1}(t) = C^{qp}_{\hat{u}_{21}}(t)\xi^{qp}_{u_{21}}(t) + v^{qp}_{u_2u_1}(t), \tag{5.4}$$

where

$$C^{qp}_{\hat{u}_{21}} \equiv \begin{bmatrix} G^{\hat{p}\hat{1}}_{\hat{u}_{21}} & \mathbf{0} \\ G^{\hat{p}\hat{1}}_{\hat{u}_{21}} & \lambda_1 \boldsymbol{I} \end{bmatrix}, \quad \xi^{qp}_{u_{21}} \equiv \begin{bmatrix} u_{21} \\ N^{n_s 1}_{L1,u_2u_1} \end{bmatrix},$$

$$G^{\hat{p}\hat{1}}_{\hat{u}_{21}} \equiv \begin{bmatrix} (g^{\hat{2}\hat{1}}_{\hat{u}_{21}})^{\mathrm{T}} \\ (g^{\hat{3}\hat{1}}_{\hat{u}_{21}})^{\mathrm{T}} \\ \vdots \\ (g^{\hat{n}_s\hat{1}}_{\hat{u}_{21}})^{\mathrm{T}} \end{bmatrix} : (n_s - 1) \times 3. \tag{5.5}$$

State Equations for Baseline Vector Estimation

In the static case for antennas, we utilize the state vector $\xi^{p1}_{u_{21}}$ in Eq. (5.4) for antennas of u_1 and u_2 ($n_r = 2$) and for n_s satellites. In order to simplify the expression, superscripts $s, 1$ and subscripts u_1,u_2 are omitted hereafter.

$$\xi_L(t+1) = \xi_L(t), \quad \xi_L \equiv \left[u^{\mathrm{T}}_{21,L}, N^{\mathrm{T}}\right]^{\mathrm{T}}, \tag{5.6}$$

where L stands for the ENU coordinates in the local frame. And the observation equation $y(t)$ is based on a local position as a origin; $\hat{u}_1$ and derived from the relation between Eq. (5.4) and the transformation by T^L_W as follows:

$$y(t) = C_{\xi_L}(t)\xi_L(t) + v(t), \tag{5.7}$$

$$C_{\xi_L}(t) = \begin{bmatrix} G^{\hat{p}\hat{1}}_{\hat{u}_{21}}(T^L_W)^{\mathrm{T}} & \boldsymbol{O} \\ G^{\hat{p}\hat{1}}_{\hat{u}_{21}}(T^L_W)^{\mathrm{T}} & \lambda_1 \boldsymbol{I} \end{bmatrix}, \tag{5.8}$$

where $G^{\hat{p}\hat{1}}_{\hat{u}_{ji}}(T^L_W)^{\mathrm{T}}$ is a $(n_s-1)\times 3$ matrix, and $\boldsymbol{O}$ is a $(n_s-1)\times(n_s-1)$ zero matrix, and $\boldsymbol{I}$ is the $(n_s-1)\times(n_s-1)$ identity matrix. The same positioning algorithms based on the Kalman filter in Eqs. (2.120)-(2.125) are applied to the state vector ξ in Eqs. (5.6) and (5.7).

Updating by Constraint Conditions

The constraint conditions are applied to update baseline-vector estimates as follows. Namely, when we have obtained the filtering estimates $\hat{\xi}_{t|t}$ and the error covariance matrix $\Sigma_{t|t}$, we apply the constraint conditions the baseline-vector length l_{ji}:

$$l_{ji,t} = ||u_{ji,t}|| + e_{l_{ji,t}}, \tag{5.9}$$

where $e_{l_{ji,t}}$ is mutually independent Gaussian white noises with

$$e_{d_{ji,t}} \sim N(0, r_{d_{ji,t}}), \tag{5.10}$$

where

$$||u_{ji}|| = \sqrt{{u_{ji}}^T u_{ji}}. \tag{5.11}$$

Define the followings as constraints:

$$l_{n_r,t} \equiv [l_{21,t}, l_{31,t}, \cdots, l_{n_r1,t}, \cdots, l_{n_r n_{r-1},t}], \tag{5.12}$$

and consider the following relations of the conditional probability density function (CPDF),

$$\begin{aligned} p(\xi_t|Y^t, l_{n_r,t}) &= \frac{p(\xi_t, Y^t, l_{n_r,t})}{p(Y^t, l_{n_r,t})} = \frac{p(\xi_t, l_{n_r,t}|Y^t)p(Y^t)}{p(Y^t, l_{n_r,t})} \\ &= \frac{p(l_{n_r,t}|\xi_t, Y^t)p(\xi_t|Y^t)p(Y^t)}{p(Y^t, l_{n_r,t})} \\ &= K_0(Y^t, l_{n_r,t})p(\xi_t|Y^t)p(l_{n_r,t}|\xi_t). \end{aligned} \tag{5.13}$$

Then we have relations from Kalman filtering methods:

$$p(\xi_t|Y^t) = \frac{1}{(2\pi)^{n'/2}|\Sigma_{\xi,t|t}|^{1/2}} \exp\Big\{ -\frac{1}{2}(\xi_t - \hat{\xi}_{t|t})^{\mathrm{T}} \Sigma^{-1}_{\xi,t|t} (\xi_t - \hat{\xi}_{t|t}) \Big\}.$$

Then we have relatins from Eq. (5.9):

$$p(l_{n_r,t}|\xi_t) = \frac{1}{\sqrt{2\pi r_{l_{ji}}}} \exp\Big\{ -\frac{\{l_{ji,t} - ||u_{ji,t}||\}^2}{2r_{l_{ji}}} \Big\}. \tag{5.14}$$

Therefore, the power terms Eq. (5.13) is expressed by the quadratic form as follows:

$$\begin{aligned} p(\xi_t|Y^t, l_{n_r,t}) = K_0(Y^t, l_{T-n_r,t}) \\ &\times \frac{1}{(2\pi)^{n'/2}|\Sigma_{\xi,t|t}|^{1/2}} \exp\Big\{ -\frac{1}{2}(\xi_t - \hat{\xi}_{t|t})^{\mathrm{T}} \Sigma^{-1}_{\xi,t|t} (\xi_t - \hat{\xi}_{t|t}) \Big\} \\ &\times \frac{1}{\sqrt{2\pi r_{l_{ji}}}} \exp\Big\{ -\frac{\{l_{ji,t} - ||u_{ji,t}||\}^2}{2r_{l_{ji}}} \Big\}, \end{aligned} \tag{5.15}$$

where the constraints are expressed by the quadratic form of ξ as follows:

$$\begin{aligned} \frac{\{l_{ji} - ||u_{ji}||\}^2}{2r_{u_{ji}}} &\cong \frac{1}{2r_{l_{ji}}}(l_{ji}^2 + u_{ji}^{\mathrm{T}} u_{ji} - 2l_{ji}\kappa_{ji}^{\mathrm{T}} u_{ji}) \\ &= \frac{1}{2}(u_{ji}^{\mathrm{T}} \frac{I}{r_{l_{ji}}} u_{ji} - \frac{2l_{ji}}{r_{l_{ji}}} \kappa_{ji}^{\mathrm{T}} u_{ji} + \frac{l_{ji}^2}{r_{l_{ji}}}) \\ &= \frac{1}{2}(\xi_{ji}^{\mathrm{T}} M_{ji} \xi_{ji} - {c_{l_{ji}}}^{\mathrm{T}} \xi_{ji} + \frac{l_{ji}^2}{r_{l_{ji}}}), \end{aligned} \tag{5.16}$$

where

$$K_{ji} \equiv \frac{I}{r_{l_{ji}}} \quad (:3\times 3), \quad c_{l_{ji}} \equiv \frac{2l_{ji}\kappa_{ji}^{\mathrm{T}}}{r_{l_{ji}}}. \tag{5.17}$$

In the case of $n_r = 2$,

$$\frac{1}{2}\frac{\{l_{21} - ||u_{21}||\}^2}{r_{l_{21}}} \cong \frac{1}{2}\{\xi^{\mathrm{T}} M_{21} \xi + c_{l_{21}}^{\mathrm{T}} \xi + \frac{l_{21}^2}{r_{l_{21}}}\}, \tag{5.18}$$

where

$$M_{21} \equiv \left[\begin{array}{c|c} K_{21} & O_{n_s-1} \\ \hline O_{n_s-1} & O_{n_s-1} \end{array}\right], \quad c_{l_{21}} \equiv \left[\begin{array}{cc} -c_{l_{12}}^{\mathrm{T}} & 0_{n_r-1}^{\mathrm{T}} \end{array}\right],$$

O_{n_s-1} is zero matrix of $(n_s-1)\times(n_s-1)$, and 0_{n_s-1} is zero vector of $1\times(n_s-1)$,

$$K_{21} \equiv \frac{I}{r_{l_{21}}}^{\mathrm{T}} \quad (:3\times 3), \qquad c_{l_{21}}^{\mathrm{T}} \equiv \frac{2l_{21}\kappa_{21}^{\mathrm{T}}}{r_{l_{21}}}.$$

Therefore, finally we have the following quadratic form as the power term of Eq. (5.15),

$$\begin{aligned}
&\frac{1}{2}(\xi-\hat{\xi})\Sigma^{-1}(\xi-\hat{\xi}) + \frac{1}{2}\frac{\{l_{21}-||u_{21}||\}^2}{r_{l_{21}}} \\
&\quad\cong \frac{1}{2}\{\xi^{\mathrm{T}}\Sigma^{-1}\xi - \xi^{\mathrm{T}}\Sigma^{-1}\hat{\xi} - \hat{\xi}^{\mathrm{T}}\Sigma^{-1}\xi + \hat{\xi}^{\mathrm{T}}\Sigma^{-1}\hat{\xi} + \xi^{\mathrm{T}}M_{\xi_{21}}\xi + c_{\xi_{21}}^{\mathrm{T}}\xi + \frac{l_{21}^2}{r_{l_{21}}}\} \\
&\quad= \frac{1}{2}\{\xi^{\mathrm{T}}(\Sigma^{-1}+M_{\xi_{21}})\xi - \xi^{\mathrm{T}}(\Sigma^{-1}\hat{\xi} - \frac{1}{2}c_{\xi_{21}}) - (\hat{\xi}^{\mathrm{T}}\Sigma^{-1} - \frac{1}{2}c_{\xi_{21}})\xi + \hat{\xi}^{\mathrm{T}}\Sigma^{-1}\hat{\xi} + \frac{l_{21}^2}{r_{l_{21}}}\} \\
&\quad= \frac{1}{2}\{[\xi-(\Sigma^{-1}+M_{\xi_{21}})^{-1}(\Sigma^{-1}\hat{\xi}-\frac{1}{2}c_{\xi_{21}})]^{\mathrm{T}}(\Sigma^{-1}+M_{\xi_{21}}) \\
&\qquad\times[\xi-(\Sigma^{-1}+M_{\xi_{21}})^{-1}(\Sigma^{-1}\hat{\xi}-\frac{1}{2}c_{\xi_{21}})] \\
&\qquad-(\Sigma^{-1}\hat{\xi}-\frac{1}{2}c_{\xi_{21}})^{\mathrm{T}}(\Sigma^{-1}+M_{\xi_{21}})^{-1}(\Sigma^{-1}\hat{\xi}-\frac{1}{2}c_{\xi_{21}}) + \hat{\xi}^{\mathrm{T}}\Sigma^{-1}\hat{\xi} + \frac{l_{21}^2}{r_{l_{21}}}\}.
\end{aligned}$$

Then the updated estimates ξ_{21} and the updated error covariance Σ_{21} of ξ_{21} based on the minimum mean square estimate are given by

$$\check{\xi}_{21} = (\Sigma_{\xi_{21}}^{-1} + M_{\xi_{21}})^{-1}(\Sigma_{\xi_{21}}^{-1}\hat{\xi}_{21} + c_{\xi_{21}}) \tag{5.19}$$

$$\check{\Sigma}_{\xi_{21}} = (\Sigma_{\xi_{21}}^{-1} + M_{\xi_{21}})^{-1}. \tag{5.20}$$

In the cases of $n_r = 3$ and $n_r = 4$, see Appendix D.

5.3 Euler Angle Estimation Algorithms

The rotation angles α, β, γ around X,Y,Z-axes, respectively, are called Euler angles, and the corresponding rotation matrixes are as follows:

$$\Gamma(X,\alpha) \equiv \begin{bmatrix} 1 & 0 & 0 \\ 0 & \cos\alpha & \sin\alpha \\ 0 & -\sin\alpha & \cos\alpha \end{bmatrix}, \Gamma(Y,\beta) \equiv \begin{bmatrix} \cos\beta & 0 & -\sin\beta \\ 0 & 1 & 0 \\ \sin\beta & 0 & \cos\beta \end{bmatrix}, \Gamma(Z,\gamma) \equiv \begin{bmatrix} \cos\gamma & \sin\gamma & 0 \\ -\sin\gamma & \cos\gamma & 0 \\ 0 & 0 & 1 \end{bmatrix}. \tag{5.21}$$

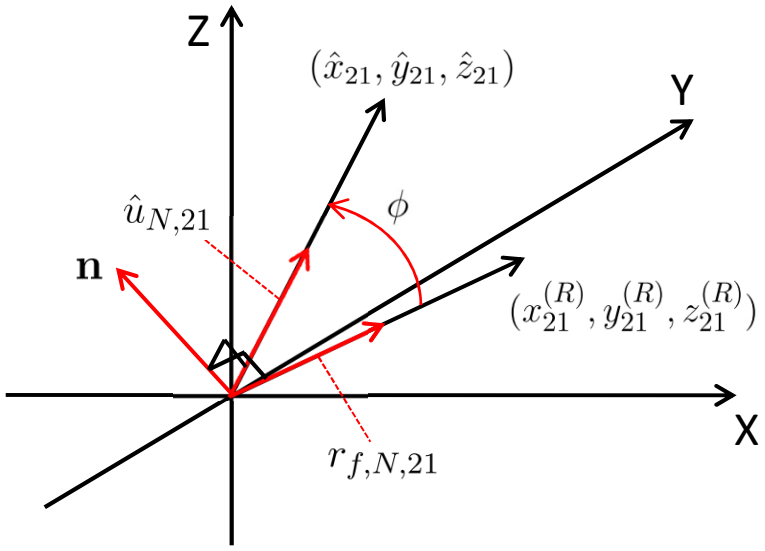

Figure 5.1: Euler's principal rotation theorem

In the case of $n_r = 2$, the rotation matrix of Z-Y-X sequence from the vector $r_{f,N,21}$ on the reference frame to the estimated baseline vector $\hat{u}_{N,21}$ on the body frame is as follows:

$$\begin{aligned} \hat{u}_{N,21} &= \Gamma(X,\alpha)\Gamma(Y,\beta)\Gamma(Z,\gamma) r_{f,N,21} \\ &= \Gamma(\alpha,\beta,\gamma) r_{f,N,21}, \end{aligned} \tag{5.22}$$

where N denotes normalized,

$$r_{f,N,21} \equiv \frac{r_{f,21}}{||r_{f,21}||} = [x_{N,21}^{(R)}, y_{N,21}^{(R)}, z_{N,21}^{(R)}]^{\mathrm{T}}, \quad \hat{u}_{N,21} \equiv \frac{\hat{u}_{21}}{||\hat{u}_{21}||} = [\hat{x}_{N,21}, \hat{y}_{N,21}, \hat{z}_{N,21}]^{\mathrm{T}}. \tag{5.23}$$

The rotation matrix $\Gamma(\alpha,\beta,\gamma)$ in Eq. (5.22) is a combined matrix of the rotation matrixes $\Gamma(\alpha)$, $\Gamma(\beta)$, $\Gamma(\gamma)$ in Eq. (5.21), and derived as shown in Eq. (5.25). Euler angles α, β, γ are derived from the elements of the rotation matrix $\Gamma(\alpha,\beta,\gamma)$ as follows:

$$\text{roll}: \ \alpha = \tan^{-1}\frac{\Gamma_{32}}{\Gamma_{33}}, \quad \text{pitch}: \ \beta = \tan^{-1}\frac{-\Gamma_{31}}{\sqrt{\Gamma_{32}^2 + \Gamma_{33}^2}}, \quad \text{yaw}: \ \gamma = \tan^{-1}\frac{\Gamma_{21}}{\Gamma_{11}}, \tag{5.24}$$

where Γ_{21} denotes the matrix element of the second row and first column.

In order to obtain Euler angles by multiple baseline vectors, we consider Euler's principal rotation theorem shown in Fig. 5.1. According to the theorem, any vector can be brought into the target vector by one rotation angle ϕ around the vector $\mathbf{n}$. The ϕ is the angle between two vectors $r_{f,N,21}$ and $\hat{u}_{N,21}$, and the $\mathbf{n}$ is the common normal vector of two vectors $r_{f,N,21}$ and $\hat{u}_{N,21}$. The vector $r_{f,N,21}$ is identical with the vector $\hat{u}_{N,21}$ by rotating of the angle ϕ around the principal axis $\mathbf{n}$. Therefore, the rotation matrix Γ is expressed by another way of the rotation matrix $\tilde{\Gamma}(\phi, \mathbf{n})$ by using the angle ϕ and the vector $\mathbf{n}$ as shown in Eq. (5.26) [47], [51]. The angle ϕ is obtained from the inner product of the two vectors, and the vector $\mathbf{n}$ is obtained from the outer product of the two vectors. Euler angles in Eq. (5.24) are similarly obtained from the elements of the rotation matrix $\tilde{\Gamma}(\phi, \mathbf{n})$.

$$
\begin{aligned}
&\Gamma(\alpha, \beta, \gamma) \\
&= \begin{bmatrix} \cos\gamma\cos\beta & -\sin\gamma\cos\alpha + \cos\gamma\sin\beta\sin\alpha & \sin\gamma\sin\alpha + \cos\gamma\sin\beta\cos\alpha \\ \sin\gamma\cos\beta & \cos\gamma\cos\alpha + \sin\gamma\sin\beta\sin\alpha & -\cos\gamma\sin\alpha + \sin\gamma\sin\beta\cos\alpha \\ -\sin\beta & \cos\beta\sin\alpha & \cos\beta\cos\alpha \end{bmatrix} \qquad (5.25) \\
&\cong \tilde{\Gamma}(\phi, \mathbf{n}) \\
&= \begin{bmatrix} \cos\phi + (1-\cos\phi){n_x}^2 & (1-\cos\phi)n_x n_y - n_z\sin\phi & (1-\cos\phi)n_z n_x + n_y\sin\phi \\ (1-\cos\phi)n_x n_y + n_z\sin\phi & \cos\phi + (1-\cos\phi){n_y}^2 & (1-\cos\phi)n_y n_z - n_x\sin\phi \\ (1-\cos\phi)n_z n_x - n_y\sin\phi & (1-\cos\phi)n_y n_z + n_x\sin\phi & \cos\phi + (1-\cos\phi){n_z}^2 \end{bmatrix}, \qquad (5.26)
\end{aligned}
$$

where

$$
\begin{aligned}
\cos\phi = r_{f,N,21} \cdot \hat{u}_{N,21} : &\quad \text{inner product}, \\
\mathbf{n} = (n_x, n_y, n_z)^{\mathrm{T}} = \frac{r_{f,N,21} \times \hat{u}_{N,21}}{||r_{f,N,21} \times \hat{u}_{N,21}||} : &\quad \text{outer product}. \qquad (5.27)
\end{aligned}
$$

In the case of multiple antennas, we derive the computational algorithms by estimating the multiple baseline vectors $\hat{u}_{N,ji}$ from the reference antenna i to other antennas j

disposed in a plane [47], [52]. The appropriate rotation matrix Γ to minimize the rotation errors from the multiple reference baseline vectors $r_{f,N,ji}$ to the multiple baseline vectors $\hat{u}_{N,ji}$ is estimated by the least-squares method, and that is the corresponding equations to estimate the parameters θ of Euler's principal rotation theorem as follows (See Appendix E):

$$\min_{\Gamma} \sum_{i<j}^{n_r} ||\hat{u}_{N,ji} - \Gamma r_{f,N,ji}||^2_{Q^{-1}_{\hat{u}_{N,ji}}} = \min_{\theta} \sum_{i<j}^{n_r} ||\hat{u}_{N,ji} - H_{ji}\theta||^2_{Q^{-1}_{\hat{u}_{N,ji}}}, \tag{5.28}$$

where

$$\hat{u}_{N,ji} \equiv \begin{bmatrix} \hat{x}_{N,ji} \\ \hat{y}_{N,ji} \\ \hat{z}_{N,ji} \end{bmatrix}, \ \theta \equiv \begin{bmatrix} \cos\phi \\ n_x \sin\phi \\ n_y \sin\phi \\ n_z \sin\phi \end{bmatrix}, \ H_{ji} \equiv \begin{bmatrix} x^{(R)}_{N,ji} & 0 & z^{(R)}_{N,ji} & -y^{(R)}_{N,ji} \\ y^{(R)}_{N,ji} & -z^{(R)}_{N,ji} & 0 & x^{(R)}_{N,ji} \\ z^{(R)}_{N,ji} & y^{(R)}_{N,ji} & -x^{(R)}_{N,ji} & 0 \end{bmatrix}, \tag{5.29}$$

and, $Q_{\hat{u}_{N,ji}}$ denotes the error covariance of the estimates $\hat{u}_{N,ji}$.

The Euler-angle estimation by the parameters of Euler's principal rotation theorem under Z-Y-X sequence is as follows. First of all, the multiple vectors $r_{f,ji}$ and $\hat{u}_{ji}$ are normalized as shown in Eq. (5.23) as follows:

$$r_{f,N,ji} \equiv \frac{r_{f,ji}}{||r_{f,ji}||} = [x^{(R)}_{N,ji}, y^{(R)}_{N,ji}, z^{(R)}_{N,ji}]^{\mathrm{T}}, \quad \hat{u}_{N,ji} \equiv \frac{\hat{u}_{ji}}{||\hat{u}_{ji}||} = [\hat{x}_{N,ji}, \hat{y}_{N,ji}, \hat{z}_{N,ji}]^{\mathrm{T}}, \tag{5.30}$$

and mapped on the X-Y,X-Z,and Y-Z planes to estimate the rotation angles in the sequence.

Then the parameters $\hat{\theta}(Z,\gamma)$, $\hat{\theta}(Y,\beta)$, and $\hat{\theta}(X,\alpha)$ for the rotations around Z-axis, Y-axis and X-axis are estimated by the least-squares method in the sequence, respectively.

Eq. (5.28) is developed and expressed by the quadratic form of θ as follows:

$$\begin{aligned}
&\sum_{i<j}^{n_r} ||\hat{u}_{N,ji} - H_{ji}\theta||^2_{Q^{-1}_{\hat{u}_{N,ji}}} \\
&= \sum_{i<j}^{n_r} (\hat{u}_{N,ji} - H_{ji}\theta)^{\mathrm{T}} Q^{-1}_{\hat{u}_{N,ji}} (\hat{u}_{N,ji} - H_{ji}\theta) \\
&= \sum_{i<j}^{n_r} (\hat{u}^{\mathrm{T}}_{N,ji} Q^{-1}_{\hat{u}_{N,ji}} \hat{u}_{N,ji} - \hat{u}^{\mathrm{T}}_{N,ji} Q^{-1}_{\hat{u}_{N,ji}} H_{ji}\theta - \theta^{\mathrm{T}} H^{\mathrm{T}}_{ji} Q^{-1}_{\hat{u}_{N,ji}} \hat{u}_{N,ji} + \theta^{\mathrm{T}} H^{\mathrm{T}}_{ji} Q^{-1}_{\hat{u}_{N,ji}} H_{ji}\theta) \\
&= \theta^{\mathrm{T}} \sum_{i<j}^{n_r} (H^{\mathrm{T}}_{ji} Q^{-1}_{\hat{u}_{N,ji}} H_{ji})\theta - \sum_{i<j}^{n_r} (\hat{u}^{\mathrm{T}}_{N,ji} Q^{-1}_{\hat{u}_{N,ji}} H_{ji})\theta \\
&\quad -\theta^{\mathrm{T}} \sum_{i<j}^{n_r} (H^{\mathrm{T}}_{ji} Q^{-1}_{\hat{u}_{N,ji}} \hat{u}_{N,ji}) + \sum_{i<j}^{n_r} (\hat{u}^{\mathrm{T}}_{N,ji} Q^{-1}_{\hat{u}_{N,ji}} \hat{u}_{N,ji}),
\end{aligned} \tag{5.31}$$

Eq. (5.31) is differenciated by θ,

$$2\sum_{i<j}^{n_r} (H^{\mathrm{T}}_{ji} Q^{-1}_{\hat{u}_{N,ji}} H_{ji})\theta - 2\sum_{i<j}^{n_r} (H^{\mathrm{T}}_{ji} Q^{-1}_{\hat{u}_{N,ji}} \hat{u}_{N,ji}) = 0, \tag{5.32}$$

and finally the estimate $\hat{\theta}$ is obtained by the weighted least squares method as follows:

$$\hat{\theta} = \left(\sum_{i<j}^{n_r} (H^{\mathrm{T}}_{ji} Q^{-1}_{\hat{u}_{N,ji}} H_{ji}) \right)^{-1} \sum_{i<j}^{n_r} (H^{\mathrm{T}}_{ji} Q^{-1}_{\hat{u}_{N,ji}} \hat{u}_{N,ji}). \tag{5.33}$$

Then each rotation matrix $\tilde{\Gamma}(Z, \phi, \mathbf{n})$, $\tilde{\Gamma}(Y, \phi, \mathbf{n})$, and $\tilde{\Gamma}(X, \phi, \mathbf{n})$ in Eq. (5.26), respectively, is derived through Eq. (5.27) from the parameter $\hat{\theta}$. Finally, Euler angles γ, β, α in Eq. (5.24) are obtained from each rotation matrix of Eq. (5.26) in the Z-Y-X sequence.

5.4 Experiments

5.4.1 Baseline Vectors Estimation

The measurement equation of the baseline-vector estimations in Eq. (5.4) is derived from the equation of the DD-PPP. The both equations estimate the DD-based integer ambiguities by Kalman filter. For the PPP method, when the estimated integer ambiguities $N^{n_s 1}_{L1,u_2u_1}$ converge to the fixed integers, the unknown antenna positions are approaching to

the real positions. As a preliminary experiment, we have checked the integer ambiguities (IA) convergence by the two antenna DD-PPP positioning. Fig. 5.2 shows the IA convergence in the two cases, (1) the synchronous processes of two receivers by a common clock, and (2) the asynchronous processes by the individual clocks. The experiments by the both processes are conducted at the same time for 10-minutes. The IA convergence of the process (1) takes approximately 200 epochs which is half of the process (2). The base clock is TCXO and the frequency accuracy is 26 MHz $\pm$0.5 ppm. In the case of (2), the different clock with the fluctuation $\pm$0.5 ppm are supplied to the two receivers, and the DD-based IA estimations based on the observables obtained by the shifted clocks could cause the delay of the IA convergence. We consider that the process (2) could cause the delay of the position convergences, and use the process (1) for the baseline-vector estimations.

The GPS observation data obtained by the experiment shown in Table 4.1 are used for

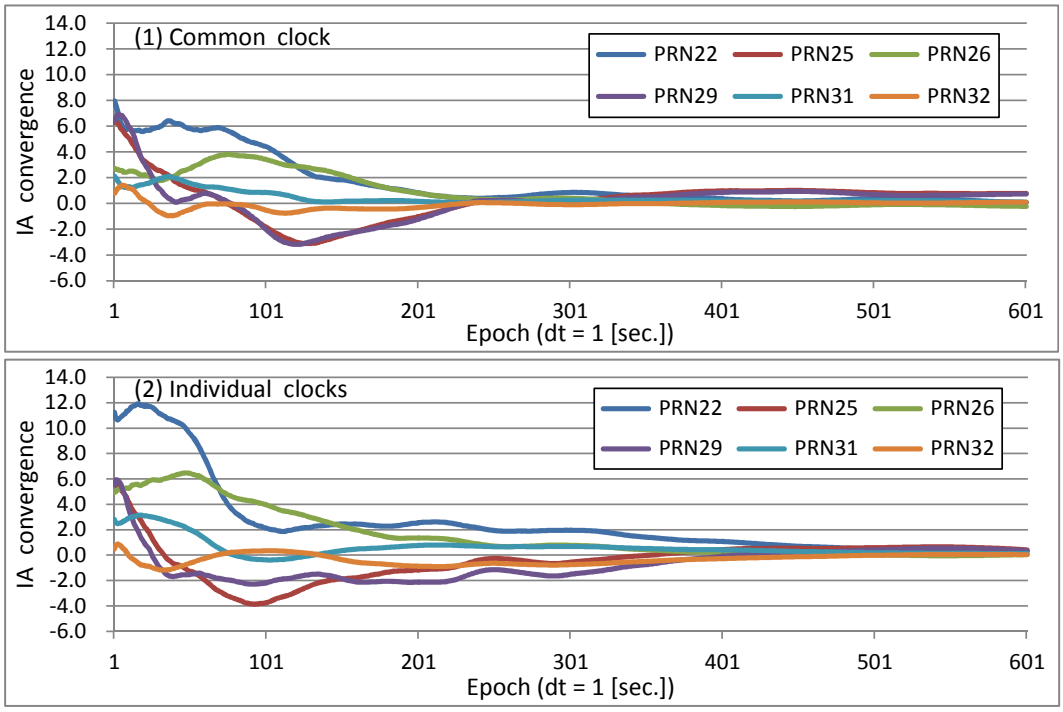

Figure 5.2: Integer Ambiguity convergence of DD-PPP

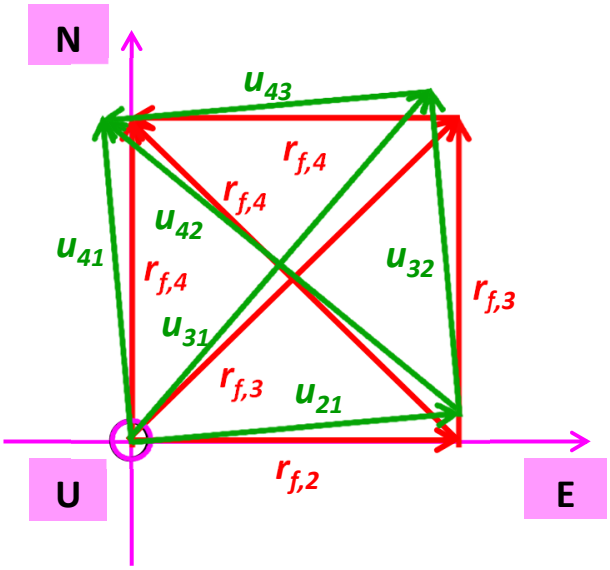

Figure 5.3: Reference and baseline vectors on ENU coordinates

Table 5.1: Six vectors on the reference and the body frame

	Reference frame				Body frame		
	E [m]	N [m]	U [m]		E [m]	N [m]	U [m]
$r_{f,21}$	1	0	0	u_{21}	0.799	-0.015	-0.006
$r_{f,31}$	1	1	0	u_{31}	0.812	0.783	-0.003
$r_{f,41}$	0	1	0	u_{41}	0.013	0.797	0.000
$r_{f,32}$	0	1	0	u_{32}	0.012	0.798	0.002
$r_{f,42}$	-1	1	0	u_{42}	-0.786	0.812	0.006
$r_{f,43}$	-1	0	0	u_{43}	-0.799	0.014	0.003

the baseline-vector estimation. The four antennas ANT-1, 2, 3, 4 are located at the corners of a square board (see Fig. 4.1). The receivers connected to the ANT-1 and ANT-2, or ANT-3 and ANT-4 are synchronized by a common clock, respectively. The coordinates of the antennas' reference positions in the WGS84 system are listed in Table 4.2, and the positioning error applying the relative positioning method is less than a few centimeters.

In general, in order to estimate three-dimensional body attitude, the reference frame and the body frame are defined. The attitude is obtained by the rotation from the ref-

erence frame to the body frame. In the case of four antennas, as shown in Fig. 5.3, there are six baseline vectors based on the number of two-antenna pairs. The red vectors $r_{f,21}, r_{f,31}, r_{f,41}, r_{f,32}, r_{f,42}, r_{f,43}$ show the reference vectors of the reference frame, and ideally located along the axes of the ENU coordinates. The green vectors $u_{21}, u_{31}, u_{41}, u_{32}, u_{42}, u_{43}$ show the baseline vectors of the body frame on the ENU coordinates, and are fixed to the body of the square board. We apply the ENU (ENU: East, North, and Height(Up)) coordinates to the both frame. The ANT-1 position is the origin of the ENU coordinates. Table 5.1 shows the six reference vectors $r_{f,ji}$ on the reference frame, and the six baseline vectors u_{ji} calculated from the relative positioning in Table 4.2. The reference vectors are reference values on the local tangent plane, namely the EN plane. The vectors' values are approximately the same, and the rotational angles of the corresponding vectors are less than a few degrees.

Fig. 5.4 shows the six baseline vectors u_{21},u_{31},u_{41},u_{32},u_{42},u_{43} estimated by Eq. (5.4) and the vector u_{21} updated by the vector length constraint in Eq. (5.9) on the EN plane. The measurement time is 20 minutes (1200 epochs). All estimates without constraints are gradually converged to the real positions which are the end points of the baseline vectors (green arrows). The ENU root-mean-square (RMS) errors of the baseline-vector estimates after 1200 epochs are approximately 10 cm as shown in Table 5.2. On the contrary, u_{21} (C) is converged adjacent to the real position in several epochs after the estimation start. Furthermore, when the IA fixed values are forced to utilize for the baseline-vector estimation in Eq. (5.4), the ENU RMS errors of the estimates are approximately less than 1 cm after setting the values as shown in Table 5.2.

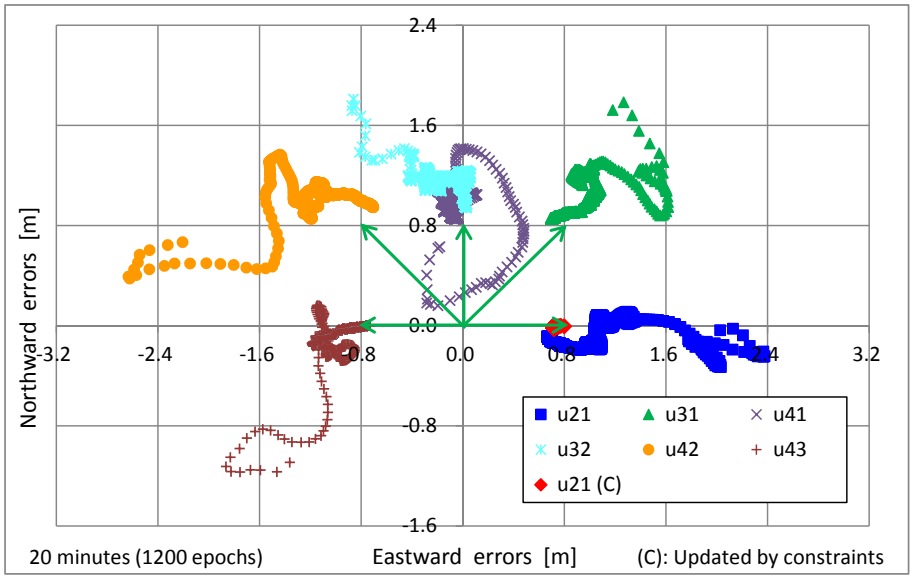

Figure 5.4: Baseline-vector estimation

Table 5.2: RMS errors of estimated baseline vectors

ENU RMS errors [m]	u_{21}	u_{31}	u_{41}	u_{32}	u_{42}	u_{43}
After 1200 epochs	0.0966	0.0873	0.0538	0.1118	0.0919	0.0724
After set IA fixed values	0.0106	0.0040	0.0058	0.0072	0.0075	0.0053

5.4.2 Euler Angle Estimation

Fig. 5.5 shows the estimation results of Euler angles from the reference frame to the body frame obtained in Eq. (5.24). The error covariance $Q_{\hat{u}_{N,ji}}$ in Eq. (5.33) is supposed to be the (3×3) identity matrix. (a) utilizes only u_{21} baseline-vector estimates, (b) utilizes six baseline-vector estimates, and (c) utilizes only u_{21} updated by constraints to estimate Euler angles. The rotation angles between the two frames obtained in Table 5.1, namely a few degrees, are utilized to correct the Euler-angle estimation results. One vector u_{21} estimates only two rotation angles γ, β in the Z-Y sequence in Table 5.3. (a) shows that the angles γ, β are approximately 10 degrees even after 1200 epochs. On the contrary, (b) shows that all rotation angles are estimated by six baseline vectors and gradually

converged as time goes by, and less than 5 degrees in approximately 600 epochs, and less than 2 degrees in approximately 1200 epochs. (c) shows that the rotation angle γ in the X-Y plane is less than 2 degrees in several epochs, because the u_{21} vector is precisely estimated by the constraints, and converge to the fixed point around the real position on the EN coordinates. However, the upward errors of the vector is not small, therefore the rotation angle β is more than 20 degrees.

The baseline-vector estimates are gradually converged to the real positions, however, it takes approximately 20 minutes. The improvements of the vector positions are caused by improving the estimation of the integer ambiguities $N^{n_s 1}_{L1,u_2u_1}$ in Eq. 5.5 with the lapse of time. When the fixed integer ambiguities are used as the initial values for the vector estimations, the more precise accuracy is obtained than usual. The Euler-angle estimation by six baseline vectors are worse than one vector just after the estimation, however, the better rotation angle estimates are obtained with the lapse of time. It is high possibility for Euler angles to be more precise for shorter time as the number of baseline vectors is increased.

5.5 Concluding Remarks

We have presented a novel baseline-vector estimation algorithms based on the double-difference (DD) positioning method, namely DD-PPP, and applied a novel update algorithm based on the vector length constraints. GPS data are applied to the coupled GR equations for multiple antennas in the case of unknown positions. The experiments for the baseline-vector estimations among four antennas in the static situation for 20 minutes have been carried out. The six baseline vectors are estimated at a time, and the vectors' positions gradually converge to the real positions. When the vector length constraints are

applied, the positions can be reached adjacent to the real position in several epochs.

We have obtained Euler angles from the reference frame to the body frame by the least-squares method of six baseline vectors through the parameters of Euler's principal rotation theorem. The experiments for Euler-angle estimation by utilizing the vectors have been carried out for 20 minutes. Euler angles by six baseline vectors are more precisely estimated compared with one vector, and gradually converged to less than 2 degrees in approximately 1200 epochs.

In general, GNSS receivers for vehicles need higher availability, therefore higher sensitivity are achieved by longer correlation time. However, the longer correlations cause the broad correlation peaks, and the tendency of worse positioning accuracy or positioning fluctuations as a result. The fluctuations directly cause the worse absolute positioning accuracy, however, the offsets toward the same direction at two antennas contribute the improvement of the baseline-vector accuracy. When the two receivers are operated by the synchronized clock, the receiver-related offset difference are reduced, and the vector accuracy are expected to be improved.

Presently the DD-based algorithms for PPP and VPPP provide the positioning accuracy in sub-meter error level, and has the potential capability for estimating the baseline vectors, namely the position differences between two antennas. When DD-PPP/VPPP positioning performance would be improved, Euler angles by multiple baseline vectors would be more precise. Furthermore, we find that the higher estimated accuracy of integer ambiguities in DD-PPP can provide the higher accuracy of baseline vectors. In the future, we will apply integer ambiguity resolution methods to DD-PPP methods.

Table 5.3: Baseline vectors for Euler-angle estimations

Estimated Euler-angles	Baseline vectors for the estimation
$\gamma \quad (Z-axis)$	$\mathrm{r}_{f,21}$, $r_{f,31}$, $r_{f,41}$, $r_{f,32}$, $r_{f,42}$, $r_{f,43}$
$\beta \quad (Y-axis)$	$\mathrm{r}_{f,21}$, $r_{f,43}$
$\alpha \quad (X-axis)$	$\mathrm{r}_{f,41}$, $r_{f,32}$

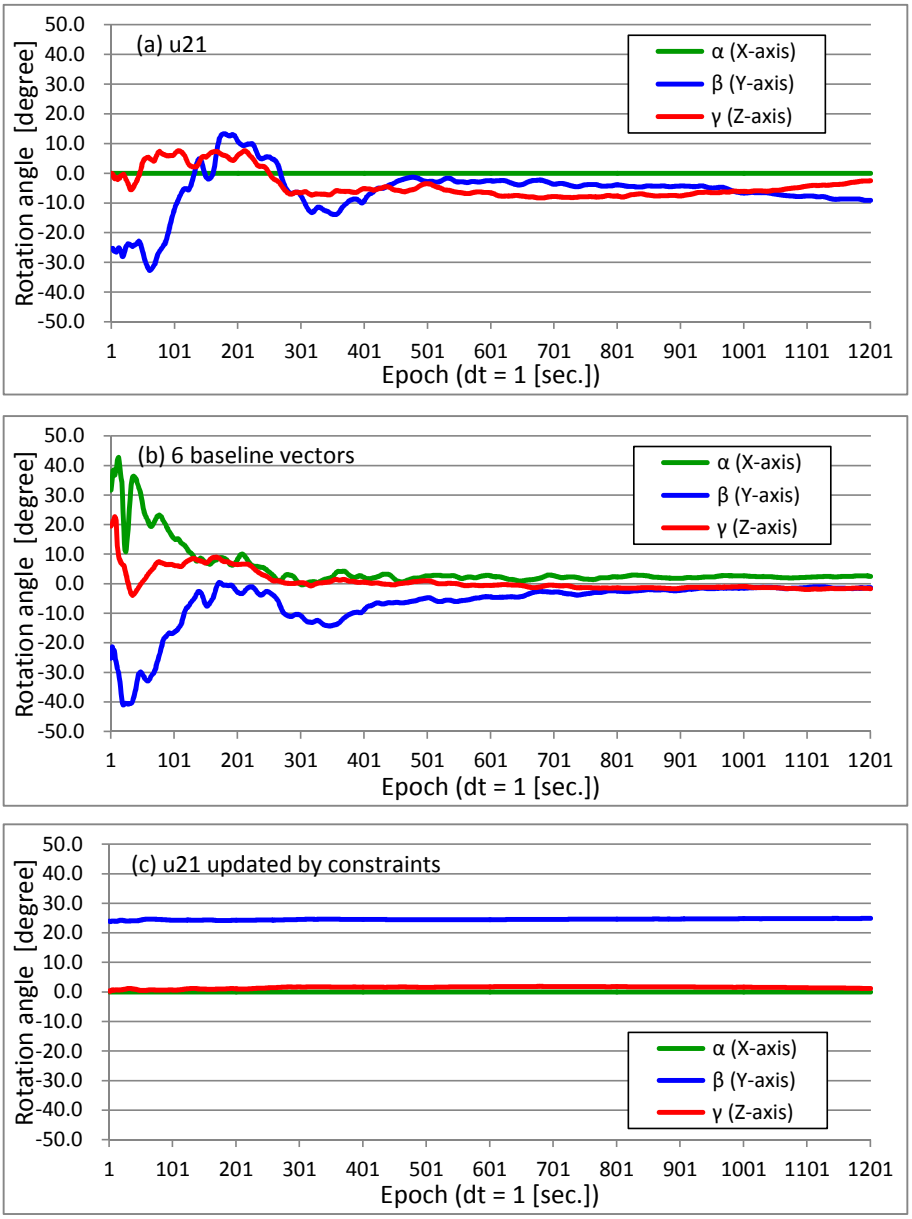

Figure 5.5: Euler-angle estimation

Chapter 6

Conclusions

The advanced GNSS positioning researches of sub-meter-level accuracy for automotive applications have been considered. In this chapter, the main findings and contributions obtained in this thesis are summarized, and recommendations are made for future research and for users of the methods.

The novel GNSS regression (GR) models for single difference (SD)/double difference (DD) based precise point positioning (PPP) have been derived in Chapter 2. The mathematical models of three types of raw measurements, namely C/A code pseudoranges, carrier-phase pseudoranges, and Doppler shift frequencies, are utilized as the basic equations for positioning. For comparison, the coupled PPP GR equations for multiple antennas are shown. The SD/DD-PPP GR models for L1 observables of multiple antennas are derived based on the mathematical models of SD/DD observables.

In order to improve observable reliability for positioning, the methods for detecting and correcting observable outliers of Doppler-aided positioning have been proposed in Chapter 3. A Doppler-aided Kalman filter positioning for single-frequency receivers are formulated from PPP GR models, and reproduced the real receiver's positioning error by Doppler bias under open sky environments. The chi-squared tests by the existing inno-

vation based detection (IBD) method and a novel measurement based detection (MBD) method are applied to detect the bias. The exclusion or the estimation correction methods combined with the detection methods are proposed, and shows the correction results of the positioning errors. The MBD and exclusion method provides the best performance among three combination methods, because it is less affected by the false detections of Doppler observables and has the smaller response delays at the start and end points of the bias-injected period. Furthermore, the MBD-method can be applied to the detection of not only Doppler outliers but also C/A code pseudorange outliers or carrier-phase cycle slips.

In order to achieve the sub-meter level positioning, the improved Very PPP (VPPP) algorithms based on the minimum mean square (MMS) methods by geometric distance constraints among multiple antennas have been derived, and applied to the PPP or the DD-PPP in Chapter 4. The experiments of four antennas (receivers) are carried out in a static situation. DD-VPPP has the smallest root-mean-square (RMS) errors among four positioning methods, namely PPP and VPPP of without DD (WOD) and DD-methods when two antennas are used. The total improvement ratio from the PPP to the DD-VPPP is approximately 84 %. The experiments of the 24-hours static positioning by using four low-end single-frequency GPS antennas are carried out. The two antenna DD-PPP/VPPP achieve less than 40-cm positioning errors on horizontal east-north (EN) coordinate after ten seconds (epochs). DD-VPPP are approximately less than half on EN coordinate, and less than 1/4 on east-north-up (ENU) coordinates compared with the u-blox NEO-M8N positioning. The improvement ratios of the averaged RMS errors from DD-PPP to DD-VPPP are approximately improved from 82 % to 66 % on EN coordinates.

The GR models for baseline-vector estimation with vector length constraints, and the

Euler-angle estimation algorithms based on the vectors have been derived in Chapter 5. The experiments for the baseline-vector estimates among four antennas in the static situation are carried out. During 20 minutes, six baseline vectors among four antennas are estimated at a time, and the vectors' positions are gradually approaching the real positions. The Euler-angle estimation from the reference frame to the body frame by the least-squares method of six baseline vectors through the parameters of Euler's principal rotation theorem are conducted. Euler angles by six baseline vectors are more precisely estimated compared with one vector, gradually converged to less than 2 degrees after 1200 epochs.

Recommendations

Future studies to improve the methods described in this thesis can be recommended.

The innovation processes of the extended Kalman filter are stated to be effective to detect the observable outliers in Chapter 3. We consider that Robust Kalman filter methods can be applied for GNSS observable outliers as a next step, because it is reported to be effective to reduce the impacts of observable spike noises [9], [10].

The ENU RMS errors of SPP methods are stated to be approximately 2.0 m at Table 4.9 in Chapter 4. The position $u1$,$u2$ estimation by Kalman filter positioning utilizes SPP results as initial values. The SPP fluctuations cause the fluctuations of the DD-PPP/DD-VPPP positioning. When the relative positioning values close to the real positions are used as the initial values, the positioning errors are reduced to less than 0.5 m from approximately 1.5 m of SPP initial values. The ionosphere delay parameters of Quasi-Zenith Satellite System (QZSS) are stated to be effective to improve SPP results, and additionally Satellite Based Augmentation System (SBAS) or International GNSS Service (IGS) pa-

rameters broadcasted from GNSS satellites can contribute to improve SPP. Furthermore, in order to get more precise initial positions of the antennas $u1$,$u2$, the receivers on the vehicles can utilize the last positions just before the stop, and the positions specified by the auxiliary sensors, namely gyro or altitude sensors, or the positions transmitted through communication means from reference stations.

The static positioning by DD-PPP/VPPP are stated to achieve approximately 50-cm RMS errors in Chapter 4. We consider the kinematic positioning of the DD-PPP/VPPP by using multiple antennas as a next step. PPP kinematic positioning algorithms by single antenna has been developed, and Singer models are applied as the state equations. Furthermore, the individual PPP kinematic positioning of two antennas (receivers) has been improved through VPPP-updating method by geometric distance constraints between two antennas. In the case of DD-PPP, we consider that the multiple unknown antenna positions are treated in a unified manner in the Kalman filter algorithms.

DD-PPP/VPPP methods are stated to have the unknown parameters of the multiple antennas' positions and the double-difference integer ambiguities which are estimated by the Kalman filter. Even though the fixed integer ambiguities and the small variances of them are set as the initial values, DD-PPP positioning results have offset values from the real antenna positions. The fixed integer values are obtained by the relative positioning in the static situation. While the baseline-vector estimates are more precisely obtained by the usage of the fixed integer ambiguities, because the offset values of two antennas can be canceled. It therefore can be effective for improving the attitude estimation among multiple antennas to converge the integer ambiguities to the fixed values in shorter time.

Publications during Doctoral Course

Journal papers:

A. Mouri, Y. Kubo, S. Sugimoto, and M. Ohashi: Detection and Correction of Doppler Outliers in Kalman Filter-based Positioning, *Transactions of The Institute of Systems, Control and Information Engineers*, Vol. 29, No. 1, pp. 18-28, January (2016).

A. Mouri, Y. Karatsu, S. Sugimoto, Y. Kubo, M. Ohashi and G. Okuda: New PPP/VPPP Algorithms by using Multiple Antennas, *Transactions of The Institute of Systems, Control and Information Engineers*, Vol. 29, No. 12, pp. 525-534, December (2016).

Conference papers:

A. Mouri, Y. Kubo and S. Sugimoto: Detection and Correction of Doppler Biases in Kalman Filter-based Positioning, *Proc. of the 46th ISCIE International Symposium on Stochastic Systems Theory and Its Applications (SSS'14)*, pp. 156-164, Kyoto, November (2014).

S. Sugimoto, Y. Suzuki, Y. Karatsu, M. Ozaki, A. Mouri, Y. Kubo: VPPP Algorithms with Multiple Antennas and their Applications, *Proc. of the 27th Int. Tech. Meeting of The Satellite Division of the Institute of Navigation (ION GNSS+ 2014)*, pp. 1073-1084, Tampa, Florida, September (2014).

Y. Karatsu, A. Mouri, Y. Kubo, and S. Sugimoto: Advancement of GNSS positioning using multiple antennas, *Proc. of the 59th Annual Conference of the Institute of Systems,*

Control and Information Engineers (ISCIE), Osaka, May 20-22 (2015) (in Japanese).

Y. Karatsu, A. Mouri, Y. Kubo and S. Sugimoto: Further Development of VPPP Algorithms with Multiple Antennas, *Proc. of the 28th Int. Tech. Meeting of The Satellite Division of the Institute of Navigation (ION GNSS+ 2015)*, pp. 1181-1192, Tampa, Florida, September (2015).

A. Mouri, Y. Karatsu, G. Okuda, S. Sugimoto, and Y. Kubo: Very Precise Point Positioning Algorithms among GNSS Antennas, *Proc. of the 60th Annual Conference of the Institute of Systems, Control and Information Engineers (ISCIE)*, Kyoto, May 25-27 (2016) (in Japanese).

A. Mouri, G. Okuda, S. Sugimoto, and Y. Kubo: VPPP Algorithms of Baseline Vector Estimation among Multiple Antennas, *Proc. of the 48th ISCIE International Symposium on Stochastic Systems Theory and Its Applications (SSS'16)*, Fukuoka, will appear in May (2017).

A. Mouri, G. Okuda, Y. Kubo and S. Sugimoto: Novel VPPP Algorithms with Multiple Antennas and Attitude Estimation, *Proc. of the 30th Int. Tech. Meeting of The Satellite Division of the Institute of Navigation (ION GNSS+ 2017)*, Moterey, California, will appear in June (2017).

Bibliography

[1] B. W. Parkinson and J. J. Spilker: *The Global Positioning System: Theory and Applications*, Vol. I, II, AIAA Publications (1996).

[2] B. Hofmann-Wellenhof, H. Lichtenegger and J. Collins: *GPS; Theory and Practice, 5th revised edition*, Springer-Verlag (2001).

[3] E. D. Kaplan and C. J. Hegarty (Eds.): *Understanding GPS: Principles and Applications 2nd edition*. Artech House, Boston and London (2006).

[4] http://www.navcen.uscg.gov/. UNITED STATES COAST GUARD Navigation Center Homepage, operated by U.S. Department of Homeland Security.

[5] http://www.glonass-iac.ru/en/. Information and Analysis Center for Positioning, Navigation and Timinig Homepage, operated by Russian Government.

[6] http://en.beidou.gov.cn/. BeiDou Navigation Satellite System Homepage, operated by Chinese Government.

[7] http://www.gsc-europa.eu/. European GNSS Service Centre Homepage, operated by European GNSS Agency.

[8] http://qzss.go.jp/en/. Michibiki (Quasi-Zenith Satellite System) Homepage, operated by Japanese Cabinet Office.

[9] T. Nakamizo: Robust Estimation (in Japanese), *Measuremnet and Control, Vol. 23, No. 6*, pp. 541-549, June (1984).

[10] Y. Kaneda, Y. Irizuki and M. Yamakita: Design Methods of Robust Kalman Filter Based on Statistics and Its Alpplication (in Japanese), *Trans. of ISCIE, Vol. 27, No. 2*, pp. 49-58, (2014).

[11] Y. Kubo, K. Sone and S. Sugimoto: Fault Detection in Carrier Phase GPS Positioning Based on Hypotheses Testing of Innovation Processes, *Int. J. of Innovative Computing, Information and Control Vol. 1*, No. 3, pp. 461-478, Sept. (2005).

[12] M. Kamimura, R. Tomita, T. Nagano, A. Chabata Y. Kubo and S. Sugimoto: Detection of Cycle Slips and Multipath in GNSS RTK Precise Point Positioning, *Proc. 24th Int. Technical Meeting of the Satellite Division of the Institute of Navigation (ION GNSS 2011)*, pp. 1056-1067, Portland, OR, Sept. (2011).

[13] International Standarss and Recommended Practices, Annex 10 to the Convention on Civil Aviation: Aeronautical Telecommunications, Vol. I: Radio Navigation Aids, 6th Ed., July (2006).

[14] R. Hirokawa, Y. Sato, S. Fujita and M. Miya: Compact SSR Messages with Integrity Information for Satellite based PPP-RTK Service, *Proc. 29th Int. Technical Meeting of the Satellite Division of the Institute of Navigation (ION GNSS+ 2016)*, pp. 3372-3376, Portland, OR, Sept. (2016).

[15] S. Sugimoto and Y. Kubo: GNSS Regressive Models and Precise Point Positioning, *Proc. of the 36th ISCIE Int. Symp. on Stochastic Systems Theory and Its Applications*, Saitama, pp. 47-48, Nov. (2004).

[16] S. Sugimoto and Y. Kubo: Carrier-Phase-Based Precise Point Positioning - a novel approach based on GNSS regression models, *Proc. GNSS 2004 Symposium*, No. P94, Sydney, NSW, Australia, Dec. (2004).

[17] Y. Kubo, A. Kitao, S. Fujita, and S. Sugimoto: A New RTK Algorithm for Carrier-Phase-Based Precise Point Positioning Based on GNSS Regression Model, *Proc. ION-GNSS 2005*, pp. 1492-1499, Long Beach, Sept. (2005).

[18] S. Sugimoto and Y. Kubo: Unified Methods of Point and Relative Positioning Based on GNSS Regression Equations, *Proc. 19th Int. Tech. Meeting of the Satellite Division of The Institute of Navigation (ION GNSS 2006)*, pp. 345-358, Fort Worth, Texas, Sep. (2006).

[19] S. Sugimoto, Y. Kubo, S. Fujta and T. Kazuno: A New GNSS Regressive Positioning Algorithm Based on GR Models, *Proc. of the 38th ISCIE Int. Symp. on Stochastic Systems Theory and Its Applications*, pp. 166-173, Suwa, Nagano, Japan, (Nov. 2006).

[20] S. Sugimoto: GNSS Positioning Algorithms based on GR Models, *Section 7.2.1 of GPS Handbook (in Japanese)* ed. by S. Sugimoto and R. Shibasaki, Asakura-Shoten, Tokyo, Japan (2010).

[21] S. Sugimoto, Y. Kubo and S. Fujita: Very Precise Point Positioning Based on GR Models, *Proc. of the 38th ISCIE Int. Symp. on Stochastic Systems Theory and Its Applications*, pp. 174-179, Suwa, Nagano, Japan, Nov. (2006).

[22] S. Sugimoto, Y. Suzuki and Y. Kubo: RTK-VPPP Algorithms in Urvan Canyons, *Proc. of the 45th ISCIE Int. Symp. on Stochastic Systems Theory and Its Applications*, pp. 178-186, Okinawa, Japan, Nov. (2013).

[23] S. Sugimoto, Y. Suzuki, Y. Karatsu, M. Ozaki, A. Mouri, Y. Kubo: VPPP Algorithms with Multiple Antennas and their Applications, *Proc. of the 27th Int. Tech. Meeting of The Satellite Division of the Institute of Navigation (ION GNSS+ 2014)*, pp. 1073-1084, Tampa, Florida, Sept. (2014),

[24] Y. Karatsu, M. Ozaki, Y. Kubo, S. Sugimoto: Further Studies on the VPPP Algorithms by using Multiple Antennas, *Proc. of the 46th ISCIE Int. Symp. on Stochastic Systems Theory and Its Applications*, pp. 171-179, Kyoto, Japan, Nov. (2014).

[25] Y. Karatsu, A. Mouri, Y. Kubo and S. Sugimoto: Further Developments of VPPP Algorithms with Multiple Antennas, *Proc. of the 28th Int. Tech. Meeting of the Satellite Division of the Institute of Navigation (ION GNSS+ 2015)*, pp. 1181 - 1192, Tampa, Florida (Sept. 2015).

[26] P. Misra and P. Enge: *Global Positioning System - Signals, Measurements, and Performance, 2nd Edition*, Ganga-Jamuna Press, Massachusetts (2006).

[27] M. Bahrami and M. Ziebart: A Kalman Filter-based Doppler-smoothing of Code Pseudoranges in GNSS-Challenged Environments, *Proc. 24th Int. Technical Meeting of the Satellite Division of the Institute of Navigation (ION GNSS 2011)*, pp. 2362-2372, Portland, OR, Sept. (2011).

[28] O. Arai: Functions of Positioning Signal Receiver Equipments *Section 5.2.7 of GPS Handbook (in Japanese)* ed. by S. Sugimoto and R. Shibasaki, Asakura-Shoten, Tokyo, Japan (2010).

[29] Y. Gao, and X. Shen: A New Method for Carrier-Phase-Based Precise Point Positioning, *Journal of the Institute of Navigation*, Vol 49, No. 2, pp. 109-116 (Summer 2002).

[30] Peter J. G. Teunissen and A. Kleusberg (Eds.): *GPS for Geodesy, 2nd Edition*, Springer-Verlag, New York (1998).

[31] A. Leick: *GPS Satellite Surveying, 3rd Edition*, John Wiley & Sons, New York (2004).

[32] Y. Gao and Z. Z. Lin: Precise Ionosphere Modeling Using Regional GPS Network Data, *J. of Global Positioning Systems*, Vol. 1, No. 1, pp. 18-24, July (2002).

[33] R. G. Brown and P. Y. C. Hwang: *Introduction to Random Signals and Applied Kalman Filtering, 3rd Edition*, John Wiley & Sons, New York (1997).

[34] A. Chabata, Y. Suzuki, Y. Kubo and S. Sugimoto: RTK-PPP Algorithms using GNSS Observables from Few Satellits, *Proc. 25th Int. Technical Meeting of the Satellite Division of the Institute of Navigation (ION GNSS 2012)*, pp. 3696-3707, Nashville, Tennessee, Sept. (2012).

[35] T. Katayama: *Applied Kalman Filtering*, New edition, Asakura, Tokyo, 2000 (in Japanese).

[36] S. Sugimoto: Stochastic Statistics and Kalman Filter, *Appendix A4 in GPS Handbook (in Japanese)*, pp. 432-460, ed. by S. Sugimoto and R. Shibasaki, Asakura-Shoten, Tokyo, Japan (2010).

[37] M. E. Cannon: High Accuracy GPS Semi-Kinematic Positioning: Modelling and Results, *Proc. 2nd Int. Tech. Meeting of the Satellite Division of the Institute of Navigation (ION GPS-89)*, pp. 405-418, (1989).

[38] M. Bahrami and M. Ziebart: Doppler-Aided Positioning: Improving Single-Frequency RTK in the Urban Environment, *GPS World*, pp. 47-56, May (2011).

[39] A. Mouri, Y. Kubo and S. Sugimoto: Detection and Correction of Doppler Biases in Kalman Filter-based Positioning, *Proc. of the 46th ISCIE International Symposium on Stochastic Systems Theory and Its Applications (SSS'14)*, pp. 156-164, Kyoto, Nov. (2014).

[40] R. A. Singer: Estimating Optimal Tracking Filter Performance for Manned Maneuvering Targets, *IEEE Trans. Aerospace and Electronic Systems*, Vol. AES-6, No. 4, pp. 473-483, July (1970).

[41] M. Basseville: Detecting Changes in Signals and Systems, *Automatica, Vol. 24, No. 3*, pp. 499-501, (1979).

[42] J. Wang and Y. Kubo: RAIM error detection based on least square residuals, *Section 7.4.3 in GPS Handbook (in Japanese)*, ed. by S. Sugimoto and R. Shibasaki, Asakura-Shoten, Tokyo, Japan (2010).

[43] Y. Kubo: Point Positioning Algorithms, *Appendix A3 in GPS Handbook (in Japanese)*, pp. 422-431, ed. by S. Sugimoto and R. Shibasaki, Asakura-Shoten, Tokyo, Japan (2010).

[44] G. Giorgi: The Multivariate Constrained LAMBDA Method for Single-epoch, Single-frequency GNSS-based Full Attitude Determination, *Proc. 23rd Int. Technical Meeting of the Satellite Division of the Institute of Navigation (ION GNSS 2010)*, pp. 1429-1439, Portland, OR, Sept. (2010).

[45] *u-blox Product Catalog Issue 18.0*, u-blox AG, Feb. (2016).

[46] S. Fujita Y. Kubo: Correction of Ionosphere Delays, *Section 4.2 in GPS Handbook (in Japanese)*, pp. 78-87, ed. by S. Sugimoto and R. Shibasaki, Asakura-Shoten, Tokyo, Japan (2010).

[47] M. Fukuda: GNSS Applications to Attitude Determination Systems, *Chapter 13 in GPS Handbook (in Japanese)*, pp. 306-330, ed. by S. Sugimoto and R. Shibasaki, Asakura-Shoten, Tokyo, Japan (2010).

[48] P. Henkel and C. Gunther: Attitude determination with low-cost GPS/INS, *Proc. ION GNSS+ 2013*, pp. 2015-2023, Nashville, Tennessee, Sept. (2013).

[49] A. Mouri, Y. Karatsu, S. Sugimoto, Y. Kubo, M. Ohashi and G. Okuda: New PPP/VPPP Algorithms by using Multiple Antennas, *Transactions of The Institute of Systems, Control and Information Engineers*, Vol. 29, No. 12, pp. 525-534, Dec. (2016).

[50] Peter J. G. Teunissen: A-PPP: Array-Aided Precise Point Positioning with Global Navigation Satellite Systems, *IEEE Trans. on Signal Processing*, Vol. 60, No. 6, pp. 1-12, June (2012).

[51] F. Landis Markley and John L. Grassidis: Attitude Representations, *2.9 in Fundamentals of Spacecraft Attitude Determination and Control*, pp. 41-59, Space Technology library, New York, USA (2014).

[52] G. Wahba: A Least Squares Estimate of Spacecraft Attitude, *SIAM Review*, Vol. 7, No. 3, p. 409, July (1965).

Appendix A

DD-PPP/VPPP Equations for Three or Four Antennas

Let us define the $(n_s - 1) \times 1$ vectors as follows:

$$\tilde{\rho}^{n_s}_{CA,ji} \equiv \begin{bmatrix} \tilde{\rho}^{\hat{2}\hat{1}}_{CA,\hat{u}_j\hat{u}_i} \\ \vdots \\ \tilde{\rho}^{\hat{n}_s\hat{1}}_{CA,\hat{u}_j\hat{u}_i} \end{bmatrix}, \quad \tilde{\Phi}^{n_s}_{L1,ji} \equiv \begin{bmatrix} \tilde{\Phi}^{\hat{2}\hat{1}}_{L1,\hat{u}_j\hat{u}_i} \\ \vdots \\ \tilde{\Phi}^{\hat{n}_s\hat{1}}_{L1,\hat{u}_j\hat{u}_i} \end{bmatrix}, \quad N^{\hat{n}_s}_{L1,ji} = \begin{bmatrix} N^{\hat{2}\hat{1}}_{L1,u_ju_i} \\ \vdots \\ N^{\hat{n}_s\hat{1}}_{L1,u_ju_i} \end{bmatrix}, \quad \text{(A.1)}$$

also define $3 \times (n_s - 1)$ matrix

$$g^{n_s}_j = \begin{bmatrix} g^{\hat{2}\hat{1}}_{\hat{u}_j} \cdots g^{\hat{n}_s\hat{1}}_{\hat{u}_j} \end{bmatrix} : \quad 3 \times (n_s - 1). \quad \text{(A.2)}$$

Measurement equation for antennas of u_1, u_2 and u_3 $(n_r = 3)$ is as follows:

$$y^{n_s}_{u_3u_2u_1} = C^{n_s}_{u_3u_2u_1}\eta^{n_s}_{u_3u_2u_1} + v^{n_s}_{u_3u_2u_1}, \quad \text{(A.3)}$$

where

$$\begin{bmatrix} \tilde{\rho}^{\hat{2}\hat{1}}_{CA,\hat{u}_2\hat{u}_1} \\ \vdots \\ \tilde{\rho}^{\hat{n}_s\hat{1}}_{CA,\hat{u}_2\hat{u}_1} \\ \tilde{\rho}^{\hat{2}\hat{1}}_{CA,\hat{u}_3\hat{u}_1} \\ \vdots \\ \tilde{\rho}^{\hat{n}_s\hat{1}}_{CA,\hat{u}_3\hat{u}_1} \\ \tilde{\rho}^{\hat{2}\hat{1}}_{CA,\hat{u}_3\hat{u}_2} \\ \vdots \\ \tilde{\rho}^{\hat{n}_s\hat{1}}_{CA,\hat{u}_3\hat{u}_2} \\ \tilde{\Phi}^{\hat{2}\hat{1}}_{L1,\hat{u}_2\hat{u}_1} \\ \vdots \\ \tilde{\Phi}^{\hat{n}_s\hat{1}}_{L1,\hat{u}_2\hat{u}_1} \\ \tilde{\Phi}^{\hat{2}\hat{1}}_{L1,\hat{u}_3\hat{u}_1} \\ \vdots \\ \tilde{\Phi}^{\hat{n}_s\hat{1}}_{L1,\hat{u}_3\hat{u}_1} \\ \tilde{\Phi}^{\hat{2}\hat{1}}_{L1,\hat{u}_3\hat{u}_2} \\ \vdots \\ \tilde{\Phi}^{\hat{n}_s\hat{1}}_{L1,\hat{u}_3\hat{u}_2} \end{bmatrix} = \begin{bmatrix} -(g^{\hat{2}\hat{1}}_{\hat{u}_1})^{\mathrm{T}} & (g^{\hat{2}\hat{1}}_{\hat{u}_2})^{\mathrm{T}} & & 0 & \cdots & & & & & 0 \\ \vdots & \vdots & & \vdots & \ddots & & & & & \vdots \\ -(g^{\hat{n}_s\hat{1}}_{\hat{u}_1})^{\mathrm{T}} & (g^{\hat{n}_s\hat{1}}_{\hat{u}_2})^{\mathrm{T}} & & \vdots & & \ddots & & & & \vdots \\ -(g^{\hat{2}\hat{1}}_{\hat{u}_1})^{\mathrm{T}} & & (g^{\hat{2}\hat{1}}_{\hat{u}_3})^{\mathrm{T}} & \vdots & & & \ddots & & & \vdots \\ \vdots & & \vdots & \vdots & & & & \ddots & & \vdots \\ -(g^{\hat{n}_s\hat{1}}_{\hat{u}_1})^{\mathrm{T}} & & (g^{\hat{n}_s\hat{1}}_{\hat{u}_3})^{\mathrm{T}} & \vdots & & & & & \ddots & \vdots \\ & -(g^{\hat{2}\hat{1}}_{\hat{u}_2})^{\mathrm{T}} & (g^{\hat{2}\hat{1}}_{\hat{u}_3})^{\mathrm{T}} & \vdots & & & & & \ddots & \vdots \\ & \vdots & \vdots & \vdots & & & & & & \ddots \\ & -(g^{\hat{n}_s\hat{1}}_{\hat{u}_2})^{\mathrm{T}} & (g^{\hat{n}_s\hat{1}}_{\hat{u}_3})^{\mathrm{T}} & \vdots & \cdots & & & & & 0 \\ -(g^{\hat{2}\hat{1}}_{\hat{u}_1})^{\mathrm{T}} & (g^{\hat{2}\hat{1}}_{\hat{u}_2})^{\mathrm{T}} & & \lambda_1 & & & & & & \\ \vdots & \vdots & & & \ddots & & & & & \\ -(g^{\hat{n}_s\hat{1}}_{\hat{u}_1})^{\mathrm{T}} & (g^{\hat{n}_s\hat{1}}_{\hat{u}_2})^{\mathrm{T}} & & & & \lambda_1 & & & & \\ -(g^{\hat{2}\hat{1}}_{\hat{u}_1})^{\mathrm{T}} & & (g^{\hat{2}\hat{1}}_{\hat{u}_3})^{\mathrm{T}} & & & & \lambda_1 & & & \\ \vdots & & \vdots & & & & & \ddots & & \\ -(g^{\hat{n}_s\hat{1}}_{\hat{u}_1})^{\mathrm{T}} & & (g^{\hat{n}_s\hat{1}}_{\hat{u}_3})^{\mathrm{T}} & & & & & & \lambda_1 & \\ & -(g^{\hat{2}\hat{1}}_{\hat{u}_2})^{\mathrm{T}} & (g^{\hat{2}\hat{1}}_{\hat{u}_3})^{\mathrm{T}} & & & & & & & \lambda_1 \\ & \vdots & \vdots & & & & & & & \ddots \\ & -(g^{\hat{n}_s\hat{1}}_{\hat{u}_2})^{\mathrm{T}} & (g^{\hat{n}_s\hat{1}}_{\hat{u}_3})^{\mathrm{T}} & & & & & & & \lambda_1 \end{bmatrix} \begin{bmatrix} u_1 \\ u_2 \\ u_3 \\ N^{21}_{L1,u_2u_1} \\ \vdots \\ N^{n_s1}_{L1,u_2u_1} \\ N^{21}_{L1,u_3u_1} \\ \vdots \\ N^{n_s1}_{L1,u_3u_1} \\ N^{21}_{L1,u_3u_2} \\ \vdots \\ N^{n_s1}_{L1,u_3u_2} \end{bmatrix} + v. \tag{A.4}$$

In this case, we have

$$M_3 \equiv \left[\begin{array}{ccc|ccc} (\frac{1}{r_{d_{21}}}+\frac{1}{r_{d_{31}}})I & -\frac{1}{r_{d_{21}}}I & -\frac{1}{r_{d_{31}}}I & 0 & \cdots & 0 \\ -\frac{1}{r_{d_{21}}}I & (\frac{1}{r_{d_{21}}}+\frac{1}{r_{d_{32}}})I & -\frac{1}{r_{d_{32}}}I & \vdots & & \vdots \\ -\frac{1}{r_{d_{31}}}I & -\frac{1}{r_{d_{32}}}I & (\frac{1}{r_{d_{31}}}+\frac{1}{r_{d_{32}}})I & 0 & \cdots & 0 \\ \hline 0 & \cdots & 0 & 0 & \cdots & 0 \\ \vdots & & \vdots & \vdots & & \vdots \\ 0 & \cdots & 0 & 0 & \cdots & 0 \end{array}\right], \tag{A.5}$$

$$c_{M_3} \equiv \left[\begin{array}{cccccc} d_{\kappa 21}^{\mathrm{T}} + d_{\kappa 31}^{\mathrm{T}} & -d_{\kappa 21}^{\mathrm{T}} + d_{\kappa 32}^{\mathrm{T}} & -d_{\kappa 31}^{\mathrm{T}} - d_{\kappa 32}^{\mathrm{T}} & 0^{\mathrm{T}} & \cdots & 0^{\mathrm{T}} \end{array} \right]. \tag{A.6}$$

Then the measurement equation for four antennas of $u_1, \cdots, u_4$ ($n_r = 4$) is as follows:

$$y_{u_4u_3u_2u_1}^{n_s} = C_{u_4u_3u_2u_1}^{n_s} \eta_{u_4u_3u_2u_1}^{n_s} + v_{u_4u_3u_2u_1}^{n_s}, \tag{A.7}$$

where

$$\left[\begin{array}{c} \tilde{\rho}_{CA,21}^{n_s} \\ \tilde{\rho}_{CA,31}^{n_s} \\ \tilde{\rho}_{CA,41}^{n_s} \\ \tilde{\rho}_{CA,32}^{n_s} \\ \tilde{\rho}_{CA,42}^{n_s} \\ \tilde{\rho}_{CA,43}^{n_s} \\ \tilde{\Phi}_{L1,21}^{n_s} \\ \tilde{\Phi}_{L1,31}^{n_s} \\ \tilde{\Phi}_{L1,41}^{n_s} \\ \tilde{\Phi}_{L1,32}^{n_s} \\ \tilde{\Phi}_{L1,42}^{n_s} \\ \tilde{\Phi}_{L1,43}^{n_s} \end{array} \right] = \left[\begin{array}{cccccccccc} -(g_1^{n_s})^{\mathrm{T}} & (g_2^{n_s})^{\mathrm{T}} & & & & & & & & \\ -(g_1^{n_s})^{\mathrm{T}} & & (g_3^{n_s})^{\mathrm{T}} & & & & & & & \\ -(g_1^{n_s})^{\mathrm{T}} & & & (g_4^{n_s})^{\mathrm{T}} & & & & & & \\ & -(g_2^{n_s})^{\mathrm{T}} & (g_3^{n_s})^{\mathrm{T}} & & & & & & & \\ & -(g_2^{n_s})^{\mathrm{T}} & & (g_4^{n_s})^{\mathrm{T}} & & & & & & \\ & & -(g_3^{n_s})^{\mathrm{T}} & (g_4^{n_s})^{\mathrm{T}} & & & & & & \\ -(g_1^{n_s})^{\mathrm{T}} & (g_2^{n_s})^{\mathrm{T}} & & & \lambda_1 I & & & & & \\ -(g_1^{n_s})^{\mathrm{T}} & & (g_3^{n_s})^{\mathrm{T}} & & & \lambda_1 I & & & & \\ -(g_1^{n_s})^{\mathrm{T}} & & & (g_4^{n_s})^{\mathrm{T}} & & & \ddots & & & \\ & -(g_2^{n_s})^{\mathrm{T}} & (g_3^{n_s})^{\mathrm{T}} & & & & & \ddots & & \\ & -(g_2^{n_s})^{\mathrm{T}} & & (g_4^{n_s})^{\mathrm{T}} & & & & & \ddots & \\ & & -(g_3^{n_s})^{\mathrm{T}} & (g_4^{n_s})^{\mathrm{T}} & & & & & & \lambda_1 I \end{array} \right] \left[\begin{array}{c} u_1 \\ u_2 \\ u_3 \\ u_4 \\ N_{L1,21}^{n_s} \\ N_{L1,31}^{n_s} \\ N_{L1,41}^{n_s} \\ N_{L1,32}^{n_s} \\ N_{L1,42}^{n_s} \\ N_{L1,43}^{n_s} \end{array} \right] + v, \tag{A.8}$$

$$M_4^{(11)} \equiv \left[\begin{array}{cc} (\frac{1}{r_{d_{21}}} + \frac{1}{r_{d_{31}}} + \frac{1}{r_{d_{41}}})I & -\frac{1}{r_{d_{21}}} I \\ -\frac{1}{r_{d_{21}}} I & (\frac{1}{r_{d_{21}}} + \frac{1}{r_{d_{32}}} + \frac{1}{r_{d_{42}}})I \end{array} \right], \quad M_4^{(12)} \equiv \left[\begin{array}{cc} -\frac{1}{r_{d_{31}}} I & -\frac{1}{r_{d_{41}}} I \\ -\frac{1}{r_{d_{32}}} I & -\frac{1}{r_{d_{42}}} I \end{array} \right],$$

$$M_4^{(21)} \equiv \left[\begin{array}{cc} -\frac{1}{r_{d_{31}}} I & -\frac{1}{r_{d_{32}}} I \\ -\frac{1}{r_{d_{41}}} I & -\frac{1}{r_{d_{42}}} I \end{array} \right], \quad M_4^{(22)} \equiv \left[\begin{array}{cc} (\frac{1}{r_{d_{31}}} + \frac{1}{r_{d_{32}}} + \frac{1}{r_{d_{43}}})I & -\frac{1}{r_{d_{43}}} I \\ -\frac{1}{r_{d_{43}}} I & (\frac{1}{r_{d_{41}}} + \frac{1}{r_{d_{42}}} + \frac{1}{r_{d_{43}}})I \end{array} \right],$$

$$M_4 \equiv \left[\begin{array}{cc|cc} M_4^{(11)} & M_4^{(12)} & O & O \\ M_4^{(21)} & M_4^{(22)} & O & O \\ \hline O & O & O & O \\ O & O & O & O \end{array}\right], \tag{A.9}$$

$$\begin{aligned} c_{M_4}^{(11)} &= d_{\kappa 21}^{\mathrm{T}} + d_{\kappa 31}^{\mathrm{T}} + d_{\kappa 41}^{\mathrm{T}}, \quad c_{M_4}^{(12)} = -d_{\kappa 21}^{\mathrm{T}} + d_{\kappa 32}^{\mathrm{T}} + d_{\kappa 42}^{\mathrm{T}}, \\ c_{M_4}^{(13)} &= -d_{\kappa 31}^{\mathrm{T}} - d_{\kappa 32}^{\mathrm{T}} + d_{\kappa 43}^{\mathrm{T}}, \quad c_{M_4}^{(14)} = -d_{\kappa 41}^{\mathrm{T}} - d_{\kappa 42}^{\mathrm{T}} - d_{\kappa 43}^{\mathrm{T}}, \\ c_{M_4} &\equiv \left[\begin{array}{cccccc} c_{M_4}^{(11)} & c_{M_4}^{(12)} & c_{M_4}^{(13)} & c_{M_4}^{(14)} & 0^{\mathrm{T}} & \cdots \quad 0^{\mathrm{T}} \end{array}\right]. \end{aligned} \tag{A.10}$$

Appendix B

Kalman Filter Estimation Methods

Kalman filter was officially announced by Rudolf E. Kalman in 1960, and is the optimum filter which successively estimates system states on the basis of the following four conditions: (1) Linearity of system equations, (2) White noises of systems and observable noises, (3) Gaussian of noises, and (4) Least square norm.

Kalman filter is also based on the discrete-time system theory, and we consider linear stochastic system models as follows:

$$\text{(State equation):}\ \ x(t+1) = Fx(t) + Gw(t), \tag{B.1}$$

$$\text{(Observation equation):}\ \ y(t) = H(t)x(t) + v(t), \tag{B.2}$$

where

$x(t) \in R^n$: State vector, $\ y(t) \in R^p$: Observation vector,

$w(t) \in R^r$: System-noise vector, $\ v(t) \in R^p$: Observation-noise vector,

$F \in R^{n\times n}$, $\ G \in R^{n\times r}$, $\ H(t) \in R^{p\times n}$: Coefficient matrix.

Eq. (B.1) shows a stochastic process of $x(t)$. Eq. (B.2) is equivalent with a linear-regression equation for unknown parameter estimation. The equations of Kalman filter

are as follows:

(System equations)

$$\hat{x}(t+1|t) = F\hat{x}(t|t) \tag{B.3}$$

$$\hat{x}(t|t) = \hat{x}(t|t-1) + K(t)\Big[y(t) - H(t)\hat{x}(t|t-1)\Big] \tag{B.4}$$

(Covariance matrix of estimation errors)

$$P(t+1|t) = FP(t|t)F^{\mathrm{T}} + GQ(t)G^{\mathrm{T}} \tag{B.5}$$

$$P(t|t) = P(t|t-1) - K(t)H(t)P(t|t-1) \tag{B.6}$$

(Kalman gain)

$$K(t) = P(t|t-1)H^{\mathrm{T}}(t)\Big[H(t)P(t|t-1)H^{\mathrm{T}}(t) + R(t)\Big]^{-1} \tag{B.7}$$

(Innovation process)

$$\nu(t) \equiv y(t) - H(t)\hat{x}(t|t-1) \tag{B.8}$$

$$M(t) \equiv H(t)P(t|t-1)H^{\mathrm{T}}(t) + R(t) \tag{B.9}$$

(Initial condition)

$$\hat{x}(0|-1) = \bar{x}(0), \quad P(0|-1) = \Sigma(0) \tag{B.10}$$

where $R(t)$ is an observation-noise covariance matrix, and $Q(t)$ is a system-noise covariance matrix. $\nu(t)$ is a Gaussian white noise process with zero mean, and independent between epochs. $M(t)$ is a covariance matrix of $\nu(t)$.

The Kalman filtering process has two steps. One is the update step of Eqs. (B.4) and (B.6). The other is the prediction step of Eqs. (B.3) and (B.5). The initial conditions generated by SPP are input into the update step. The observables $y(t)$ and $R(t)$ are input into the update step, and $Q(t)$ is input into the prediction step every epoch, respectively.

GNSS observation equations are nonlinear functions, therefore extended Kalman filter

is utilized for state estimation. In general, nonlinear system models are as follows:

$$\text{(State equation):}\ \ x(t+1) = f_t(x(t)) + w(t), \tag{B.11}$$

$$\text{(Observation equation):}\ \ y(t) = h_t(x(t)) + v(t). \tag{B.12}$$

The nonlinear functions f_t and h_t are expanded by Taylor series around the estimate values $\hat{x}(t|t)$ and $\hat{x}(t|t-1)$, respectively, as follows:

$$f_t(x(t)) = f_t(\hat{x}(t|t)) + \hat{F}_t(x(t) - \hat{x}(t|t)) + \cdots, \tag{B.13}$$

$$h_t(x(t)) = h_t(\hat{x}(t|t-1)) + \hat{H}_t(x(t) - \hat{x}(t|t-1)) + \cdots, \tag{B.14}$$

where

$$\hat{F}_t = \left(\frac{\partial f_t}{\partial x(t)}\right)_{x=\hat{x}(t|t)}, \quad \hat{H}_t = \left(\frac{\partial h_t}{\partial x(t)}\right)_{x=\hat{x}(t|t-1)}. \tag{B.15}$$

The terms greater than the first-order term of Taylor series in Eqs. (B.13) and (B.14) are negligible. Then, they are input into Eqs. (B.11) and (B.12), respectively, as follows:

$$x(t+1) = \hat{F}_t x(t) + w(t) + f_t(\hat{x}(t|t)) - \hat{F}_t\hat{x}(t|t), \tag{B.16}$$

$$y(t) = \hat{H}_t x(t) + v(t) + h_t(\hat{x}(t|t-1)) - \hat{H}_t\hat{x}(t|t-1). \tag{B.17}$$

Then, we obtain linearized system models as follows:

$$\tilde{x}(t+1) = x(t+1) - f_t(\hat{x}(t|t)) + \hat{F}_t\hat{x}(t|t) = \hat{F}_t x(t) + w(t), \tag{B.18}$$

$$\tilde{y}(t) = y(t) - h_t(\hat{x}(t|t-1)) + \hat{H}_t\hat{x}(t|t-1) = \hat{H}_t x(t) + v(t). \tag{B.19}$$

We consider that $\hat{H}_t = C_{\eta_L}$ and the state equation $x(t+1) = x(t)$ in a static observation environment of GNSS signals, Eqs. (2.120)-(2.125) are derived as extended Kalman filter.

Appendix C

Antennas' Height Constraints for DD-VPPP

If we can assume that the heights of two antennas are approximately same. Namely, the local East, North, Up (ENU) coordinates of antennas' positions u_1 and u_2 are described by

$$u_1 = \begin{bmatrix} u_{1,\mathrm{E}} \\ u_{1,\mathrm{N}} \\ u_{1,\mathrm{U}} \end{bmatrix}, \quad u_2 = \begin{bmatrix} u_{2,\mathrm{E}} \\ u_{2,\mathrm{N}} \\ u_{2,\mathrm{U}} \end{bmatrix}, \tag{C.1}$$

respectively. Then we assume that

$$u_{1,\mathrm{U}} \cong u_{2,\mathrm{U}}, \tag{C.2}$$

or

$$d_{21} \equiv ||u_{2,\mathrm{EN}} - u_{1,\mathrm{EN}}|| + e_{d_{21}}, \tag{C.3}$$

$$a_{21} \equiv 0 = (u_{2,\mathrm{U}} - u_{1,\mathrm{U}}) + e_{a_{21}}, \tag{C.4}$$

where $e_{d_{21}}$, $e_{a_{21}}$ are assumed as zero mean Gaussian white noises such as

$$e_{a_{21}} \sim \mathrm{N}(0, r_{e_{a_{21}}}), \quad e_{a_{21}} \sim \mathrm{N}(0, r_{e_{a_{21}}}).$$

Then the constraint (or the so-called pseudo-observation) updates the CPDF of the state vector η as follows:

$$\begin{aligned} & p(\eta_t|Y^t, d_{21,t}, a_{21,t}) \\ &= K_0(Y^t, d_{21,t}) p(\eta_t|Y^t) p(d_{21,t}, a_{21,t}|\eta_t). \end{aligned} \tag{C.5}$$

Then we have

$$\begin{aligned} p(d_{21,t}, a_{21,t}|\eta_t) = & \frac{1}{\sqrt{2\pi r_{d_{21}}}} \exp\Big\{ - \frac{[d_{21} - ||u_{2,\mathrm{EN}} - u_{1,\mathrm{EN}}||]^2}{2r_{d_{21}}} \Big\} \\ & \times \frac{1}{\sqrt{2\pi r_{a_{21}}}} \exp\Big\{ - \frac{[a_{21} - (u_{2,\mathrm{U}} - u_{1,\mathrm{U}})]^2}{2r_{a_{21}}} \Big\}. \end{aligned} \tag{C.6}$$

Therefore, $p(\eta_t|Y^t, d_{21,t}, a_{21,t})$ in Eq. (C.5) is expressed as follows:

$$\begin{aligned} p(\eta_t|Y^t, d_{21,t}, a_{21,t}) = & K_0(Y^t, d_{21,t}, a_{21,t}) \frac{1}{(2\pi)^{n'/2} |\Sigma_{\eta,t|t}|^{1/2}} \\ & \times \exp\Big\{ - \frac{1}{2} [\eta_t - \hat{\eta}_{t|t}]^{\mathrm{T}} \Sigma_{\eta,t|t}^{-1} [\eta_t - \hat{\eta}_{t|t}] \Big\} \\ & \times \frac{1}{\sqrt{2\pi r_{d_{21}}}} \exp\Big\{ - \frac{[||u_{2,\mathrm{EN}} - u_{1,\mathrm{EN}}||]^2}{2r_{d_{21}}} \Big\} \\ & \times \frac{1}{\sqrt{2\pi r_{a_{21}}}} \exp\Big\{ - \frac{[a_{21} - (u_{2,\mathrm{U}} - u_{1,\mathrm{U}})]^2}{2r_{a_{21}}} \Big\}. \end{aligned} \tag{C.7}$$

The power term of the exponential in Eq. (C.6) can be expressed by the quadratic form of the state vector η as follows:

$$\begin{aligned} & \frac{[d_{21} - ||u_{2,\mathrm{EN}} - u_{1,\mathrm{EN}}||]^2}{2r_{d_{21}}} \\ &= \frac{1}{2r_{d_{21}}} \Big\{ d_{21}^2 + ||u_{2,\mathrm{EN}} - u_{1,\mathrm{EN}}||^2 - 2d_{21}||u_{2,\mathrm{EN}} - u_{1,\mathrm{EN}}|| \Big\} \\ &= \frac{1}{2r_{d_{21}}} \Big\{ d_{21}^2 + (u_{2,\mathrm{EN}} - u_{1,\mathrm{EN}})^{\mathrm{T}} (u_{2,\mathrm{EN}} - u_{1,\mathrm{EN}}) - 2d_{21}||u_{2,\mathrm{EN}} - u_{1,\mathrm{EN}}|| \Big\} \\ &\cong \frac{1}{2} \Big\{ \frac{d_{21}^2}{r_{d_{21}}} + \frac{1}{r_{d_{21}}} u_{2,\mathrm{EN}}^{\mathrm{T}} u_{2,\mathrm{EN}} - \frac{1}{r_{d_{21}}} u_{2,\mathrm{EN}}^{\mathrm{T}} u_{1,\mathrm{EN}} - \frac{1}{r_{d_{21}}} u_{1,\mathrm{EN}}^{\mathrm{T}} u_{2,\mathrm{EN}} + \frac{1}{r_{d_{21}}} u_{1,\mathrm{EN}}^{\mathrm{T}} u_{1,\mathrm{EN}} \\ & - c_{21,\mathrm{EN}}^{\mathrm{T}} u_2 + c_{21,\mathrm{EN}}^{\mathrm{T}} u_1 \Big\}, \end{aligned} \tag{C.8}$$

where

$$||u_{2,\mathrm{EN}} - u_{1,\mathrm{EN}}|| \cong \frac{(\hat{u}_{2,\mathrm{EN}} - \hat{u}_{1,\mathrm{EN}})^{\mathrm{T}}}{||\hat{u}_{2,\mathrm{EN}} - \hat{u}_{1,\mathrm{EN}}||^2}(u_{2,\mathrm{EN}} - u_{1,\mathrm{EN}}) \equiv \kappa_{21,\mathrm{EN}}^{\mathrm{T}}(u_{2,\mathrm{EN}} - u_{1,\mathrm{EN}}), \tag{C.9}$$

and

$$c_{21,\mathrm{EN}}^{\mathrm{T}} = \frac{2d_{21}\kappa_{21,\mathrm{EN}}^{\mathrm{T}}}{r_{d_{21}}}. \tag{C.10}$$

Finally, we have the expression of the quadratic form:

$$\frac{1}{2}\frac{[d_{21} - ||u_{2,\mathrm{EN}} - u_{1,\mathrm{EN}}||]^2}{r_{d_{21}}} \cong \frac{1}{2}\Big\{\eta^{\mathrm{T}} M_{2,\mathrm{EN}}\eta + c_{M_{2,\mathrm{EN}}}^{\mathrm{T}}\eta + \frac{d_{21}^2}{r_{d_{21}}}\Big\}, \tag{C.11}$$

where

$$M_{2,\mathrm{EN}} \equiv \left[\begin{array}{ccc|ccc} \frac{1}{r_{d_{21}}}B_{\mathrm{EN}} & & -\frac{1}{r_{d_{21}}}B_{\mathrm{EN}} & 0 & \cdots & 0 \\ -\frac{1}{r_{d_{21}}}B_{\mathrm{EN}} & & \frac{1}{r_{d_{21}}}B_{\mathrm{EN}} & 0 & \cdots & 0 \\ \hline 0 & \cdots & 0 & 0 & \cdots & 0 \\ \vdots & & \vdots & & \vdots & \\ 0 & \cdots & 0 & 0 & \cdots & 0 \end{array}\right], \quad B_{\mathrm{EN}} \equiv \begin{bmatrix} 1 & 0 & 0 \\ 0 & 1 & 0 \\ 0 & 0 & 0 \end{bmatrix}, \tag{C.12}$$

$$c_{M_{2,\mathrm{EN}}}^{\mathrm{T}} \equiv \begin{bmatrix} c_{21,\mathrm{EN}}^{\mathrm{T}} & -c_{21,\mathrm{EN}}^{\mathrm{T}} & 0^{\mathrm{T}} & \cdots & 0^{\mathrm{T}} \end{bmatrix}. \tag{C.13}$$

And then

$$\begin{aligned} &\frac{[0 - (u_{2,\mathrm{U}} - u_{1,\mathrm{U}})]^2}{2r_{a_{21}}} \\ &= \frac{1}{2r_{a_{21}}}\left\{u_{2,\mathrm{U}}^2 + u_{1,\mathrm{U}}^2 - u_{2,\mathrm{U}}u_{1,\mathrm{U}} - u_{1,\mathrm{U}}u_{2,\mathrm{U}}\right\} \\ &= \frac{1}{2}\Big\{u_{2,\mathrm{U}}\frac{1}{r_{a_{21}}}u_{2,\mathrm{U}} + u_{1,\mathrm{U}}\frac{1}{r_{a_{21}}}u_{1,\mathrm{U}} - u_{2,\mathrm{U}}\frac{1}{r_{a_{21}}}u_{1,\mathrm{U}} - u_{2,\mathrm{U}}\frac{1}{r_{a_{21}}}u_{1,\mathrm{U}}\Big\} \\ &= \frac{1}{2}\eta^{\mathrm{T}} M_{2,\mathrm{U}}\eta, \end{aligned} \tag{C.14}$$

where

$$M_{2,\mathrm{U}} \equiv \left[\begin{array}{ccc|ccc} \frac{1}{r_{a21}}B_{\mathrm{U}} & & -\frac{1}{r_{a21}}B_{\mathrm{U}} & 0 & \cdots & 0 \\ -\frac{1}{r_{a21}}B_{\mathrm{U}} & & \frac{1}{r_{a21}}B_{\mathrm{U}} & 0 & \cdots & 0 \\ \hline 0 & \cdots & 0 & 0 & \cdots & 0 \\ \vdots & & \vdots & & \vdots & \\ 0 & \cdots & 0 & 0 & \cdots & 0 \end{array}\right], \quad B_{\mathrm{U}} \equiv \left[\begin{array}{ccc} 0 & 0 & 0 \\ 0 & 0 & 0 \\ 0 & 0 & 1 \end{array}\right]. \quad \text{(C.15)}$$

Then we have the following quadratic form for the power term of the CPDF of Eq. (C.5):

$$\begin{aligned} &\frac{1}{2}(\eta-\hat{\eta})\Sigma_{\eta}^{-1}(\eta-\hat{\eta}) + \frac{1}{2}\frac{[d_{21}-||u_{2\mathrm{EN}}-u_{1,\mathrm{EN}}||]^2}{r_{d_{21}}} + \frac{1}{2}\frac{[0-(u_{2,\mathrm{U}}-u_{1,\mathrm{U}})]^2}{r_{a_{21}}} \\ &= \frac{1}{2}\Big\{\eta^{\mathrm{T}}\Sigma_{\eta}^{-1}\eta - \eta^{\mathrm{T}}\Sigma_{\eta}^{-1}\hat{\eta} - \hat{\eta}^{\mathrm{T}}\Sigma_{\eta}^{-1}\eta + \hat{\eta}^{\mathrm{T}}\Sigma_{\eta}^{-1}\hat{\eta} + \eta^{\mathrm{T}}M_{2,\mathrm{EN}}\eta + c_{M_{2,\mathrm{EN}}}^{\mathrm{T}}\eta + \frac{d_{21}^2}{r_{d_{21}}} + \eta^{\mathrm{T}}M_{2,\mathrm{U}}\eta\Big\} \\ &= \frac{1}{2}\Big\{\eta^{\mathrm{T}}(\Sigma_{\eta}^{-1}+M_{2,\mathrm{EN}}+M_{2,\mathrm{U}})\eta - \eta^{\mathrm{T}}(\Sigma_{\eta}^{-1}\hat{\eta}-\frac{1}{2}c_{M_{2,\mathrm{EN}}}) - (\hat{\eta}^{\mathrm{T}}\Sigma_{\eta}^{-1}-\frac{1}{2}c_{M_{2,\mathrm{EN}}})\eta + \hat{\eta}^{\mathrm{T}}\Sigma_{\eta}^{-1}\hat{\eta} + \frac{d_{21}^2}{r_{d_{21}}}\Big\} \\ &= \frac{1}{2}\Big\{[\eta-(\Sigma_{\eta}^{-1}+M_{2,\mathrm{EN}}+M_{2,\mathrm{U}})^{-1}(\Sigma_{\eta}^{-1}\hat{\eta}-\frac{1}{2}c_{M_{2,\mathrm{EN}}})]^{\mathrm{T}}(\Sigma_{\eta}^{-1}+M_{2,\mathrm{EN}}+M_{2,\mathrm{U}}) \\ &\quad \times[\eta-(\Sigma_{\eta}^{-1}+M_{2,\mathrm{EN}}+M_{2,\mathrm{U}})^{-1}(\Sigma_{\eta}^{-1}\hat{\eta}-\frac{1}{2}c_{M_{2,\mathrm{EN}}})] \\ &\quad -(\Sigma_{\eta}^{-1}\hat{\eta}-\frac{1}{2}c_{M_{2,\mathrm{EN}}})^{\mathrm{T}}(\Sigma_{\eta}^{-1}+M_{2,\mathrm{EN}}+M_{2,\mathrm{U}})^{-1}(\Sigma_{\eta}^{-1}\hat{\eta}-\frac{1}{2}c_{M_{2,\mathrm{EN}}}) + \hat{\eta}^{\mathrm{T}}\Sigma^{-1}\hat{\eta} + \frac{d_{21}^2}{r_{d_{21}}}\Big\}. \end{aligned}$$

Then the update estimated vector $\check{\eta}$ and error covariance matrix $\check{\Sigma}_{\eta}$ of η based on the minimum mean square estimate are given by

$$\begin{aligned} \check{\eta} &= \big(\Sigma_{\eta}^{-1}+M_{2,\mathrm{EN}}+M_{2,\mathrm{U}}\big)^{-1}(\Sigma_{\eta}^{-1}\eta-\frac{1}{2}c_{M_{2,\mathrm{EN}}}), \\ \check{\Sigma}_{\eta} &= \big(\Sigma_{\eta}^{-1}+M_{2,\mathrm{EN}}+M_{2,\mathrm{U}}\big)^{-1}. \end{aligned} \quad \text{(C.16)}$$

Appendix D

Baseline Vector Estimation for Three or Four Antennas

Let us define the $(n_s - 1) \times 1$ vectors as follows:

$$\tilde{\rho}^{n_s}_{CA,ji} \equiv \begin{bmatrix} \tilde{\rho}^{\hat{2}\hat{1}}_{CA,\hat{u}_j\hat{u}_i} \\ \vdots \\ \tilde{\rho}^{\hat{n}_s\hat{1}}_{CA,\hat{u}_j\hat{u}_i} \end{bmatrix}, \quad \tilde{\Phi}^{n_s}_{L1,ji} \equiv \begin{bmatrix} \tilde{\Phi}^{\hat{2}\hat{1}}_{L1,\hat{u}_j\hat{u}_i} \\ \vdots \\ \tilde{\Phi}^{\hat{n}_s\hat{1}}_{L1,\hat{u}_j\hat{u}_i} \end{bmatrix}, \quad N^{\hat{n}_s}_{L1,ji} = \begin{bmatrix} N^{\hat{2}\hat{1}}_{L1,u_ju_i} \\ \vdots \\ N^{\hat{n}_s\hat{1}}_{L1,u_ju_i} \end{bmatrix}, \quad \text{(D.1)}$$

also define $3 \times (n_s - 1)$ matrix

$$g^{n_s}_{ji} = \begin{bmatrix} g^{\hat{2}\hat{1}}_{\hat{u}_{ji}} \cdots g^{\hat{n}_s\hat{1}}_{\hat{u}_{ji}} \end{bmatrix} : \quad 3 \times (n_s - 1). \quad \text{(D.2)}$$

Measurement equation for antennas of u_1, u_2 and u_3 $(n_r = 3)$ is as follows:

$$y^{n_s}_{u_3u_2u_1} = C^{n_s}_{u_{21}u_{31}u_{32}}\xi^{n_s}_{u_{21}u_{31}u_{32}} + v^{n_s}_{u_3u_2u_1}, \quad \text{(D.3)}$$

where

$$
\begin{bmatrix}
\tilde{\rho}^{\hat{2}\hat{1}}_{CA,\hat{u}_2\hat{u}_1} \\ \vdots \\ \tilde{\rho}^{\hat{n}_s\hat{1}}_{CA,\hat{u}_2\hat{u}_1} \\ \tilde{\rho}^{\hat{2}\hat{1}}_{CA,\hat{u}_3\hat{u}_1} \\ \vdots \\ \tilde{\rho}^{\hat{n}_s\hat{1}}_{CA,\hat{u}_3\hat{u}_1} \\ \tilde{\rho}^{\hat{2}\hat{1}}_{CA,\hat{u}_3\hat{u}_2} \\ \vdots \\ \tilde{\rho}^{\hat{n}_s\hat{1}}_{CA,\hat{u}_3\hat{u}_2} \\ \tilde{\Phi}^{\hat{2}\hat{1}}_{L1,\hat{u}_2\hat{u}_1} \\ \vdots \\ \tilde{\Phi}^{\hat{n}_s\hat{1}}_{L1,\hat{u}_2\hat{u}_1} \\ \tilde{\Phi}^{\hat{2}\hat{1}}_{L1,\hat{u}_3\hat{u}_1} \\ \vdots \\ \tilde{\Phi}^{\hat{n}_s\hat{1}}_{L1,\hat{u}_3\hat{u}_1} \\ \tilde{\Phi}^{\hat{2}\hat{1}}_{L1,\hat{u}_3\hat{u}_2} \\ \vdots \\ \tilde{\Phi}^{\hat{n}_s\hat{1}}_{L1,\hat{u}_3\hat{u}_2}
\end{bmatrix}
=
\begin{bmatrix}
(g^{\hat{2}\hat{1}}_{\hat{u}_{21}})^{\mathrm{T}} & & & 0 & \cdots & 0 \\
\vdots & & & \vdots & \ddots & \vdots \\
(g^{\hat{n}_s\hat{1}}_{\hat{u}_{21}})^{\mathrm{T}} & & & \vdots & \ddots & \vdots \\
& (g^{\hat{2}\hat{1}}_{\hat{u}_{31}})^{\mathrm{T}} & & \vdots & \ddots & \vdots \\
& \vdots & & \vdots & \ddots & \vdots \\
& (g^{\hat{n}_s\hat{1}}_{\hat{u}_{31}})^{\mathrm{T}} & & \vdots & \ddots & \vdots \\
& & (g^{\hat{2}\hat{1}}_{\hat{u}_{32}})^{\mathrm{T}} & \vdots & \ddots & \vdots \\
& & \vdots & \vdots & \ddots & \vdots \\
& & (g^{\hat{n}_s\hat{1}}_{\hat{u}_{32}})^{\mathrm{T}} & \vdots & \cdots & 0 \\
(g^{\hat{2}\hat{1}}_{\hat{u}_{21}})^{\mathrm{T}} & & & \lambda_1 & & \\
\vdots & & & & \ddots & \\
(g^{\hat{n}_s\hat{1}}_{\hat{u}_{21}})^{\mathrm{T}} & & & & \lambda_1 & \\
& (g^{\hat{2}\hat{1}}_{\hat{u}_{31}})^{\mathrm{T}} & & & & \lambda_1 \\
& \vdots & & \vdots & & \ddots \\
& (g^{\hat{n}_s\hat{1}}_{\hat{u}_{31}})^{\mathrm{T}} & & & & \lambda_1 \\
& & (g^{\hat{2}\hat{1}}_{\hat{u}_{32}})^{\mathrm{T}} & & & \lambda_1 \\
& & \vdots & \vdots & & \ddots \\
& & (g^{\hat{n}_s\hat{1}}_{\hat{u}_{32}})^{\mathrm{T}} & & & \lambda_1
\end{bmatrix}
\begin{bmatrix}
u_{21} \\ u_{31} \\ u_{32} \\ N^{21}_{L1,u_2u_1} \\ \vdots \\ N^{n_s1}_{L1,u_2u_1} \\ N^{21}_{L1,u_3u_1} \\ \vdots \\ N^{n_s1}_{L1,u_3u_1} \\ N^{21}_{L1,u_3u_2} \\ \vdots \\ N^{n_s1}_{L1,u_3u_2}
\end{bmatrix}
+ v. \tag{D.4}
$$

In this case, we have

$$
M_3 \equiv \left[\begin{array}{ccc|ccc}
\frac{1}{r_{l_{21}}} I & & & 0 & \cdots & 0 \\
& \frac{1}{r_{l_{31}}} I & & \vdots & & \vdots \\
& & \frac{1}{r_{l_{32}}} I & 0 & \cdots & 0 \\
\hline
0 & \cdots & 0 & 0 & \cdots & 0 \\
\vdots & & \vdots & \vdots & & \vdots \\
0 & \cdots & 0 & 0 & \cdots & 0
\end{array}\right], \tag{D.5}
$$

$$c_{M_3} \equiv \left[\begin{array}{cccccc} -c_{l_{21}}^{\mathrm{T}} & -c_{l_{31}}^{\mathrm{T}} & -c_{l_{32}}^{\mathrm{T}} & 0^{\mathrm{T}} & \cdots & 0^{\mathrm{T}} \end{array} \right]. \tag{D.6}$$

Then the measurement equation for four antennas of $u_1, \cdots, u_4$ ($n_r = 4$) is as follows:

$$y_{u_4 u_3 u_2 u_1}^{n_s} = C_{u_{21} u_{31} u_{41} u_{32} u_{42} u_{43}}^{n_s} \xi_{u_{21} u_{31} u_{41} u_{32} u_{42} u_{43}}^{n_s} + v_{u_4 u_3 u_2 u_1}^{n_s}, \tag{D.7}$$

where

$$\begin{bmatrix} \tilde{\rho}_{CA,21}^{n_s} \\ \tilde{\rho}_{CA,31}^{n_s} \\ \tilde{\rho}_{CA,41}^{n_s} \\ \tilde{\rho}_{CA,32}^{n_s} \\ \tilde{\rho}_{CA,42}^{n_s} \\ \tilde{\rho}_{CA,43}^{n_s} \\ \tilde{\Phi}_{L1,21}^{n_s} \\ \tilde{\Phi}_{L1,31}^{n_s} \\ \tilde{\Phi}_{L1,41}^{n_s} \\ \tilde{\Phi}_{L1,32}^{n_s} \\ \tilde{\Phi}_{L1,42}^{n_s} \\ \tilde{\Phi}_{L1,43}^{n_s} \end{bmatrix} = \begin{bmatrix} (g_{21}^{n_s})^{\mathrm{T}} & & & & & & & & & & & \\ & (g_{31}^{n_s})^{\mathrm{T}} & & & & & & & & & & \\ & & (g_{41}^{n_s})^{\mathrm{T}} & & & & & & & & & \\ & & & (g_{32}^{n_s})^{\mathrm{T}} & & & & & & & & \\ & & & & (g_{42}^{n_s})^{\mathrm{T}} & & & & & & & \\ & & & & & (g_{43}^{n_s})^{\mathrm{T}} & & & & & & \\ (g_{21}^{n_s})^{\mathrm{T}} & & & & & & \lambda_1 I & & & & & \\ & (g_{21}^{n_s})^{\mathrm{T}} & & & & & & \lambda_1 I & & & & \\ & & (g_{21}^{n_s})^{\mathrm{T}} & & & & & & \ddots & & & \\ & & & (g_{21}^{n_s})^{\mathrm{T}} & & & & & & \ddots & & \\ & & & & (g_{21}^{n_s})^{\mathrm{T}} & & & & & & \ddots & \\ & & & & & (g_{21}^{n_s})^{\mathrm{T}} & & & & & & \lambda_1 I \end{bmatrix} \begin{bmatrix} u_{21} \\ u_{31} \\ u_{41} \\ u_{32} \\ u_{42} \\ u_{43} \\ N_{L1,21}^{n_s} \\ N_{L1,31}^{n_s} \\ N_{L1,41}^{n_s} \\ N_{L1,32}^{n_s} \\ N_{L1,42}^{n_s} \\ N_{L1,43}^{n_s} \end{bmatrix} + v, \tag{D.8}$$

$$M_4 \equiv \left[\begin{array}{cccccc|ccc} \frac{1}{r_{l_{21}}}I & & & & & & 0 & \cdots & 0 \\ & \frac{1}{r_{l_{31}}}I & & & & & \vdots & & \vdots \\ & & \frac{1}{r_{l_{41}}}I & & & & \vdots & & \vdots \\ & & & \frac{1}{r_{l_{32}}}I & & & \vdots & & \vdots \\ & & & & \frac{1}{r_{l_{42}}}I & & \vdots & & \vdots \\ & & & & & \frac{1}{r_{l_{43}}}I & 0 & \cdots & 0 \\ \hline 0 & \cdots & \cdots & \cdots & \cdots & 0 & 0 & \cdots & 0 \\ \vdots & & & & & \vdots & \vdots & & \vdots \\ 0 & \cdots & \cdots & \cdots & \cdots & 0 & 0 & \cdots & 0 \end{array}\right], \tag{D.9}$$

$$c_{M_4} \equiv \left[\begin{array}{cccccccccc} -c_{l_{21}}^{\mathrm{T}} & -c_{l_{31}}^{\mathrm{T}} & -c_{l_{41}}^{\mathrm{T}} & -c_{l_{32}}^{\mathrm{T}} & -c_{l_{42}}^{\mathrm{T}} & -c_{l_{43}}^{\mathrm{T}} & 0^{\mathrm{T}} & \cdots & 0^{\mathrm{T}} \end{array}\right]. \tag{D.10}$$

Appendix E

Rotation Matrix by Euler's Principal Rotation Theorem

Let us define the rotation angle ϕ and the normal vector $\mathbf{n}$ between two normalized baseline vectors $\mathbf{s}$,$\mathbf{t}$:

$$\mathbf{s} = (x_0, y_0, z_0), \quad \mathbf{t} = (x_1, y_1, z_1). \tag{E.1}$$

According to the Euler's principal rotation theorem, the position of $\mathbf{s}$ is moved to the position of $\mathbf{t}$ by the rotation of the angle ϕ around the normal vector which is called Euler axis. $\cos\phi$ is obtained from the inner product of two vectors $\mathbf{s}$, $\mathbf{t}$, and the normal vector $\mathbf{n}$ is obtained from the outer product of two vectors $\mathbf{s}$,$\mathbf{t}$.

$$\begin{aligned} \cos\phi &= \mathbf{s} \cdot \mathbf{t} \\ &= x_0 x_1 + y_0 y_1 + z_0 z_1, \end{aligned} \tag{E.2}$$

$$\begin{aligned} \mathbf{n} = (n_x, n_y, n_z)^{\mathrm{T}} &= \frac{\mathbf{s} \times \mathbf{t}}{||\mathbf{s} \times \mathbf{t}||} \\ &= \frac{1}{\sin\phi}(y_0 z_1 - z_0 y_1, z_0 x_1 - x_0 z_1, x_0 y_1 - y_0 x_1). \end{aligned} \tag{E.3}$$

From Eq.(E.2)-(E.3), we have following equations:

$$\cos\phi = x_0x_1 + y_0y_1 + z_0z_1, \tag{E.4}$$

$$n_x\sin\phi = y_0z_1 - z_0y_1, \tag{E.5}$$

$$n_y\sin\phi = z_0x_1 - x_0z_1, \tag{E.6}$$

$$n_z\sin\phi = x_0y_1 - y_0x_1. \tag{E.7}$$

Transforming Eq.(E.4)-(E.7), (x_1, y_1, z_1) are expressed by (x_0, y_0, z_0),(n_x, n_y, n_z), and ϕ:

$$x_1 = x_0\cos\phi + z_0n_y\sin\phi - y_0n_z\sin\phi, \tag{E.8}$$

$$y_1 = y_0\cos\phi - z_0n_x\sin\phi + x_0n_z\sin\phi, \tag{E.9}$$

$$z_1 = z_0\cos\phi + y_0n_x\sin\phi - x_0n_y\sin\phi. \tag{E.10}$$

Eq.(E.8)-(E.10) are expressed by matrix form as follows:

$$\begin{bmatrix} x_1 \\ y_1 \\ z_1 \end{bmatrix} = \begin{bmatrix} x_0 & 0 & z_0 & -y_0 \\ y_0 & -z_0 & 0 & x_0 \\ z_0 & y_0 & -x_0 & 0 \end{bmatrix} \begin{bmatrix} \cos\phi \\ n_x\sin\phi \\ n_y\sin\phi \\ n_z\sin\phi \end{bmatrix}. \tag{E.11}$$

When we obtain two baseline vectors **s**,**t**, we estimate the parameters (n_x, n_y, n_z),$\cos\phi$, and $\sin\phi$. Then we derive the rotation matrix in Eq.(5.26) by the estimates.